University of Alberta

# The Behaviour of Composite Bell-shaped Deviators with Multistrand Post-Tensioned Tendons

by

Neilu Rishi 

A thesis submitted to the Faculty of Graduate Studies and Research
in
partial fulfillment of the requirements for the degree of Master of Science
in
Structural Engineering

Department of Civil and Environmental Engineering

Edmonton, Alberta

Fall 2006

*Your file Votre référence*
*ISBN: 978-0-494-22358-1*
*Our file Notre référence*
*ISBN: 978-0-494-22358-1*

# ABSTRACT

Deviators are critical components in external post-tensioning systems. Current Canadian and American design codes restrict the type of deviator that can be employed to a bent-steel pipe deviator. Less prescriptive code requirements should be considered.

This study examines a composite bell-shaped deviator. The objective was to validate design concepts proposed and to acquire data for the design of diablo deviators. The scope of the study includes a literature review, design of a bell-shaped deviator, and testing prototypes of such deviators with multistrand tendons.

Tests were performed on two different sized deviators to ascertain the friction characteristics, deviator behaviour, and tendon efficiency that result from tendon deviation. The friction coefficient between the tendon and high-density polyethylene sheathing ranged between 0.11 and 0.13. Wedge hardware, as opposed to the tendon radius of curvature, controlled tendon efficiency. Deviator behaviour was examined, from which deviator design recommendations are made.

# ACKNOWLEDGEMENTS

This study was performed at the I. F. Morrison Structural Engineering Laboratory at the University of Alberta. The funding was provided, in large part, by the University of Alberta. Additional thanks go to Con-force Structures Limited for their work in making the deviators and to VSL International for the single-use anchorages they provided.

There are many people who contributed to this project. I owe much gratitude to Dr. D.M. Rogowsky, who saw me through the project from beginning to end. Without his guidance and expertise, I would have been lost. Thank you for all your help and for simply being so smart.

The help of Richard Helfrich and Larry Burden was invaluable. Richard and Larry were my heroes in the lab, helping me throughout the many stages of testing and making sure I kept five digits on each hand and foot. To them, I owe many thanks.

Dr. A.E. Elwi also provided assistance and guidance as he navigated me through much of the paperwork necessary to get my degree.

To the Razavys, thank you for making sure I got to and from the university without breaking a student's budget.

Finally, I owe an incredible debt of thanks to my friends and family. They kept me afloat over the many years this project took, keeping faith in me throughout it all. Thank you to all who kept my spirit well nourished and helped me retain some perspective throughout this venture. I appreciate all of you more than I can express and am blessed to have you in my life.

# TABLE OF CONTENTS

# LIST OF TABLES

# LIST OF FIGURES

## LIST OF SYMBOLS

$a$ = $I_s / A_{sec} R_c^2$

$A_{ret}$ = effective area of ram piston at retraction end

$A_{sec}$ = cross-sectional area of steel pipe

$b$ = $F E_s I_s / G A_{sec} R_c^2$

$D_{sh}$ = outside diameter of sheathing

$\Delta D_H$ = horizontal diameter change of deviator

$E_g$ = modulus of elasticity of deviator grout

$E_s$ = modulus of elasticity of deviator steel pipe

$f_p$ = stress in tendon

$f_{pj}$ = jacking stress in tendon, in MPa

$f_{pu}$ = ultimate tensile strength of tendon, in MPa

$F$ = shape factor for the steel pipe cross-section (0.878 for 1500 mm radius deviators and 0.870 for 4500 mm radius deviators)

$F_{dvi}$ = driving force

$F_{fr}$ = friction force between two surfaces

$F_{f_N}$ = friction force in north ram

$F_{f_S}$ = friction force in south ram

$F_n$ = normal force acting between two surfaces

$FR$ = tendon stress loss due to friction

$G$ = shear modulus of elasticity of steel pipe

$I_{comp}$ = moment of inertia of composite section of deviator, transformed to grout

$= I_g + nI_s$

$I_g$ = moment of inertia of grout cross-section in deviator

$I_s$ = moment of inertia of deviator steel pipe cross-section

$k_3$ = $1 - a - b$

$K$ = wobble coefficient ( /m)

$l$ = deviator cantilever length (distance between deviator support face and deviator end)

$l_c$ = length from deviator support face over which there is tendon contact

$l_e$ = length from deviator end upon which there is no tendon contact

$M_p$ = moment in deviator due to tendon deviation

$n$ = $E_s / E_g$

$P_1$ = tendon force at dead end of deviator, in kN

$P_2$ = tendon force at live end of deviator, in kN

$P_f$ = friction force between tendon and sheathing at deviator, in kN

$P_l$ = lateral force due to tendon deviation

$P_{N_{EXT}}$ = load applied to tendon at north ram (with piston extending), in kN

$P_{N_{RET}}$ = load applied to tendon at north ram (with piston retracting), in kN

$P_{ret}$ = load at retraction end of ram, in kN

$P$ = force in tendon, in kN

$P_o$ = jacking force in tendon, in kN

$P_{S_{EXT}}$ = load applied to tendon at south ram (with piston extending), in kN

$P_{S_{RET}}$ = load applied to tendon at south ram (with piston retracting), in kN

$P_u$ = ultimate load in tendon, in kN

$R$ = radius of curvature of tendon deviation

$R_c$ = radius to the centroid of the cross-section

$R_{min}$ = minimum allowable radius of curvature of tendon deviation, in metres

$R_s$ = outer radius of deviator steel pipe

$V_p$ = shear force in deviator due to tendon deviation

$w_p$ = distributed load on deviator from tendon deviation

= P/R

$W$ = resultant vertical load acting on deviator

$x$ = tendon length, in metres

$z$ = distance from deviator end in millimetres

$y$ = distance from deviator cross-section centroid to point of interest for strain

$\alpha$ = overall angle change tendon undergoes at deviator (in radians)

$\alpha_N$ = angle change of tendon over north portion of deviator (in radians)

$\alpha_S$ = angle change of tendon over south portion of deviator (in radians)

$\beta$ = additional unintended angle change tolerance at deviator (in radians)

$\delta_{comp}$ = deviator deflection (fully composite)

$\varepsilon_{comp}$ = strain in deviator (fully composite)

$\varepsilon_{ps}$ = strain in prestressing tendon

$\mu$ = friction coefficient

$\theta_{comp}$ = slope of deviator due to elastic bending, in radians (fully composite)

$\sigma_n$ = north ram pressure reading at expansion/stroke end

$\sigma_{ret}$ = pressure reading at retraction end of ram

$\sigma_s$ = south ram pressure reading at expansion/stroke end

# 1 INTRODUCTION

## 1.1 OVERVIEW

The use of external post-tensioning is increasing in both new design and in the rehabilitation of old structures. External post-tensioning is unique from other forms of prestressing in that the tendon is located outside the member and is only connected to the structure at anchorage ends and at isolated locations, referred to as deviators, along the member's length. Figure 1.1 shows an example of a common application of external tendons inside the cell of a box girder.

The use of deviators is critical in the effectiveness of external post-tensioning. The use of deviators in external post-tensioning is twofold:

1) The deviator is the only place, with the exception of the anchorages, where the prestressing tendon is connected to the structure. This connection is important in limiting the loss of eccentricity of the tendon, and the corresponding reduction in member strength, due to deflections of a structure.
2) The deviator controls the angle changes in the tendon profile.

This study focuses on the second point. Presently, Canadian (CAN/CSA S6-00, 2000) and American (AASHTO LRFD, 2000) codes limit the type of deviator that can be employed to a bent-steel pipe deviator. An alternative design, a composite "diablo" (or bell-shaped) deviator, is examined in this study, with emphasis on the

friction characteristics, deviator behaviour and tendon efficiency that result from a tendon angle change.

## 1.2 OBJECTIVES AND SCOPE OF THESIS

The goal of the study is to explore the design of deviators for use with multistrand external post-tensioning tendons. The scope of the study includes a review of the literature, design of a new type of deviator, and testing prototypes of such deviators. Emphasis is on a new type of deviator that is not covered by Canadian and American design codes, referred to as a composite diablo deviator. The objectives of the experiments are as follows:

1) Validate the design concept (i.e. proof of concept tests)
2) Acquire data that will facilitate the practical design of the deviators.

The behaviour of the composite diablo deviator is examined. Four deviators are tested to see if their behaviour is consistent with predictions and to see if their performance satisfies the required design criteria. The friction coefficient, $\mu$, is assessed throughout the tests to determine the range of the friction coefficient that one might use in design. Tests to failure examine the overall behaviour of the deviators and determine the extent to which the deviators reduce the strength and ductility of the tendon. Finally, a design model and design criteria suitable for use in codes are proposed.

## 1.3 ORGANIZATION OF THESIS

This thesis is organized in five chapters and two appendices.

In Chapter 2, literature is reviewed for information regarding external post-tensioning and the use of deviators. Gaps in knowledge and areas of improvement in design codes are identified.

Chapter 3 describes the experimental program, which presents proof of concept tests and the acquisition of additional data that will facilitate the design of deviators. This chapter includes descriptions of the test specimen, the materials used, the test set-up and instrumentation used, and the test procedure.

Chapter 4 presents a summary of the test results along with a detailed analysis and discussion of the results. This chapter includes comparisons between predictions and actual results, as well the development of useful design information and recommendations.

Chapter 5 provides a summary of the conclusions and recommendations.

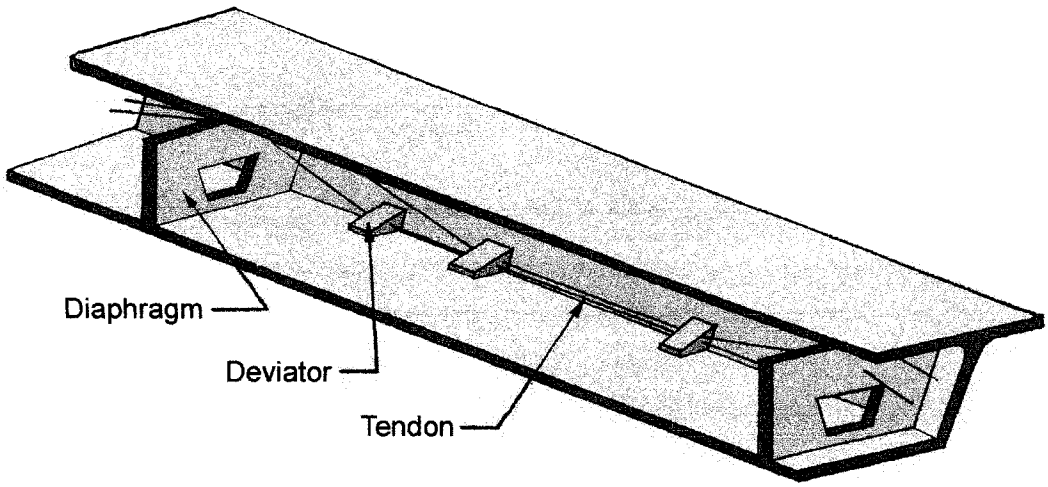


**Figure 1.1: Example of typical external post-tensioning in a box girder (adapted from Macovei-Benczur and Rogowsky, 2002)**

# 2 LITERATURE REVIEW

## 2.1 INTRODUCTION

This chapter focuses on the technical literature regarding the use and effect of deviators in external post-tensioning applications. The review begins with a discussion of the written works on types of deviators, friction at deviators, and other issues concerning deviators such as the forces acting on the deviator and its interior radius of curvature. The second section in the literature review provides an overview of various codes' requirements pertaining to external post-tensioning. The discussion outlines the requirements from the various codes as well as a presentation of areas the author feels warrant further examination.

## 2.2 REVIEW OF LITERATURE CONCERNING EXTERNAL POST-TENSIONING AND DEVIATORS

An external post-tensioning system can be looked at as two substructures – the concrete beam and the external tendons – with interaction between the two substructures only at anchorage zones and deviators (Pisani and Nicoli, 1996). The reliability of an external prestressing system entirely depends on these tendon fixing points (Manisekar and Rao, 2003). The deviator, while maintaining tendon eccentricity at deviator locations, is also typically used to deflect the tendon to give it a draped profile.

### 2.2.1 DEVIATOR TYPES

The deviator is supported and positioned with deviator supports. The three primary types of deviator supports used include the diaphragm, rib, and saddle deviator supports, all seen in Figure 2.1. In addition, cross beams are often used as deviator supports. The deviator is occasionally placed within steel deviator supports as well (Figure 2.1(d)) (Manisekar and Rao, 2003).

The forces from tendon deviation are transferred from the deviator through the deviator support to the superstructure. The deviator support and deviator together are referred to as the deviator block. The tendon passes through the deviator, which controls the tendon geometry. Common types of deviators are shown in Figure 2.2 (Hewson, 2003). The bent-steel pipe deviator is very common (Figure 2.2(a) and (b)). This deviator consists of a steel pipe bent to the tendon profile. Typically, this deviator doubles as sheathing, with high-density polyethylene (HDPE) sheathing connected to the deviator at its ends (Figure 2.2(a)). However, this is not always the case and the HDPE sheathing can be continuous through the deviator (Figure 2.2(b)). A deviator can also be formed within the deviator support by casting the deviator support with formed holes to control the tendon deviation (Figure 2.2(c)). With the deviators discussed thus far, problems may arise in aligning the deviator hole because setting all the deviators at their correct angles and positions can be very difficult. Any misalignments result in the tendon bearing against the lip of the deviator, causing kinks in the tendon and/or possible spalling of the concrete support (Hewson, 2003). To reduce this problem, Hewson (2003) suggests incorporating a bell-mouthed

arrangement at the ends of the deviator hole as shown in Figure 2.2(c) and (d). A bell-mouthed arrangement at the ends of the deviator hole would allow the tendons to deviate at the required angle while reducing the possibility of kinks in the tendon at the deviator ends (Hewson, 2003). Macovei-Benczur and Rogowsky (2002) suggest the use of a continuous bell-shaped interior through the deviator as opposed to restricting the bell to the deviator ends (Figure 2.3). The misalignments can be eliminated if the deviator is dimensioned to accommodate the intended angle change plus tolerance ($\beta$). The Bangkok Second Stage Expressway used this type of deviator. The deviator was formed with concrete, using a mould that was extracted early after concrete setting to leave a smooth surface (Hewson, 1993).

### 2.2.2 FRICTION AT DEVIATORS

In the prestressing process, the tendon experiences a loss in its prestress due to friction along the tendon. Friction between the tendon and its sheathing can result in a considerable loss of force in the tendon and can be a problem if not correctly considered in the design of the post-tensioned system (Manisekar and Rao, 2003; Hewson, 2003). Friction is a force component at the interface of two materials that restricts or tends to retard the motion of one object with respect to another (Burns, 1991). The two basic laws of friction are (Bowden and Tabor, 1956):

1) Frictional resistance is proportional to the normal force
2) Friction is independent of the area of the sliding surfaces

Based on these principles, the friction force, $F_{fr}$, can be expressed as

$$F_{fr} = \mu F_n \qquad \textbf{(Eq. 2.1)}$$

in which $\mu$ is the coefficient of friction and $F_n$ is the normal force acting between the surfaces.

Determining the coefficient of friction between two surfaces can be difficult as many factors influence the friction properties. All material surfaces are rough at an atomic level and will exhibit peaks and valleys. When two surfaces are placed against each other, only a few points are actually in contact with one another and the pressure at these points is 10 to 100 times higher than the average pressure over the whole contact surface. When movement between the surfaces occurs, the peaks of the materials come into contact with one another and the harder peaks will wear away the softer ones. With greater contact pressure the peaks will interlock and will shear away one another. After some movement, the most prominent peaks will have been sheared off and the material will fill up the valleys, increasing the contact points and creating a smoother contact surface. Thus, when movement is initiated, the coefficient of friction tends to be higher and, as movement continues, the coefficient of friction drops and typically plateaus (Figure 2.4). The high friction value necessary to initiate movement is referred to as static friction while the friction value between the moving surfaces is referred to as kinetic friction. When sliding in one direction, the peaks are bent over in that direction. If the direction of travel is reversed, the bent-over peaks will initially apply an extra restraint and the static friction will be greater than it was before. If a lubricant such as oil is used, the surfaces will float on each other and the contact between the peaks of the two materials will be reduced,

resulting in significantly less frictional resistance (Bowden and Tabor, 1956; Leonhardt, 1964).

When the jack pulls a profiled multistrand tendon, the movement of the strand is resisted by friction against the duct (Hewson, 2003). Leonhardt (1964) lists the following as factors influencing the friction between prestressing tendons and their ducts:

1. The surface condition of the sliding surfaces;
2. The hardness of each of the two materials sliding upon each other, and the ratio of these two hardnesses;
3. The dryness of the surfaces or the wetting thereof by a lubricant;
4. The speed of the movement: $\mu$ has its maximum value when starting from rest and it usually decreases during movement and with increasing speed;
5. The contact pressure which is produced by the force exerted upon the sliding surface;
6. Molecular force (if the pressure exerted upon the sliding surface is very high);
7. Foreign bodies between the sliding surfaces; for example, flakes of mill scale or rust cause a substantial increase in friction; both of these substances have an action similar to that of fine sand; and
8. The duration of the movement or the distance travelled – because the sliding surfaces become polished by the movement.

It is apparent that, due to the many factors that influence the friction coefficient, it can be highly variable and difficult to predict. Typically, a range of values or an average

coefficient value is specified in codes. A typical friction coefficient value between high-density polyethylene and flat steel plate would be 0.26 (Dow Chemical Company, 2006), though the friction coefficient will largely depend on the roughness of the steel surface (Kinsella et al., 2005).

Friction between the tendon and the duct results in a variation of the prestress force along the length of the member. Figure 2.5 shows a typical force profile along an internal multistrand tendon stressed from one end. The force on the jacking end is notably higher than that at the anchorage end. A report by the Transport Research Laboratory on an externally prestressed box girder model showed as much as 10% lower prestress at the dead end anchorage due to friction losses (Manisekar and Rao, 2003). Prestress losses due to friction can be compensated for by double-end stressing, where the tendon is jacked from both ends. Nonetheless, even when double-end stressed, the friction losses can be significant for internal post-tensioned tendons longer than 120m and for external post-tensioned tendons longer than 300m. (Hewson, 2003).

The condition of tendon slip at a deviator depends on the tendon force on either side of the deviator, the friction between the cable and deviator, and the angle of deviation (Diep and Tanabe, 2000; Diep and Umehara, 2002; Rao and Mathew, 1996; Tan and Ng, 1997). The forces at each deviator can be modeled as shown in Figure 2.6. Rao and Mathew (1996) defined the "driving" force ($F_{dvi}$), the force causing the tendon to slip, and the friction force ($F_{fr}$) as

$$F_{dvi} = (P_2 - P_1)\cos\left(\frac{\alpha}{2}\right), \quad \textbf{(Eq. 2.2)}$$

$$F_{fr} = \mu(P_2 + P_1)\sin\left(\frac{\alpha}{2}\right) = \mu F_n \quad \textbf{(Eq. 2.3)}$$

in which $P_1$ and $P_2$ are the tendon forces on either side of the deviator and $\alpha$ is the overall tendon angle change at the deviator, all shown in Figure 2.6. Tendon slip occurs at a deviator when the driving force exceeds the friction force; otherwise, no slip occurs.

The friction force can also be expressed with the Euler-Eytelwin-Grashof formula, as shown below (Leonhardt, 1964)

$$F_{fr} = P_o\left(1 - e^{-\mu\alpha}\right) \quad \textbf{(Eq. 2.4)}$$

where $P_o$ is the jacking force in the tendon, and the force in the tendon, $P$, can be defined as

$$P = P_o e^{-\mu\alpha} \quad \textbf{(Eq. 2.5)}$$

For $\mu\alpha < \sim 0.1$, the following approximation is acceptable (Leonhardt, 1964)

$$P = P_o(1 - \mu\alpha) \quad \textbf{(Eq. 2.6)}$$

In addition to the friction forces resulting from intended directional change of the tendon, friction is induced from unintended directional changes called tendon wobble. This unintentional wobble produces additional rubbing between the tendon and the duct surfaces (Hewson, 2003; Burns et al., 1991). Considering the friction resulting from both tendon curvature and wobble, the force, $P$, at any point along the tendon, $x$

metres from the stressing anchor, is commonly determined by (Hewson, 2003; Aeberhard et al., 1992)

$$P = P_o e^{-(\mu\alpha + Kx)} \qquad \textbf{(Eq. 2.7)}$$

The wobble coefficient, $K$, is a measure of the unintentional angle change along the duct. The amount of wobble depends on the tendon size, the prestressing system (sheathing type and size, prestressing steel, spacing of supports, etc.), and the quality of workmanship. The wobble is also dependent on the tendon curvature. The wobble is greater for straight tendons and decreases with increased curvature as the strands, when changing direction, tend to arrange themselves in the smoothest possible curves (Leonhardt, 1964).

The type of sheathing employed is a significant factor affecting the friction properties of the system. While external tendons are typically placed inside HDPE sheathing (Hewson, 2003), metal sheathing is commonly employed at deviators. Plastic sheathing, however, results in less friction and, therefore, higher effective stresses in the prestressing (Macovei-Benczur and Rogowsky, 2002). The friction properties of plastic sheathing also reduce fretting fatigue and increase the allowable stress range by almost a factor of two compared to steel duct (Macovei-Benczur and Rogowsky, 2002).

The wobble and friction coefficients in any particular installation depend on a number of factors, including surface conditions of the steel, the type, diameter, condition and support of the sheathing, and the installation method adopted (Hewson, 2003).

Typical coefficient values specified by Hewson (2003) and Aeberhard et al. (1992) are shown in Table 2.1. In the case of the Bangkok Second Stage Expressway, which used the bell-shaped deviator, HDPE sheathing was employed and designed using a coefficient of friction of 0.15 at deviators and a wobble coefficient of friction of 0.002/m over the length of the diaphragm. During the stressing of the tendons, the typical friction losses observed corresponded to $K = 0.001$ and $\mu = 0.100$, based on Equation 2.7. (Hewson, 1993).

### 2.2.3 Other Deviator Considerations

The design of the deviator must consider the transverse and horizontal forces resulting from tendon deviation (Bruggeling, 1990). The transverse force per unit length, $w_p$, over the contact length between the deviator and tendon is

$$w_p = \frac{P}{R} \qquad \textbf{(Eq. 2.8)}$$

in which $R$ is the radius of curvature of tendon deviation. In addition to the transverse forces from tendon deviation, the tendons produce out-of-plane forces (Rogowsky and Marti, 1991). These forces occur in multistrand or multiwire tendons as a result of the vertical radial forces pushing the tendon against the duct (see Figure 2.7). The total lateral force that results from these out-of-plane forces depends primarily on the tendon force, radius of curvature, and depth of strands within the duct. For VSL tendons in normal size ducts, the horizontal force is approximately equal to 25% of the transverse force (Rogowsky and Marti, 1991). For oversized ducts, the bundle flattening forces are significantly reduced. To determine the magnitude of the horizontal forces, a to-scale schematic of the tendons in the sheathing can be drawn.

From the drawing, the forces acting on the sheathing (see Figure 2.7) can be determined and divided into their horizontal and vertical components.

Multistrand tendons often follow a profile of tight curves. The practical minimum radius of tendon curvature can be governed by the ability to bend the duct without damage (Hewson, 2003) or the reduction of strand strength that results from tendon curvature (Bruggeling, 1990). Hewson (2003) and Aeberhard et al. (1992) stated the minimum bending radii listed in Table 2.2 must be respected in order to avoid damage of the prestressing steel and the plastic sheathing. Chevron (2004) states that the cold bending radius for plastic pipe is dependent on the pipe outside diameter and DR sizing classification. For its DRISCOPIPE® 8100 pipe (which meets the requirements for plastic sheathing set by CAN/CSA S6-00 (2000) and AASHTO LRFD (2000)), the following minimum bending radii, $R_{min}$, are allowed:

$$R_{min} = 20D_{sh} \quad \text{if } DR \leq 9$$

$$R_{min} = 25D_{sh} \quad \text{if } 9 < DR \leq 13.5$$

where $D_{sh}$ is the outside diameter of HDPE sheathing. Rogowsky and Marti (1991) state that, while the minimum radius of tendon curvature is affected by many factors, it is primarily a function of the tendon force. They propose the following formulation for minimum radius of curvature:

$$R_{min} = 3\sqrt{P_u/1000} \qquad \textbf{(Eq. 2.9)}$$

for multistrand tendons in corrugated metal sheathing and:

$$R_{min} = 1.5\sqrt{P_u/1000} \qquad \textbf{(Eq. 2.10)}$$

for multistrand tendons in plastic sheathing. In equations 2.9 and 2.10, $P_u$ is the ultimate load in the tendon, in kN. These equations were proposed assuming that the strands occupy no more than 40% of the duct cross section. Rogowsky and Marti (1991) further stipulated that $R_{min}$ should not be less than 2.5m for constructability reasons.

The sheathing employed must be strong enough to withstand the abrasion from the strands as they are threaded and stressed, the pressure from the strands as they go around any curves in the tendon alignment, and the pressure from grouting. In addition, the internal area of the duct is typically at least twice the tendon area (Hewson, 2003). As the duct area to tendon area ratio increases, there will be fewer layers of strand piled up in the curves. This reduces contact stresses between duct and tendon, improving fretting fatigue resistance. There is also reduced friction because the horizontal forces on the side walls of the duct are reduced.

Excessive kinking of the strands at anchorages can occur if the tendon length between the deviator and anchorage hardware is too short. Such kinking can adversely affect the fatigue life and anchorage efficiency. Rogowsky and Marti (1991) provide a chart (Figure 2.8) for the recommended minimum tangent lengths at stressing anchorages. Figure 2.8 is applicable for the VSL post-tensioning system. Other post-tensioning systems may require other minimum tangent lengths between the anchorage and the start of tendon curvature.

## 2.3 CODE REQUIREMENTS AND RECOMMENDATIONS FOR EXTERNAL POST-TENSIONING

This section reviews and examines the design requirements pertaining to external post-tensioning from CAN/CSA S6-00 (2000), AASHTO LRFD (2000), CSA A23.3-94 (1995), CEB-FIP Model Code 1990 (1993), and ACI 318-02 (2002). CSA A23.3-94 (1995) and ACI 318-02 (2002) discuss design considerations for external post-tensioning, but do not make any mention of considerations for deviators.

### 2.3.1 POST-TENSIONING MATERIALS

All codes reviewed require tendons to be in the form of uncoated, stress-relieved or low-relaxation, seven-wire strand, or uncoated plain or deformed high-strength bars. While the various codes reference different standards for their prestress strand properties, the required strand properties are very similar.

CAN/CSA S6-00 (2000), AASHTO LRFD (2000), and ACI 318-02 (2002) require anchorage hardware for these tendons to develop at least 95% tendon efficiency (i.e., 95% of the specified tensile strength of the tendons). In addition, the anchorage hardware must be able to withstand the applied load without slippage, distortion, or other changes that result in the loss of prestress. CSA A23.3-94 (1995) and CEB-FIP 1990 (1993) simply stipulate that anchorage hardware be able to transfer the design strength of the tendon to the concrete.

CAN/CSA S6-00 (2000) requires sheathing for external post-tensioning to be made of high-density polyethylene plastic conforming to ASTM Standard D 3350, Cell

Classification 324420C, and manufactured in accordance with ASTM Standard D 2239. The tendon duct requirements from AASHTO LRFD (2000) are similar to those from CAN/CSA S6-00 (2000). The code states tendon ducts shall be made of rigid or semirigid galvanized or ferrous materials or of polyethylene, though polyethylene is recommended in corrosive environments. ACI 318-02 (2002) is less specific about the exact materials required, simply stating that the sheathing is to be watertight and continuous over the full length of the tendon and that the material be mortar tight and non-reactive with other materials in the system. CAN/CSA S6-00 (2000) allows the use of plastic sheaths when the radius of tendon curvature is at least 10 m, while AASHTO LRFD (2000) sets this limit at 9 m. CAN/CSA S6-00 (2000) also states the sheathing wall must not be less than 1 mm after a tendon movement of 750 mm at a tendon stress of 80% of its ultimate tensile strength ($0.80f_{pu}$) and the inside cross-sectional area of the sheath for a multiple strand tendon must be at least twice the net area of the prestressing steel. CAN/CSA S6-00 (2000), AASHTO LRFD (2000) and ACI 318-02 (2002) have the same cross-sectional area requirements, but AASHTO LRFD (2000) further stipulates that, when the pull-through method of tendon placement is employed, the cross-sectional area of the duct shall be at least 2.5 times the net area of prestressing steel. CSA A23.3-94 (1995) and CEB-FIP 1990 (1993) make no stipulations regarding tendon sheathing.

### 2.3.2 Design Considerations for Deviation Points

#### 2.3.2.1 Friction Losses in Prestress

Friction between the tendon and its sheathing can result in significant losses in prestress force. These losses in stress from friction, *FR*, are defined by CAN/CSA S6-00 (2000), CEB-FIP 1990 (1993), CSA A23.3-94 (1995) and ACI 318-02 as

$$FR = f_{pj}\left(1 - e^{-(Kx+\mu\alpha)}\right) \qquad \textbf{(Eq. 2.11)}$$

where $f_{pj}$ is the jacking stress in the tendon. AASHTO LRFD (2000), on the other hand, defines the friction losses as

$$FR = f_{pj}\left(1 - e^{-\mu(\alpha+0.04)}\right) \qquad \textbf{(Eq. 2.12)}$$

If $(Kx + \mu\alpha)$ is not greater than 0.3, ACI 318-02 (2002) allows one to determine the friction loss by

$$FR = f_{pj}\left(Kx + \mu\alpha\right) \qquad \textbf{(Eq. 2.13)}$$

The wobble and friction coefficients recommended by each code are shown in Table 2.1. The codes nonetheless recommend that these coefficients be determined experimentally, if possible. CSA A23.3-94 (1995) does not provide coefficient values and indicates that coefficient values should be obtained from the manufacturer of the tendons. Since CAN/CSA S6-00 (2000) and AASHTO LRFD (2000) specify steel sheathing at deviators, the coefficients of friction provided in Table 2.1 are those recommended with internal post-tensioning. ACI 318-02 (2002) and CSA A23.3-94 (1995) warn that overestimation or underestimation of the prestress losses may result in serviceability problems. The friction coefficient between strand and plastic sheathing may warrant further study as AASHTO LRFD (2000) uses a considerably

different value for the coefficient than the other codes.

Equation 2.12 differs from the other codes with the addition of a 0.04 rad angle change in lieu of consideration to wobble. The 0.04 rad value accounts for an inadvertent angle change in the tendon and corresponds to a tolerance of 10 mm in 1000 mm (or 3/8 in. in 3 ft.), as shown in Figure 2.9. This tolerance may vary depending on deviator placement and other job-specific aspects. Thus, AASHTO LRFD (2000) allows that the 0.04 rad tolerance need not be applied in cases where the deviation angle is strictly controlled or precisely known. As an example of when the tolerance may be eliminated or reduced, the code commentary presents the case of continuous ducts passing through separate longitudinal bell-shaped holes at deviators. This type of deviator, however, is not in accordance with the bent-steel pipe deviator stipulated in AASHTO LRFD (2000). To support the use of the 0.04 rad tolerance, the AASHTO LRFD (2000) commentary cites the results from field tests on external tendons of a segmental viaduct in San Antonio, Texas (Roberts, 1993). The external tendons in this case experienced more friction than predicted (with no additional angle tolerance). They claimed this additional loss seemed to be partly due to small misalignments in the bent-steel pipe deviators, resulting in significantly increased angle changes of the tendons at the deviation points. The 0.04 rad angle tolerance at each deviator, however, accounted for the discrepancy in results.

#### 2.3.2.2 Deviator Design

At deviation points, both CAN/CSA S6-00 (2000) and AASHTO LRFD (2000) require sheathing to be comprised of galvanized steel pipe conforming to ASTM Standard A53, Type E, Grade B, with a wall thickness not less than 3 mm. The bent-steel pipe is to be supported and connected to the superstructure by reinforced concrete deviation blocks or diaphragms.

CEB-FIP 1990 (1993) is less prescriptive in its requirements at deviation points than AASHTO LRFD (2000) and CAN/CSA S6-00 (2000). It states that deviating devices need to be able to transfer the design action, taking permissible tolerances into account and that the deviators must be designed assuming that a relative displacement of the tendon takes place, resulting in friction at the deviator.

Macovei-Benczur and Rogowsky (2002) state that CAN/CSA S6-00 (2000) and AASHTO LRFD (2000) are overprescriptive in their deviator requirements, both for deviators and for deviator blocks. The author agrees that the singular option of a bent-steel pipe deviator "inhibits innovation and improvements" (Macovei-Benczur and Rogowsky, 2002) in deviator design. The less specific nature of the CEB-FIP 1990 (1993) requirements is preferable, as it simply requires consideration to the deviator action without reducing innovation to a singular form of deviator. AASHTO LRFD (2000) mentions the use of bell-shaped deviators as a tool to improve the alignment of and reduce the amount of friction at deviators; nonetheless, it retains the singular deviator option of the bent-steel pipe in its requirements.

The use of plastic sheathing at deviators should be permitted provided that the design and detailing are satisfactory. As noted earlier, friction can significantly reduce the prestress at the dead end anchorage. Plastic sheathing will induce less friction and thus reduce the loss in prestress. The requirement for reinforced concrete deviator blocks also eliminates the possibilities for other alternatives such as steel deviator blocks.

The minimum radius of curvature at deviators should also be investigated further. CAN/CSA S6-00 (2000) and AASHTO LRFD (2000) do not define a minimum radius of curvature for the bent-steel pipe deviator. CAN/CSA S6-00 (2000) does, however, define a minimum inside radius of curvature of 9m (without distress) for steel sheaths and this value can be presumed to hold for the bent-steel pipe deviator. AASHTO LRFD (2000), on the other hand, allows for a minimum radius of curvature of 6000 mm for steel sheathing. As previously stated, Hewson (2003), Aeberhard et al. (1992), Chevron (2004), and Rogowsky and Marti (1991) indicate that, depending on tendon size, the minimum radius of curvature for the tendons can be less than those required by CAN/CSA S6-00 (2000) and AASHTO LRFD (2000). Rogowsky and Marti (1991) set the minimum radius of curvature for tendons with plastic sheathing at $1.5\sqrt{P_u/1000}$.

#### 2.3.2.3 Deviation Forces

CAN/CSA S6-00 (2000) and AASHTO LRFD (2000) model the forces acting on the deviator as shown in Figure 2.10. The transverse force, as noted earlier, is defined as

$$w_p = \frac{P}{R} \qquad \textbf{(Eq. 2.14)}$$

The lateral forces, $P_l$, resulting from the directional change of the tendons (see Figure 2.11), are defined by CAN/CSA S6-00 (2000) and AASHTO LRFD (2000) as

$$P_l = \frac{P}{\pi R} \qquad \textbf{(Eq. 2.15)}$$

Equation 2.15 is based on the assumption that the strands occupy one-half of the duct. The transverse and lateral forces must be investigated and resisted by the deviator's surrounding substructure. The spreading of the strands at deviation points also results in a change in eccentricity of the tendon relative to the sheathing. CAN/CSA S6-00 (2000) gives the eccentricity of curved tendons with respect to the centre of the duct, as shown in

Figure 2.12. If the duct diameter is oversized or the number of strands reduced (strands occupy less than one-half of the duct), a random packing of the strands should be drawn and the corresponding eccentricity computed.

## 2.4 SUMMARY

The reliability of external prestressing greatly depends on the effective use of deviators. Deviators control tendon profile and transfer tendon forces into the concrete substructure. Misalignments in deviators and ducts can be a considerable

problem and should be considered in design. The bell-shaped deviator reduces misalignment problems.

Frictional forces induced at deviators can also result in significant prestress loss. The amount of slip at each deviator depends on the tendon force on either side of the deviator, the friction coefficient between the tendon and its sheathing, and the angle of deviation of the tendon. The codes overviewed present frictional loss in similar manners, with minor variations.

The author feels that certain areas of the Canadian and American bridge codes warrant further investigation. The singular requirement for bent-steel pipe deviators disallows the use of alternate types of deviators such as the bell-shaped deviator. The improved alignment associated with the use of such a deviator would result in lower prestress losses due to friction. The minimum radius of curvature at deviators should also be investigated as the findings of Hewson (2003), Aeberhard et al. (1992), Chevron (2004), and Rogowsky and Marti (1991) show that smaller radii of curvature than stipulated by present codes may be feasible. There is also literature that supports the use of plastic sheathing at deviators. The lower friction forces associated with plastic duct would result in a reduction in prestress losses due to friction, as well as in better fretting fatigue performance.

The following chapters explore some of the issues discussed by investigating the behaviour of a composite deviator. The evidence thus gained could be used to facilitate improvements in code requirements for deviators.

**Table 2.1: Friction and wobble coefficients***

| Reference | Friction Coefficient, $\mu$ | Wobble Coefficient, $K$ ( /m) |
|---|---|---|
| CAN/CSA S6-00 (2000) | 0.14 | 0.002 |
| ACI 318-02 (2002) | 0.05 – 0.15 | 0.0010 - 0.0020 |
| CEB-FIP 1990 (1993) ** | 0.12 – 0.15 | 0 |
| AASHTO LRFD (2000) | 0.23 | N/A |
| Hewson (2003) | 0.15 | 0.001 |
| Aeberhard et al. (1992) | 0.12 – 0.15 | 0 |
| Hewson (1993) (Bangkok Expressway) | 0.10 | 0.001 |

* Values of friction coefficients for multistrand tendons with polyethylene sheathing
** Coefficient values correspond to a saddle radius of 2.5m to 4.0m. For lower radii, CEB-FIP 1990 (1993) states further test evidence is required.

**Table 2.2: Minimum bending radii for tendons in plastic sheathing at deviators**

| Reference | Tendon Size | Minimum Radius (m) |
|---|---|---|
| Hewson (2003) | 4 x 15 mm | 3.00 |
| | 12 x 15 mm | 5.00 |
| | 31 x 15 mm | 8.00 |
| Aeberhard et al. (1992) | 19 x 12.7mm or 12 x 15 mm | 2.50 |
| | 31 x 12.7mm or 19 x 15 mm | 3.00 |
| | 55 x 12.7mm or 37 x 15 mm | 5.00 |
| Rogowsky and Marti (1991) | Tendon ultimate strength $P_u = A_p f_{pu}$ (in MN) | $1.5\sqrt{P_u/1000}$ but not less than 2.5 m |
| Chevron (2004)* | DR ≤ 9 | $20D_{sh}$ |
| | 9 < DR ≤ 13.5 | $25D_{sh}$ |

*Instead of tendon size, the DR rating refers to the size of plastic pipe used as sheathing

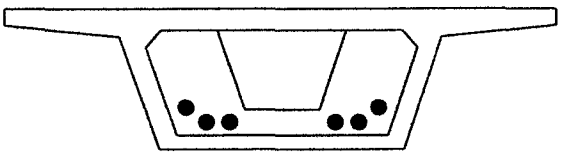

(a) Diaphragm

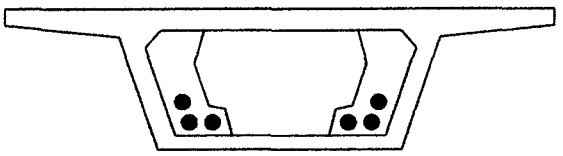

(b) Rib

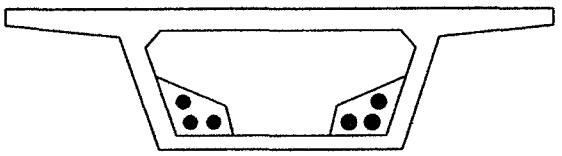

(c) Saddle

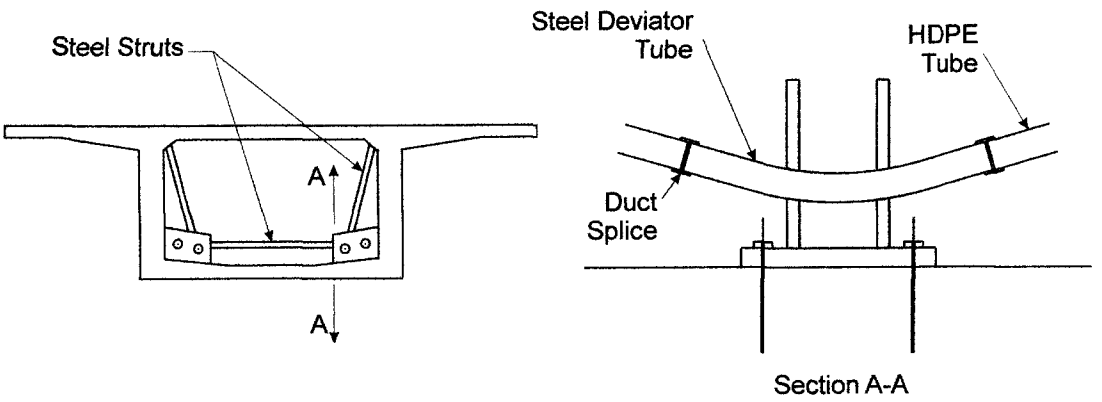


(d) Steel deviator support (adapted from Hewson, 2003)

**Figure 2.1: Common deviator supports**

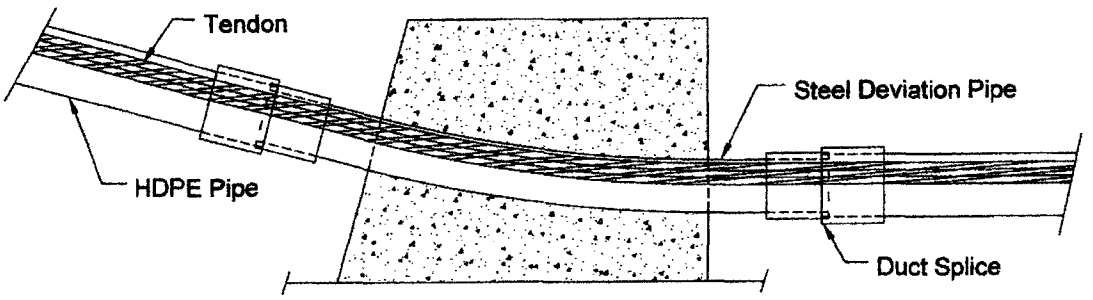


(a) Bent-steel pipe deviator with discontinuous HDPE sheathing

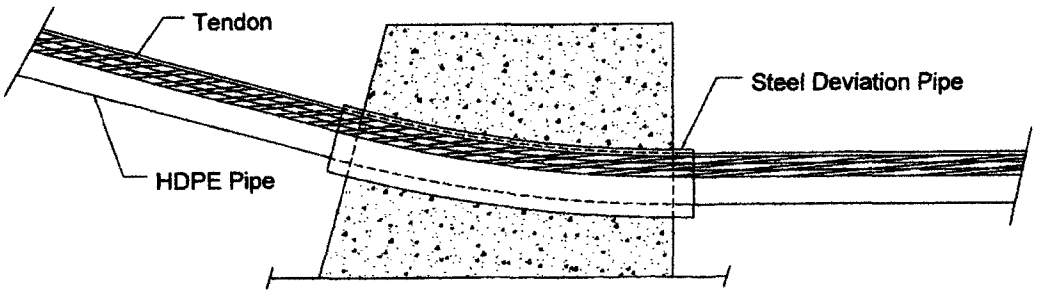


(b) Bent-steel pipe deviator with continuous HDPE sheathing

**Figure 2.2: Common types of deviators**

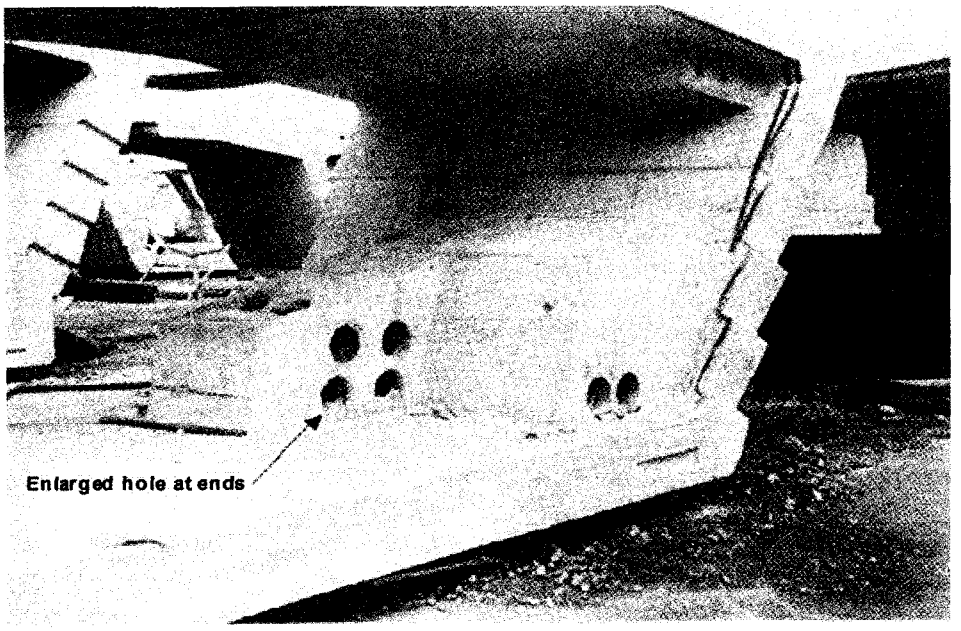


(c) Deviators formed within deviator supports (adapted from Hewson, 2003)

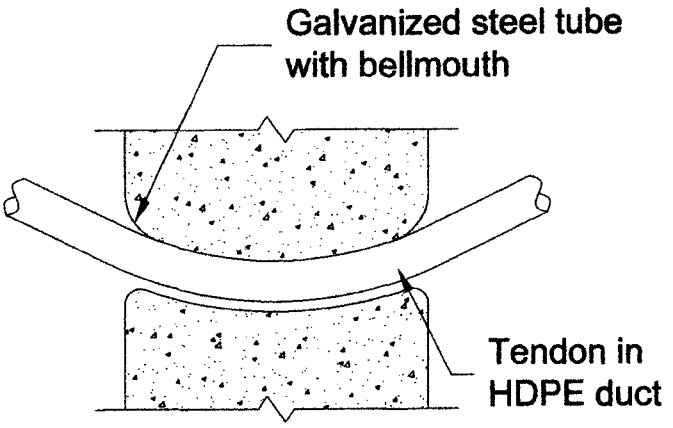


(d) Deviator with bell-mouth configuration

**Figure 2.2: (Cont'd)**

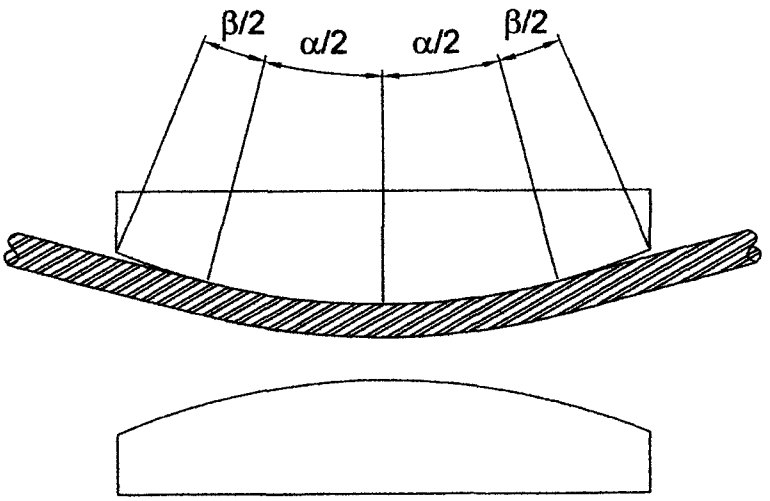


**Figure 2.3: Bell-shaped deviator profile**

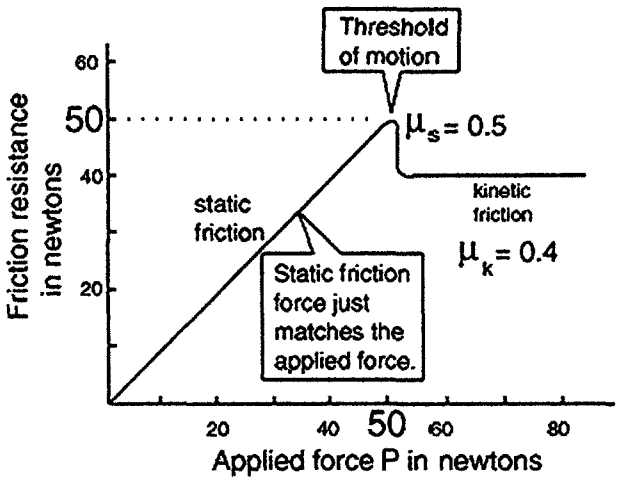


**Figure 2.4: General relationship of applied force and friction force (adapted from Nave)**

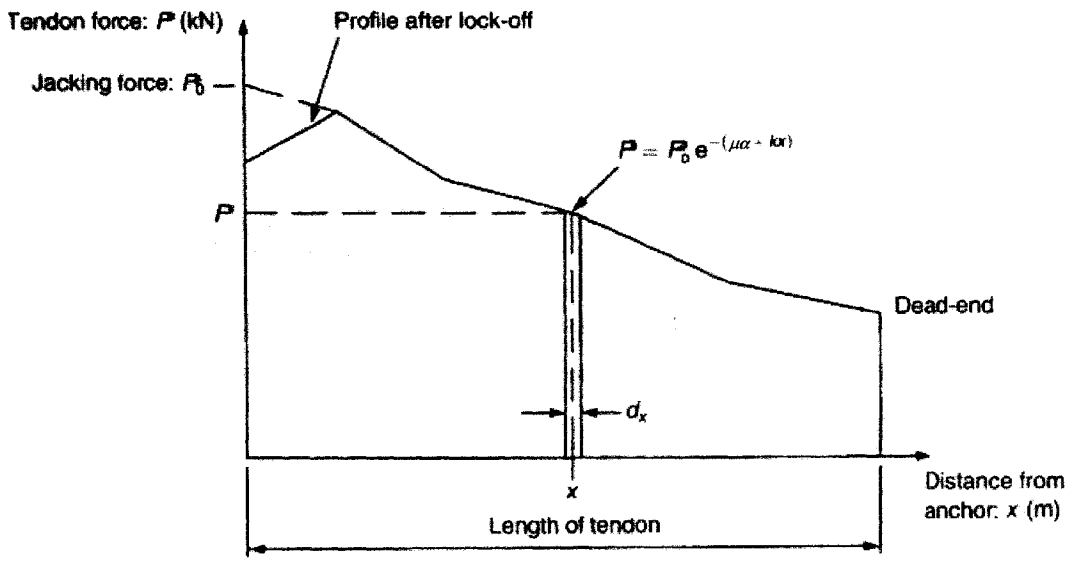


**Figure 2.5: Tendon force over the length of the tendon considering losses due to friction and anchorage seating (adapted from Hewson, 2003)**

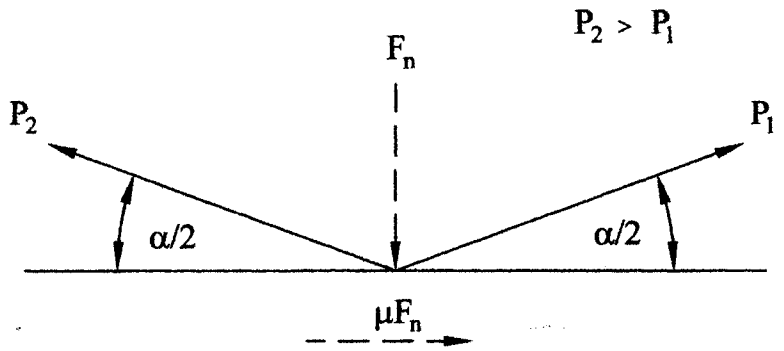


**Figure 2.6: Deviator forces**

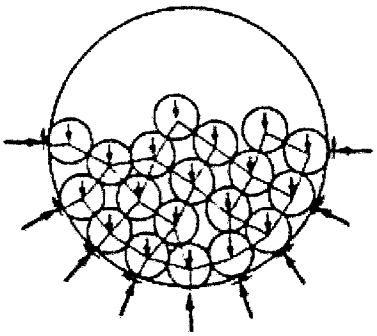

**Figure 2.7: Lateral forces acting at deviator (adapted from Rogowsky and Marti, 1991)**

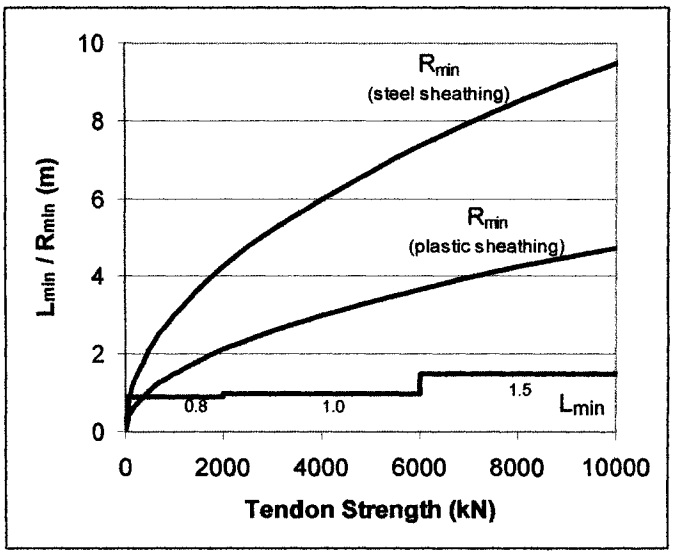


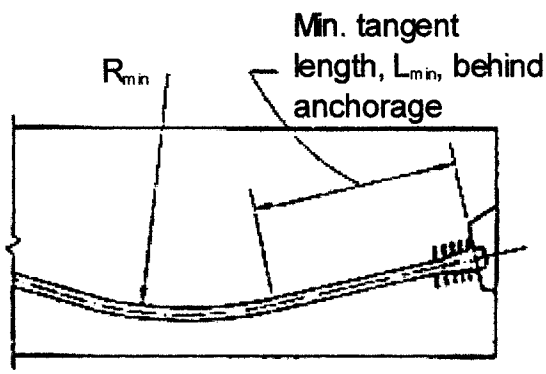


**Figure 2.8: Minimum radii of tendon curvature and minimum tendon tangent lengths (adapted from Rogowsky and Marti, 1991)**

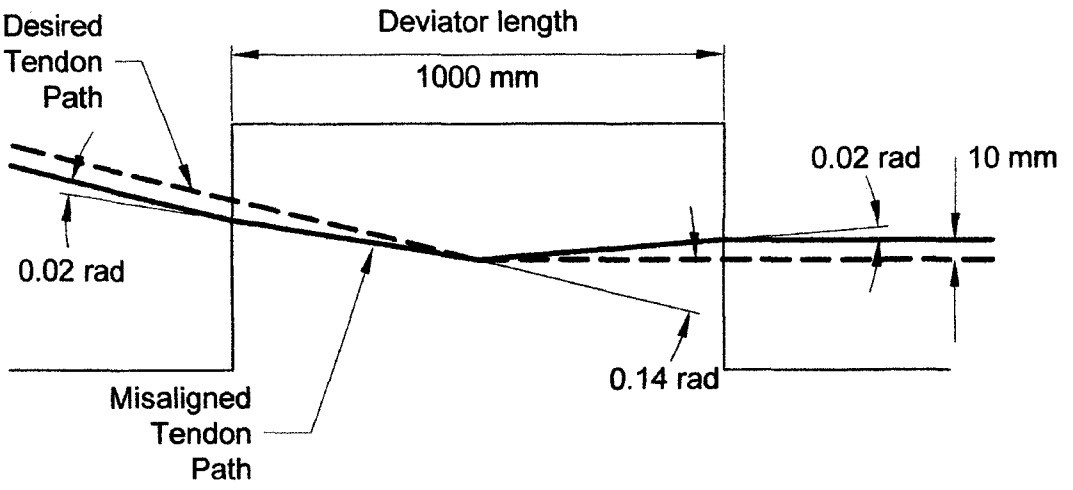


**Figure 2.9: Effect of deviator duct misalignment**

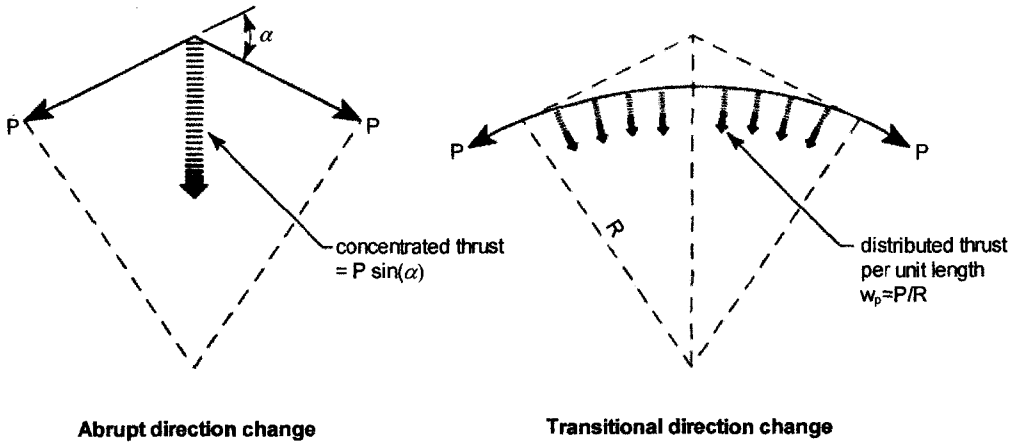


**Figure 2.10: Forces due to tendon deviation (adapted from CAN/CSA S6-00, 2000)**

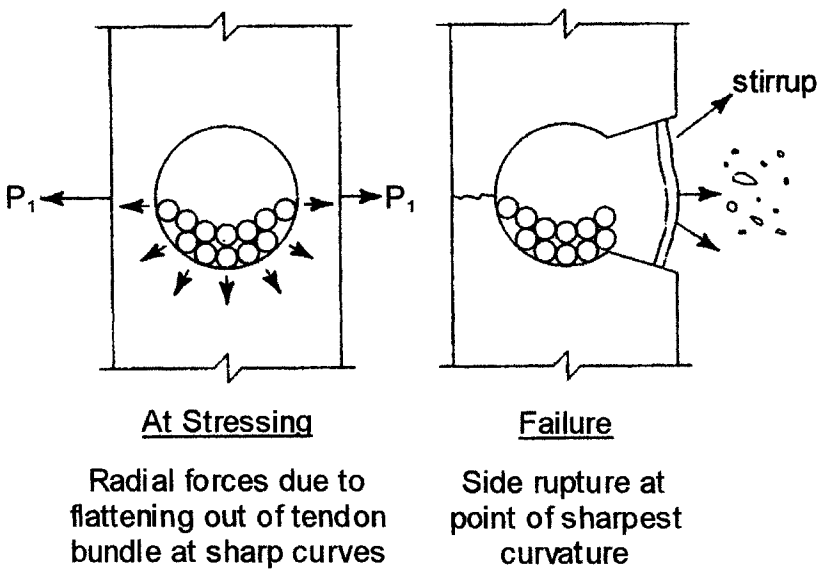


**Figure 2.11: Forces due to strand bunching (adapted from CAN/CSA S6.1-00, 2001)**

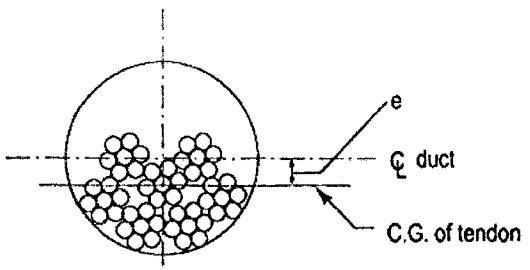


| Duct Diameter | e |
|---|---|
| 75 mm or less | 12 mm |
| over 75 mm to 100 mm | 20 mm |
| over 100 mm | 25 mm |

**Figure 2.12: Tendon eccentricity at deviation points (adapted from CAN/CSA S6-00, 2000)**

# 3 EXPERIMENTAL PROGRAM

## 3.1 INTRODUCTION

The objective of the experimental program was to investigate the behaviour of the composite diablo deviator. The "diablo" deviator is a deviator with a bell-shaped interior void through which a prestressing tendon is placed (see Figure 3.1). Diablo deviators with internal radius of curvatures of 1.5m and 4.5m were tested. The 1.5m radius was based on the Rogowsky and Marti (1991) recommendation that the minimum radius of curvature of plastic sheathed external tendons be

$$R_{\min} = 1.5\sqrt{P_u / 1000} \qquad \text{(Eq. 3.1)}$$

For the tendons tested, $P_u$ = 756 kN, and $R_{min}$ = 1.31 m. The radius of curvature for the smaller deviators was set at 1.5 m. Practical limitations in the laboratory restricted tendon size to 756 kN breaking load. The 4.5 m radius was considered sufficiently larger than 1.5 m for comparison. The deviators were designed as precast composite members, with an exterior steel pipe and a grout interior. The reason for the steel pipe was to allow the deviation to be connected to steel diaphragms or steel structures, as well as embedment in concrete diaphragms. The throat of the deviator was sized to allow passage of a continuous plastic sheath through the deviator. The bell shapes were proportioned to accommodate a wide range of deviation angles with a single design. This avoids the need to produce different components every time the tendon deviation angle changes.

As noted in the literature review, friction in the deviator can have an effect on the load carrying capacity of an external post-tensioning system. In addition, the desired failure mechanism for a deviated tendon is for the strand to exhibit overall yielding before the deviator or tendon fails. Thus, experiments were designed to examine friction characteristics at the deviator, deviator behaviour during stressing, and tendon behaviour under ultimate loading. The data collected from the experiments was used to validate a design concept for the deviators, as well as to gain information on and develop design recommendations for the deviators.

Four specimens were tested. Two of these specimens were deviators with an interior radius of curvature of 1500 mm. The other two specimens had an interior radius of curvature of 4500 mm. All tendons consisted of four 13 mm prestressing 7-wire strands, undergoing an angle change of approximately 0.14 rad (8°) at the deviator.

Each deviator had two sequential sets of tests performed on it. The first set of tests investigated the friction coefficient between the tendon and the sheathing at various load levels. It was assumed throughout these tests that the friction force between the deviator grout interior and tendon sheathing was larger than that between the tendon and its sheathing and thus, the sheathing would not be moving through the deviator. In addition, the strands in the tendon were assumed to move together as a unit, with no relative motion allowed. The test was designed to have the tendon shift back and forth through the deviator. The friction coefficient was determined from

measurements of the tendon force on each side of the deviator during each tendon shift.

The second set of tests brought the tendon to failure while strand and deviator behaviour were monitored. These tests were designed such that the tendon was pulled with approximately equal forces at each of its ends. Based on this condition, friction forces through the deviator would be negligible and the tensile force in each strand is considered constant along the tendon length. The load in the tendon was increased until failure, with the behaviour of the tendon and the deviator monitored throughout loading.

After the above two sets of tests were performed on the deviators, it was noted that there was no apparent damage to the deviators. New tendons were installed and an additional set of friction and failure tests were then performed on one deviator of each size; thus, a total of six tests were performed on deviators.

In addition to these tests, two control tests were performed in which four strand undeviated tendons were stressed to failure. The results from the control tests were compared to those from the failure tests to examine the effect of the deviator on tendon behaviour.

A description of each test specimen, the material properties, the test set-up, the instrumentation, and the test procedure are presented in the following sections.

## 3.2 TEST SPECIMENS

### 3.2.1 DEVIATOR DESIGNATION

The four deviators tested consisted of two deviators with an interior radius of curvature of 1500 mm and two deviators with an interior radius of curvature of 4500 mm. The smaller deviators were designated as Deviators 1500A and 1500B and the larger deviators were designated as Deviators 4500A and 4500B. When the deviators were used for a second set of tests with new tendons, they were designated as Deviators 1500A2 and 4500A2.

### 3.2.2 DETAILS OF SPECIMENS

Figure 3.2 shows the design specifications for the deviators. The deviators were designed to have four 13 mm diameter 7-wire prestressing strands undergo an angle change of 0.14 rad (8°) at the deviator. In practice, tendon deviation angles are typically less than 0.13 rad (7.2°) and are rarely, if more, greater than the 0.14 rad. The deviator was designed for a 0.14 rad tendon angle change and an additional 0.04 rad (2.3°) angle tolerance for alignment errors.

The exterior of the deviator is steel pipe, chosen to be in accordance with the bent-steel pipe requirements stipulated by CAN/CSA S6-00 (2000) and AASHTO LRFD (2000). The pipe sizes are DN 125 for Deviators 1500A and 1500B and DN 150 for Deviators 4500A and 4500B. The dimensions of the pipe can be seen in Figure 3.2.

The flared hole through the deviator was formed with a diablo shaped insert, which was removed after the grout hardened. The insert separated in the middle and was removed from each end of the deviator. Sizing of the diameter of the deviators was based on having a minimum throat diameter of 60 mm and a minimum grout thickness of 25 mm. High-density polyethylene pipe was used to sheath the tendon through the deviator. The 60 mm minimum deviator throat diameter was sufficiently large for the sheathing of the four strands to pass through. While thinner pipe walls could have been used, standard pipe was used for practical convenience.

The deviators were cast into concrete supports to hold and position the deviators during testing. The supports were 142 mm wide and located at midspan of the deviator. It was judged that this would be the minimum support length that one could use in practice. Thus, it gives the longest cantilever lengths for the deviators. Schematics of the deviators and supports can be seen in Figure 3.3.

## 3.3 Materials and Material Properties

### 3.3.1 Diablo Deviator

The deviator was a composite member, consisting of an exterior steel pipe and a grout interior. The exterior steel pipe had specified yield and tensile strengths of 240 MPa and 415 MPa, respectively. For purpose of analysis, a modulus of elasticity of 200,000 MPa was assumed.

100 x 200 mm grout cylinders were cast at the same time and from the same grout batch as the deviators. Four compression tests were performed on these cylinders in accordance with ASTM Standard C39. The modulus of elasticity of the grout was 28,750 MPa. The compression strength of the grout was 61.0 MPa.

All deviators were cast by Con-force Structures Limited at its Calgary, Alberta precast plant.

### 3.3.2 PRESTRESSING STRANDS

Four 13 mm diameter seven-wire prestressing strands were used in each test. The measured properties of these strands are shown in Table 3.1.

The actual diameter of the strands was determined from the average of 10 measurements of the strand diameter, wire crown to wire crown, made with callipers. The diameter of each wire was calculated from an average of 36 king wire diameter readings and 36 diameter readings for each outer wire (total of 216 outer wire readings), also made with callipers. From these values, the area of each wire was computed, the sum of which became the overall strand area.

The strength of the strand was determined from three tensile tests performed with an MTS 1000 universal testing machine, in accordance with ASTM Standard A370-02. The strands were loaded at a stroke rate of 3 mm per minute, with the MTS 1000 reading the load applied to the strand (in kN) and an extensometer reading the

elongation of the strands (in mm) over an extensometer gauge length of approximately 590 mm. From the data collected, a Ramberg-Osgood function, as reported by Collins and Mitchell (1987), was fitted to the data to mathematically define a curve for the stress-strain relationship in the strand. The resulting equation for stress in the strand was:

$$f_p = 193700\varepsilon_{ps}\left\{0.0196 + \frac{1-0.0196}{\left[1+\left(110.7\varepsilon_{ps}\right)^{8.52}\right]^{1/8.52}}\right\} \le 1917.4\,\text{MPa} \qquad \textbf{(Eq. 3.2)}$$

where $f_p$ and $\varepsilon_{ps}$ are the stress and strain in the tendon, respectively. This formulation, as shown in

Figure 3.4 defines the typical stress-strain relationship for the prestressing strands used.

### 3.3.3 SHEATHING

Plastic sheathing for the strands was supplied in accordance with the requirements of CAN/CSA S6-00 (2000). The sheathing was high-density polyethylene pipe with a size designation of IPS 1.5" DR11 (1.5 inch inside diameter and wall thickness of 0.173 inch). The sheathing had an actual outside diameter of 48.1 mm and wall thickness of 4.7 mm. These values are the average of 6 measurements of the sheathing diameters. The pipe conformed to ASTM D3350 with Material Designation Code PE3408.

### 3.3.4 WEDGE CHUCKS

Two types of wedge chucks were employed in the testing. The first type of wedge chuck was a multi-use wedge chuck. The second type of wedge chuck used was a single use wedge chuck. In preliminary tests with both wedge chucks, prestressing strands were stressed to more than $0.95f_{pu}$ and strand strains up to approximately 25000 με were achieved. With preliminary testing on both types of wedge chucks, it was found that considerable effort and attention to details of the wedge installation was required to obtain consistent and high anchorage hardware efficiency. The high efficiency was required so that the influence of the deviator on the breaking load of the deviated tendon could be isolated with no losses in the anchorage interfering with the test results.

### 3.3.5 DEVIATOR SUPPORTS

Figure 3.3 shows a typical deviator support with deviator. The mix design for the concrete had a specified strength of 30MPa. All deviator supports were cast in the structural laboratory at the University of Alberta. The actual strength and modulus of elasticity of the concrete were 32.6MPa and 22,800MPa respectively.

The deviator support was reinforced with 6 mm diameter and 10M steel reinforcement, as shown in Figure 3.3(c). The steel had a specified strength of 400 MPa.

## 3.4 TEST SET-UP

### 3.4.1 CONTROL TESTS

Figure 3.5 shows a typical test set up for the control tests. Four prestressing strands were stressed in the test frame. The strands were situated 44 mm apart at the wedge chucks, as seen in Figure 3.6. A tension plate was placed along the strands to simulate the angle changes that occurred in the friction and failure tests.

Two 100-ton centre hole rams at the test frame ends applied load to the prestressing strands. The strands were separated by wooden separator plates and then converged to tension plates at each tendon end. The separator plates ensured that the strands were parallel as they entered the wedge chuck in order to preserve the efficiency of the wedge chucks. The tension plates brought the strands to a spacing that would occur in practice with typical multistrand tendons. The breaking force obtained in the control tests established the undeviated tendon strength with the materials and equipment used. The results are shown in Table 3.2.

### 3.4.2 FRICTION AND FAILURE TESTS

A schematic of a typical test set-up can be seen in Figure 3.7. The test specimens were placed in the concrete test frame as shown in Figure 3.8. The deviator was supported in the frame by the concrete deviator support. To inhibit movement of the deviator, the deviator support was braced vertically and along the length of the test frame as shown in Figure 3.9.

Four 13 mm diameter 7-wire strands passed through the deviator, undergoing an overall angle change of 0.12 rad to 0.14 rad. Variation in the angle change existed due to placement of the deviator (see Table 3.3 for actual tendon angle changes in each test). Polyethylene tubing sheathed the tendons along the portion passing through the deviator.

The tendons were stressed with 100-ton centre hole rams at each end of the test frame. The centre hole rams pressed against bearing plates (Bearing Plate 1 in Figure 3.7), which in turn transferred the load into the concrete test frame. The strands were once again situated 44 mm apart at the wedge chucks. The strands were separated by wooden separator plates and then converged to the tension plate. From the tension plate, the strands continued to merge towards the deviator and were fully converged as they entered the deviator.

The double acting rams were connected with a hydraulic hose configuration (Figure 3.10) that allowed independent or simultaneous ram operation. The rams were operated simultaneously under stroke control to tension the tendon to the desired load. One ram could then be stroked out while the other ram simultaneously retracted, thus maintaining a constant average load while moving the tendon. Such control over the movement in the tendon, while maintaining a constant load, was particularly important in the friction portion of the tests.

High-density polyethylene tubing was placed through the deviator, acting as the tendon sheathing. Thus, there was contact in the deviator between the polyethylene tubing and prestress strands, as well as between the deviator grout surface and the polyethylene tubing.

## 3.5 INSTRUMENTATION[NR18]

Two 100-ton centre hole rams were used in the stressing of the tendon. The pressure in each ram was monitored by both electronic pressure gauges and dial gauges. The electronic pressure gauges were situated between the hoses and rams, while the dial gauge readings were taken at the hydraulic pump. Prior to testing, each ram was calibrated in a universal testing machine to determine the load-pressure relationship for each ram. The electronic pressure gauges, once calibrated to read load, read to an accuracy of ±1.8 kN. The mechanical dial pressure gauges were used to provide an independent check on the electronic readings. The mechanical pressure gauges were read to an accuracy of ±50 psi (0.346 MPa). With an effective ram piston area of 20.6 $in^2$ (13,300 $mm^2$) and 13.5 $in^2$ (8710 $mm^2$) for the extension and retraction piston ends respectively, this translates to a reading accuracy of ±4.6 kN and ±3.0 kN in tendon force.

For more precise measurements of the force in the tendon, the strands were strain gauged. For all tests except the 1500A2 and 4500A2 series, four strain gauges were placed on each strand (two on each end of the strand). The strain gauges were placed on opposite sides of the strand to allow compensation for bending effects. The strain

gauges used read to a maximum of approximately 20,000 με with 1% accuracy. After the strands were strain gauged, the strands were individually tensioned up to 70% $f_{pu}$ and calibrated with a load cell. This was done because the strain gauges were placed parallel to the axis of the outer wire rather than parallel to the axis of the strand.

Deviator strains and deformations were measured. Strain gauges were placed on the deviator as shown in Figure 3.3 to measure the longitudinal strain in the steel pipe. The strain gauges read up to approximately 20000 με with 1% accuracy. Two LVDTs were used, as shown in Figure 3.11 to measure the vertical deflection of the deviator. These LVDTs were placed within 3 mm of the outermost ends of the deviator. The LVDT at the north end of the deviator read to an accuracy of 0.010 mm, while that on the south end of the deviator read to an accuracy of 0.005 mm. Both LVDTs read up to 25 mm. In addition, a calliper was used to manually measure the horizontal diameters of the R4500 deviators at various points. The deviator was marked along the horizontal length of the deviator at distances of 10 mm, 150 mm, and 300 mm from the deviator support face, as shown in Figure 3.3, at which points the deviator diameters were measured. The callipers used read to an accuracy of 0.02 mm and up to 450 mm.

Movement of the tendon ends and of the tendon relative to the deviator were measured. LVDTs were placed on the ends of each strand as shown in Figure 3.7. These LVDTs were used to measure the elongation of each strand in the tendon. The

initial length of each strand, wedge to wedge, was measured with an accuracy of 10 mm. From the elongations and initial length of the strand, the strain in each strand was determined. The LVDTs measured to an accuracy of 1.0 mm and up to 75 mm. In addition to the LVDTs at the strand ends, LVDTs were used to measure the stroke on each ram. These latter LVDTs read up to 75 mm with an accuracy of 0.3 mm. For the friction tests, another LVDT was placed between the deviator and the tendon. This LVDT was used to detect any relative movement between the tendon and the deviator and read up to 75 mm with an accuracy of 0.3 mm. Its location is shown in Figure 3.7 (LVDT 4). Figure 3.12 shows a photograph of the LVDT and its connection to the tendon. All LVDTs were calibrated before and after testing was completed. The accuracies stated are from those calibrations.

A FLUKE data acquisition system was used throughout the tests. All instruments were calibrated with this system before and after testing. The data acquisition system recorded readings for pressure in the rams, wire strains in the strands, and strains in the deviators. In addition, it recorded LVDT readings for the elongation in the strands, the deflection of the deviators, the ram strokes, and the relative movement between the tendon and the deviator.

## 3.6 Test Procedure

### 3.6.1 Overview

Prior to the testing of any of the deviators, two control failure tests on undeviated tendons were performed. Each deviator had two sequential sets of tests performed on

it. The first set of tests was the friction tests. The second set of tests was the failure test, in which the tendon was stressed until failure.

### 3.6.2 Test Designations

The control tests are referred to as Control Test 1 and Control Test 2.

The friction tests are referenced by deviator specimen (1500A, 1500B, 1500A2, 4500A, 4500B, or 4500A2), load level (friction tests were performed at 50%, 60%, and 70% $f_{pu}$), and test methodology employed in the test (two procedures, referred to as A and B, were employed for ascertaining friction values). For example, for friction tests on Deviator 1500A at a load level of 60% using method B, the test is referred to as Test 1500A-60%B.

The failure tests are referenced by deviator specimen, followed by the word "Ultimate". For example, the failure test on Deviator 1500A is referred to as Test 4500A-Ultimate.

### 3.6.3 Control Failure Test

The tendon was stressed to 50% $f_{pu}$ to lock the wedge chucks in place and the load was subsequently released. Once the wedges were locked, individual strands were shimmed to achieve approximately equal load and strain in all strands. Both rams were simultaneously stroked at a tendon elongation rate of approximately 6 mm per minute until a wire failed in a strand (indicated by a loud snapping sound). Testing

was briefly paused to ensure the test was safe and equipment was in working order. Stroking was then resumed until a second wire failed, after which the load was removed from the system by simultaneously releasing the pressure in each ram. This marked the end of the test. The data acquisition system took readings at 1.5 second intervals throughout the testing. The locations of the wire breaks were determined when the test was disassembled.

### 3.6.4 FRICTION TESTS

Before any stressing of the tendon, each ram was extended at least 75 mm. The tendon was then stressed to approximately $0.50f_{pu}$ to lock the strands in their wedges. The load was then removed from the system by simultaneously releasing the pressure in both rams. Shims were then placed under strand wedge chucks to equalize the load and strain in each strand.

For each load level (50%, 60%, or 70% $f_{pu}$), the friction tests were performed as follows. Both rams were simultaneously stroked to increase the load to a specified load level, with measurements being taken by the data acquisition system. Testing was paused once the load level was achieved, during which time an LVDT was installed to measure the movement of the tendon through the deviator (see Figure 3.12). The stationary end of the LVDT was attached to the test frame, extended upward to be parallel with the tendon. The moving end of the LVDT was attached to a hose clamp on one of the strands, located a short distance (0-75 mm) from the deviator end.

The outsides of all the strands at a specific point were match marked to ensure the assumption that the strands moved as a unit was valid. In addition, the sheathing was also marked at the deviator face to validate the assumption that the friction partners are the sheathing and the tendon and the sheathing, therefore, would not move through the deviator.

With the data acquisition system taking incremental readings, the tendon was then moved (shifted) through the deviator for a specified distance. This movement was done by pumping oil into the retraction valve of one ram with the release to the opposite ram's retraction valve open, all while the release to both rams' stroke ends were closed. For example, to simultaneously extend the north ram and retract the south ram, oil would be pumped into the retraction end of the south ram and released from the retraction end of the north ram. Once the tendon moved the desired distance, testing was paused. Testing resumed after a few minutes as the tendon was shifted again in the north-south direction. The shifting of the tendon was performed in two ways. The first procedure, Method A, involved moving the tendon back and forth, north to south to north, etc., with pauses between changes in tendon movement direction. The second method, Method B, involved movements in the same direction at least three times in a row, with pauses between every shift. Table A.1 to Table A.6 in Appendix A list the shifting sequence and distances the tendon was shifted for each test).

### 3.6.5 Failure Tests

Following the friction tests, the failure tests were performed. Both rams were simultaneously stroked at a tendon elongation rate of approximately 6 mm per minute until a wire failed in a strand (indicated by a loud snapping sound). Testing was briefly paused to ensure the test was safe and equipment was in working order. The loading resumed until a second strand wire failed, after which the load was removed from the system by simultaneously releasing the pressure in the rams. This marked the end of the test. The data acquisition system took readings at 1.5 second intervals throughout the testing. The locations of the wire breaks were determined when the test was disassembled.

## 3.7 Test Results

Test results are presented in Table 3.4 to Table 3.5. Table 3.4 shows the average load level, the tendon angle changes, and the average load differences between the north and south ends of the tendons in the friction tests. Table 3.2 provides a summary of the most important data from the failure tests: the ultimate loads and tendon elongations, where the tendon broke, as well as the maximum deflections and strains in the deviators. Table 3.5 presents the diameter measurements for tests 4500A and 4500A2.

Analysis and discussion of the test results are presented in Chapter 4.

**Table 3.1: Measured strand properties**

| | Measured Value |
|---|---|
| Average Strand Diameter (mm) | 12.81 |
| Computed Strand Cross-Sectional Area ($mm^2$) | 98.7 |
| Ultimate Strength (MPa) | 1920 |
| Modulus of Elasticity (MPa) | 193700 |
| Average Outside Wire Diameter (mm) | 4.21 |
| King Wire Diameter (mm) | 4.38 |

**Table 3.2: Failure test data**

| Test | Wires Broken | Break Location | Tendon Load (kN) | Tendon Elongation (mm) | Tendon Initial Length (mm) | Max. Deviator Deflection (mm) | | Max. Deviator Strain (με) | | | | | | | |
|---|---|---|---|---|---|---|---|---|---|---|---|---|---|---|---|
| | | | | | | North | South | Top N20 | Top N40 | Top S20 | Top S40 | Bot N20 | Bot N40 | Bot S20 | Bot S40 |
| Control 1 | Break 1 | Wedge | 742.3 | 126.5 | 4807 | – | – | – | – | – | – | – | – | – | – |
| | Break 2 | Wedge | 722.1 | 148.8 | 4807 | – | – | – | – | – | – | – | – | – | – |
| Control 2 | Break 1 | Wedge | 740.4 | 132.7 | 4789 | – | – | – | – | – | – | – | – | – | – |
| | Break 2 | Wedge | 728.4 | 155.0 | 4789 | – | – | – | – | – | – | – | – | – | – |
| 1500A | Break 1 | Wedge | 732.2 | 94.6 | 4412 | – | – | 4 | – | 6 | – | 77 | – | – | – |
| 1500B | Break 1 | Wedge | 745.3 | 139.0 | 4815 | 18.5 | 6.9 | 1 | – | 6 | – | – | – | 25 | – |
| | Break 2 | Wedge | 720.5 | 145.6 | 4815 | 16.1 | 7.1 | 1 | – | 6 | – | – | – | 27 | – |
| 1500A2 | Break 1 | Wedge | 732.5 | 100.2 | 4853 | 6.3 | 4.0 | 2 | – | 5 | – | 60 | – | 12 | – |
| | Break 2 | Wedge | 712.0 | 105.4 | 4853 | 3.6 | 4.0 | 3 | – | 4 | – | 60 | – | 16 | – |
| 4500A | Break 1 | Wedge | 717.8 | 72.9 | 4795 | 53.3 | – | 132 | 106 | 102 | 83 | 143 | – | 79 | 42 |
| | Break 2 | Wedge | 720.2 | 127.1 | 4795 | 48.5 | – | 132 | 106 | 102 | 83 | 147 | – | 84 | 42 |
| 4500B | Break 1 | Wedge | 662.6 | 46.4 | 4818 | 42.8 | 14.6 | 121 | – | – | – | 111 | 91 | – | – |
| | Break 2 | Wedge | 669.2 | 52.6 | 4818 | 33.6 | 14.4 | 127 | – | – | – | 122 | 94 | – | – |
| | Break 3 | Wedge | 675.5 | 70.2 | 4818 | – | – | 129 | – | – | – | 119 | 95 | – | – |
| 4500A2 | Break 1 | Wedge | 735.4 | 107.2 | 4817 | – | 15.6 | 133 | 97 | 126 | – | 123 | 59 | 91 | – |
| | Break 2 | Wedge | 707.9 | 114.2 | 4817 | – | 15.5 | 137 | 98 | 129 | – | 122 | 60 | 93 | – |

Notes: 1) N20 and N40 measured 20 mm and 40 mm north of the deviator support face respectively. S20 and S40 measured 20 mm and 40 mm south of the deviator support face respectively.

2) Test values listed are the average of 3 measurements with one standard deviation, varying from 0.00 mm to 0.27 mm.

**Table 3.3: Tendon angle changes**

| Test Series | Tendon Angle Change |
|---|---|
| 1500A | 0.121 rad ± 0.005 rad |
| 1500B | 0.130 rad ± 0.005 rad |
| 1500A2 | 0.128 rad ± 0.004 rad |
| 4500A | 0.128 rad ± 0.005 rad |
| 4500B | 0.140 rad ± 0.006 rad |
| 4500A2 | 0.128 rad ± 0.005 rad |

Note: Angle accuracies listed are one standard deviation

**Table 3.4: Friction test data**

| Test | Ave. Load Level (kN) | Ave. Press. at Retraction end of Ram (psi) | $\alpha$ (radians) |
|---|---|---|---|
| R1500A-60% | 476.5 | 401 | 0.121 |
| R1500B-50% | 388.7 | 338 | 0.130 |
| R1500B-60% | 470.5 | 374 | 0.130 |
| R1500B-70% | 554.8 | 401 | 0.130 |
| R1500A2-50% | 384.3 | 383 | 0.128 |
| R1500A2-60% | 473.9 | 354 | 0.128 |
| R1500A2-70% | 543.9 | 426 | 0.128 |
| R4500A-50% | 382.8 | 391 | 0.128 |
| R4500A-60% | 470.5 | 421 | 0.128 |
| R4500A-70% | 542.3 | 467 | 0.128 |
| R4500B-60% | 473.1 | 374 | 0.140 |
| R4500A2-50% | 383.5 | 323 | 0.128 |
| R4500A2-60% | 469.2 | 401 | 0.128 |
| R4500A2-70% | 544.8 | | 0.128 |

**Table 3.5: Horizontal diameter measurements of deviators**

| | Test No. | Load (kN) | Dia. N1 (mm) | Dia. N2 (mm) | Dia. N3 (mm) | Dia. S1 (mm) | Dia. S2 (mm) | Dia. S3 (mm) |
|---|---|---|---|---|---|---|---|---|
| No load | 4500A | 0 | 158.62 | 158.66 | 158.33 | 159.47 | 159.08 | 158.65 |
| | 4500A2 | 0 | 158.48 | 158.53 | 158.67 | 158.28 | 158.41 | 158.84 |
| Under load | 4500A | 546 | 158.8 | 158.77 | 158.42 | 159.47 | 159.11 | 158.18 |
| | 4500A2 | 558 | 158.847 | 158.74 | 158.91 | 158.35 | 158.45 | 158.75 |

Note: N1, N2, and N3 measured 10 mm, 150 mm, and 300 mm north of the deviator support face respectively. S1, S2, and S3 measured 10 mm, 150 mm, and 300 mm south of the deviator support face respectively.

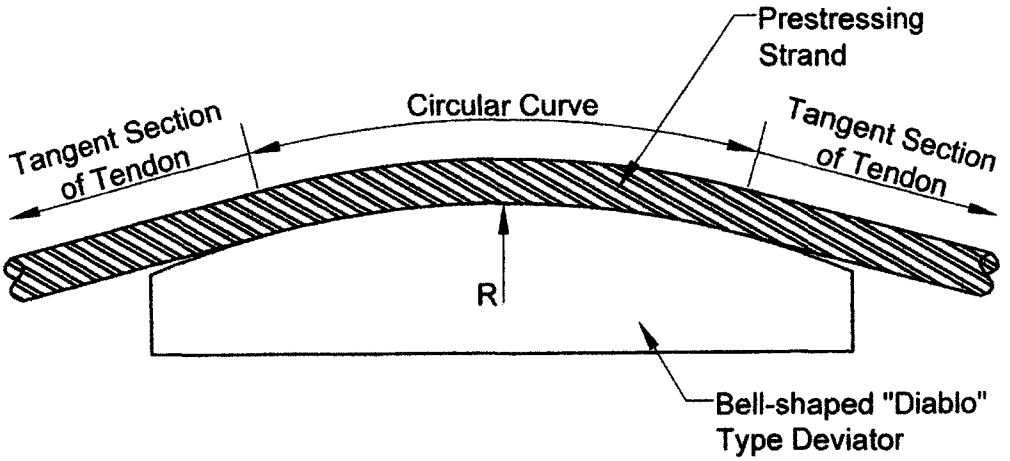


**Figure 3.1: Deviation of prestressing strand with "diablo" type deviator**

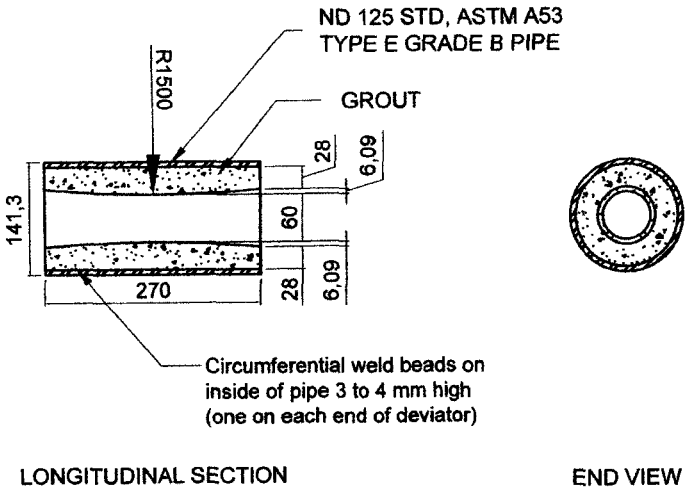


(a) Diablo with 1500 mm radius

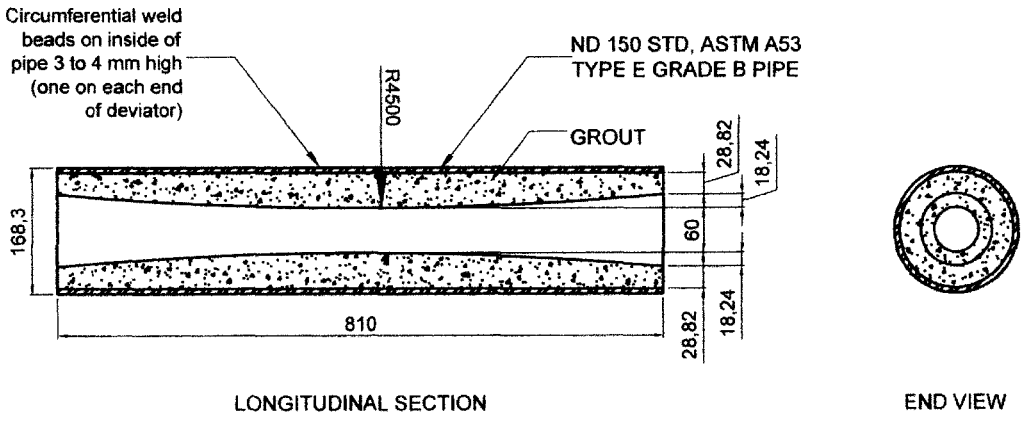


(b) Diablo with 4500 mm radius

**Figure 3.2: Diablo deviator test specimens**

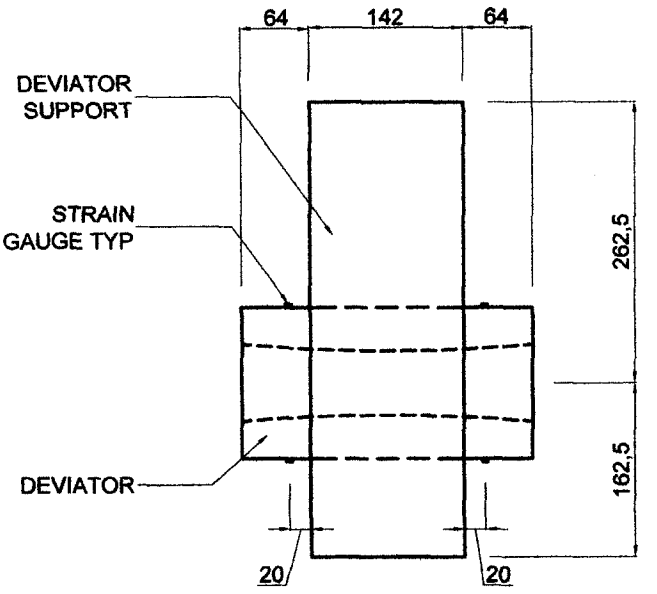


(a) Diablo with 1500 mm radius

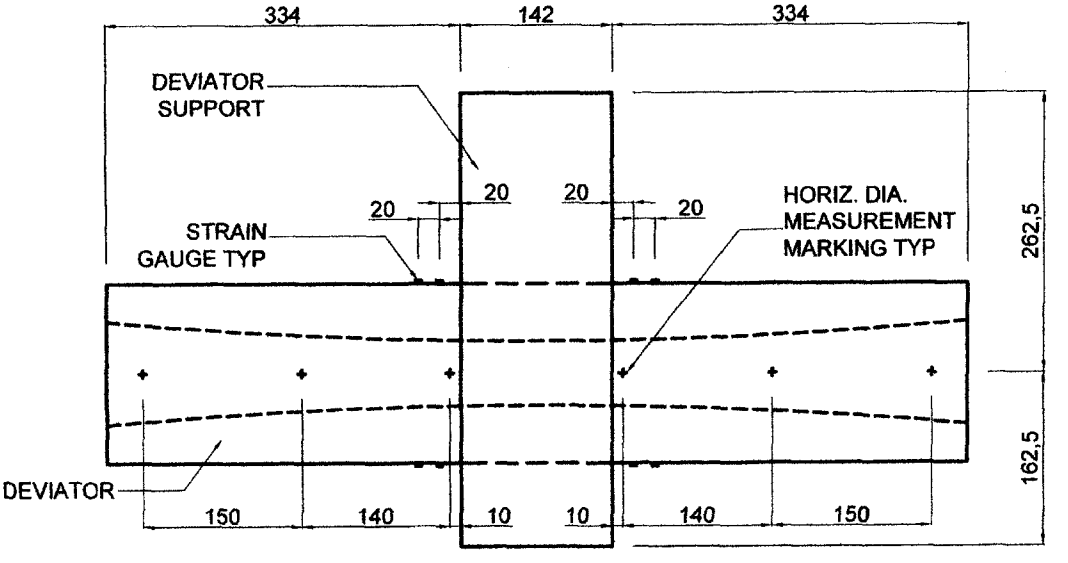


(b) Diablo with 4500 mm radius

**Figure 3.3: Deviators in concrete supports**

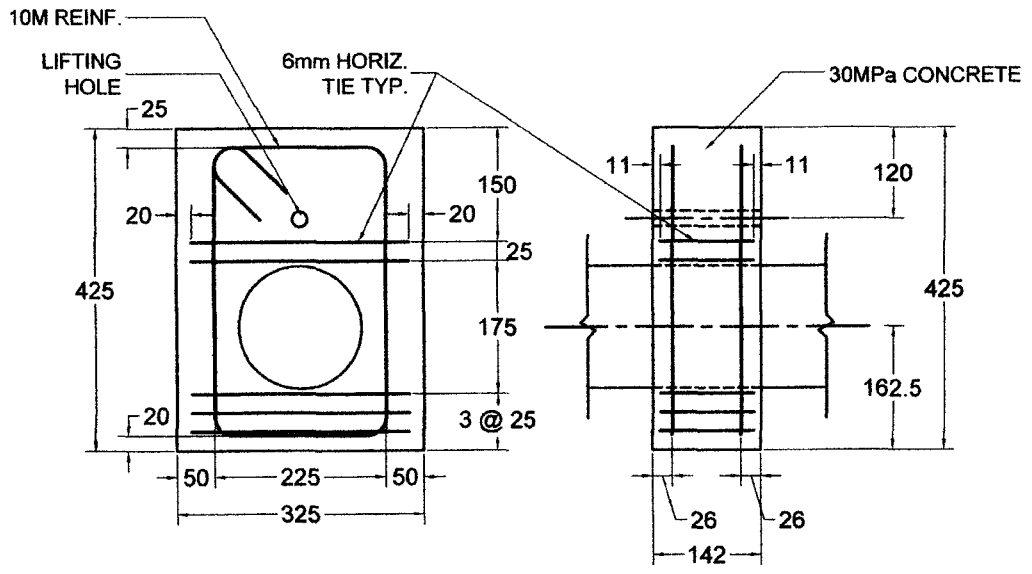


(c) Deviator Support Detailing

**Figure 3.3: (Cont'd)**

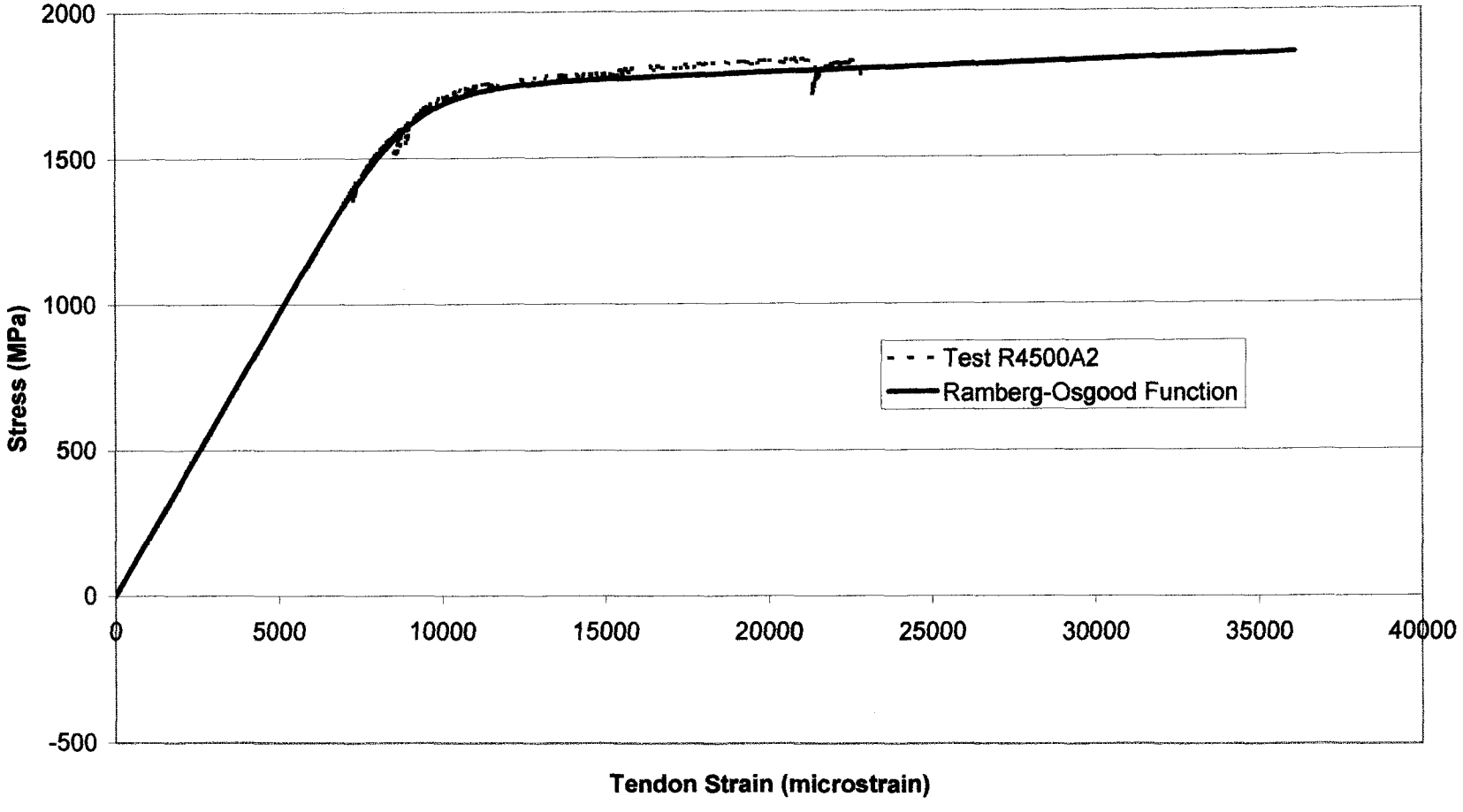


**Figure 3.4: Typical stress vs. strain relationship for prestressing strand**

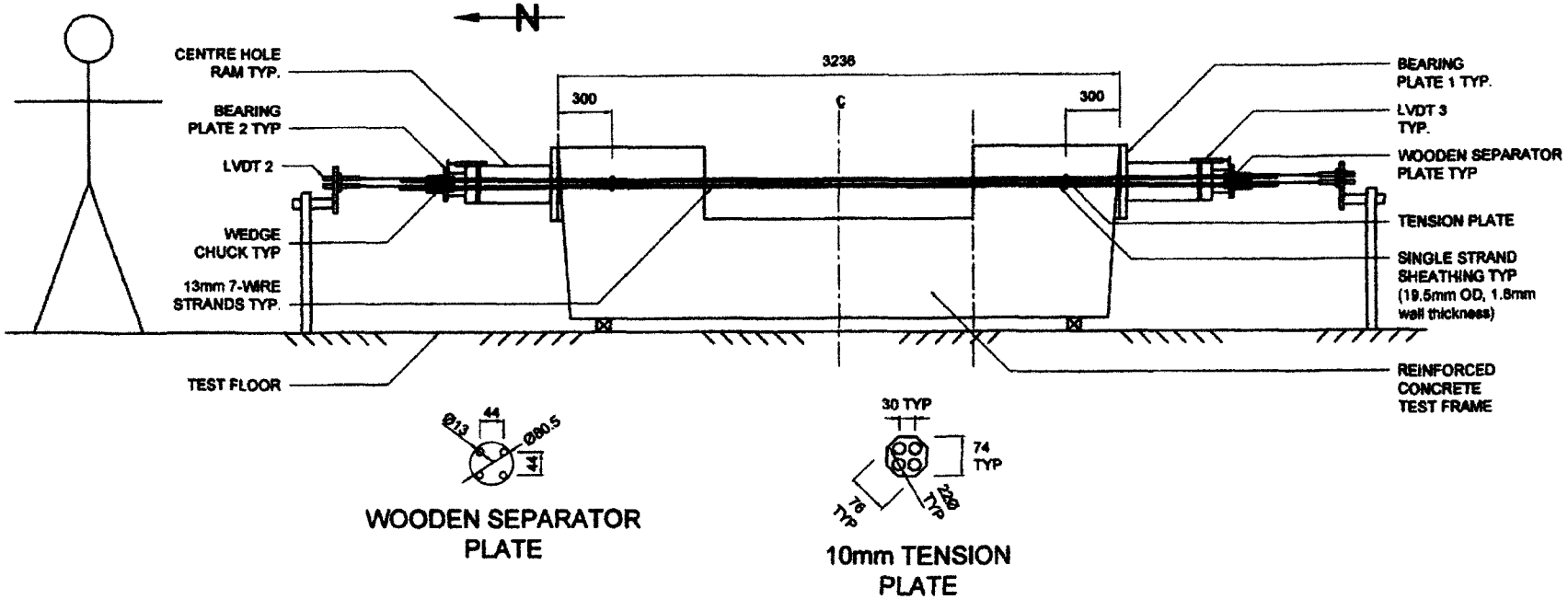


**Figure 3.5: Control test set-up**

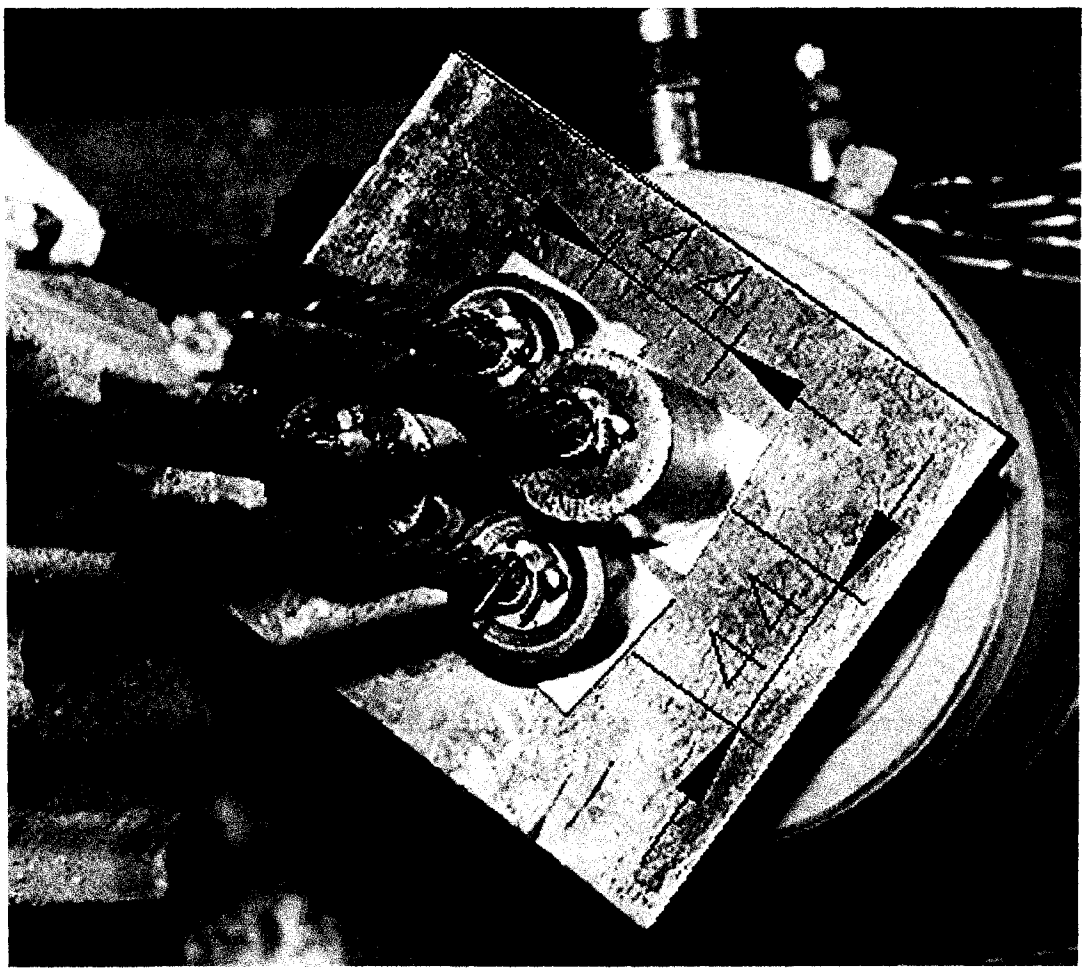

**Figure 3.6: Strand wedge chucks**

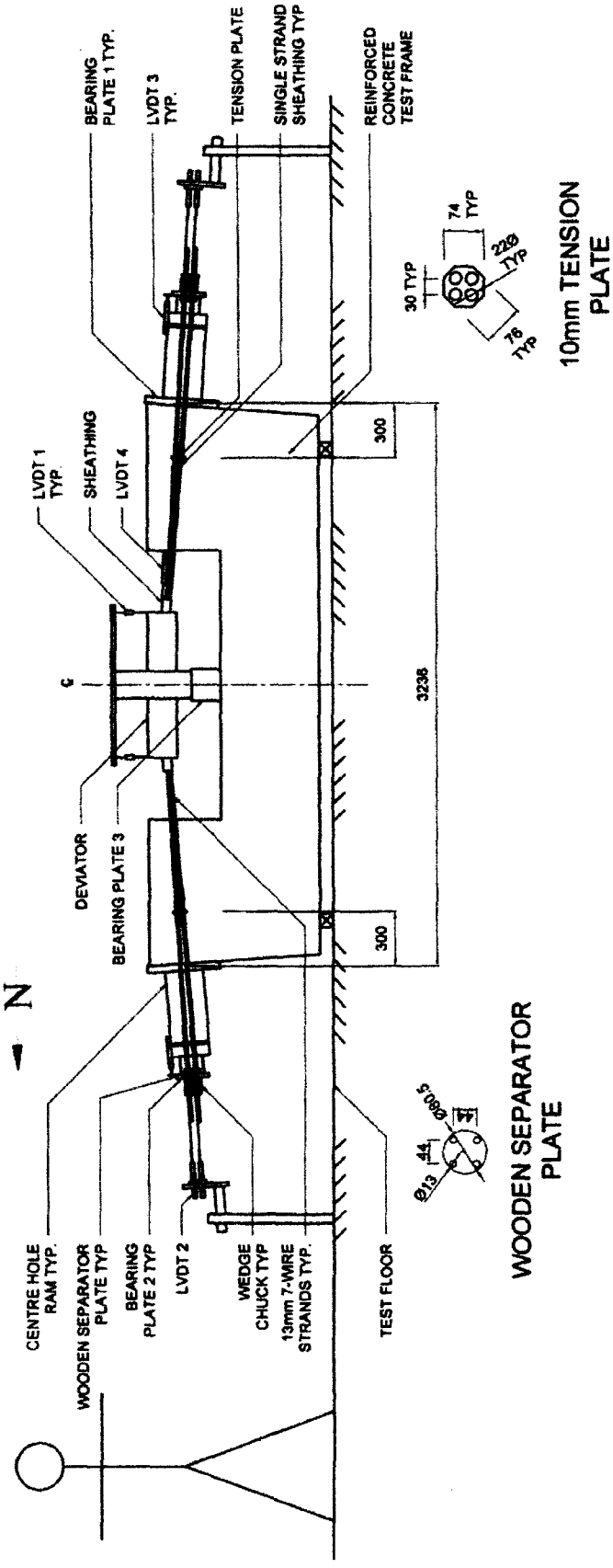


Figure 3.7: Test set-up

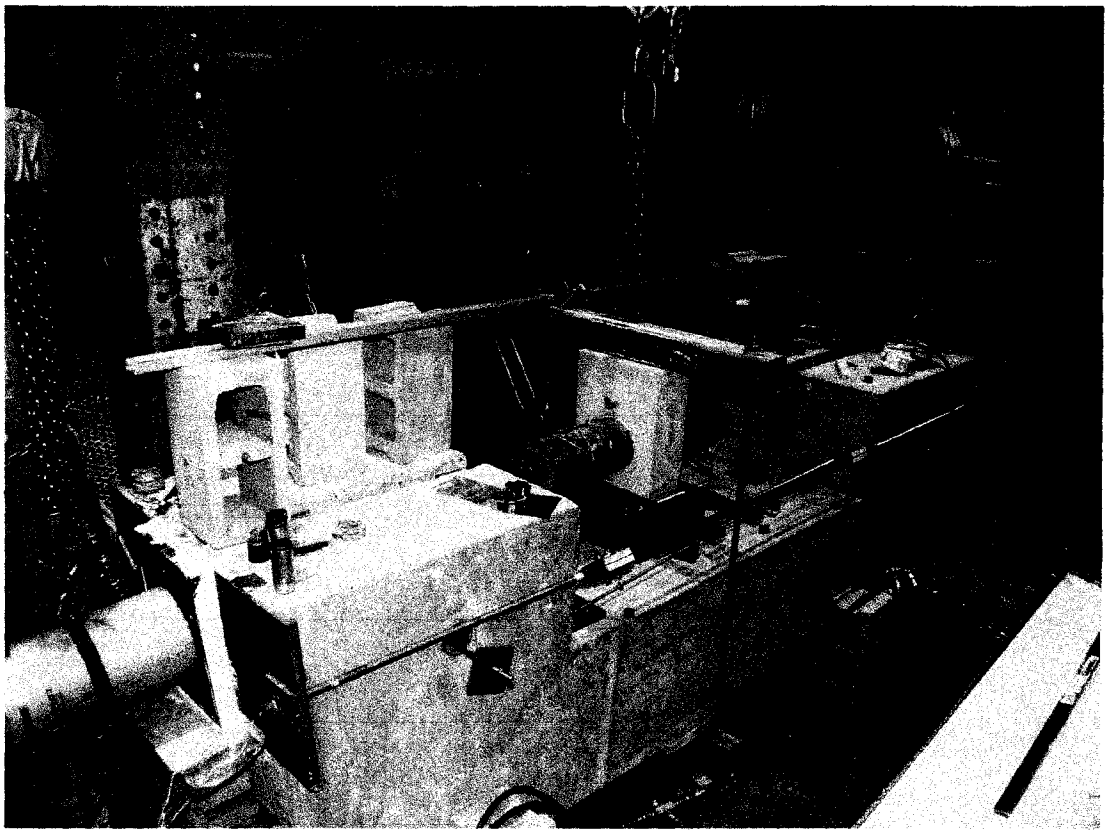

**Figure 3.8: Test frame and deviator**

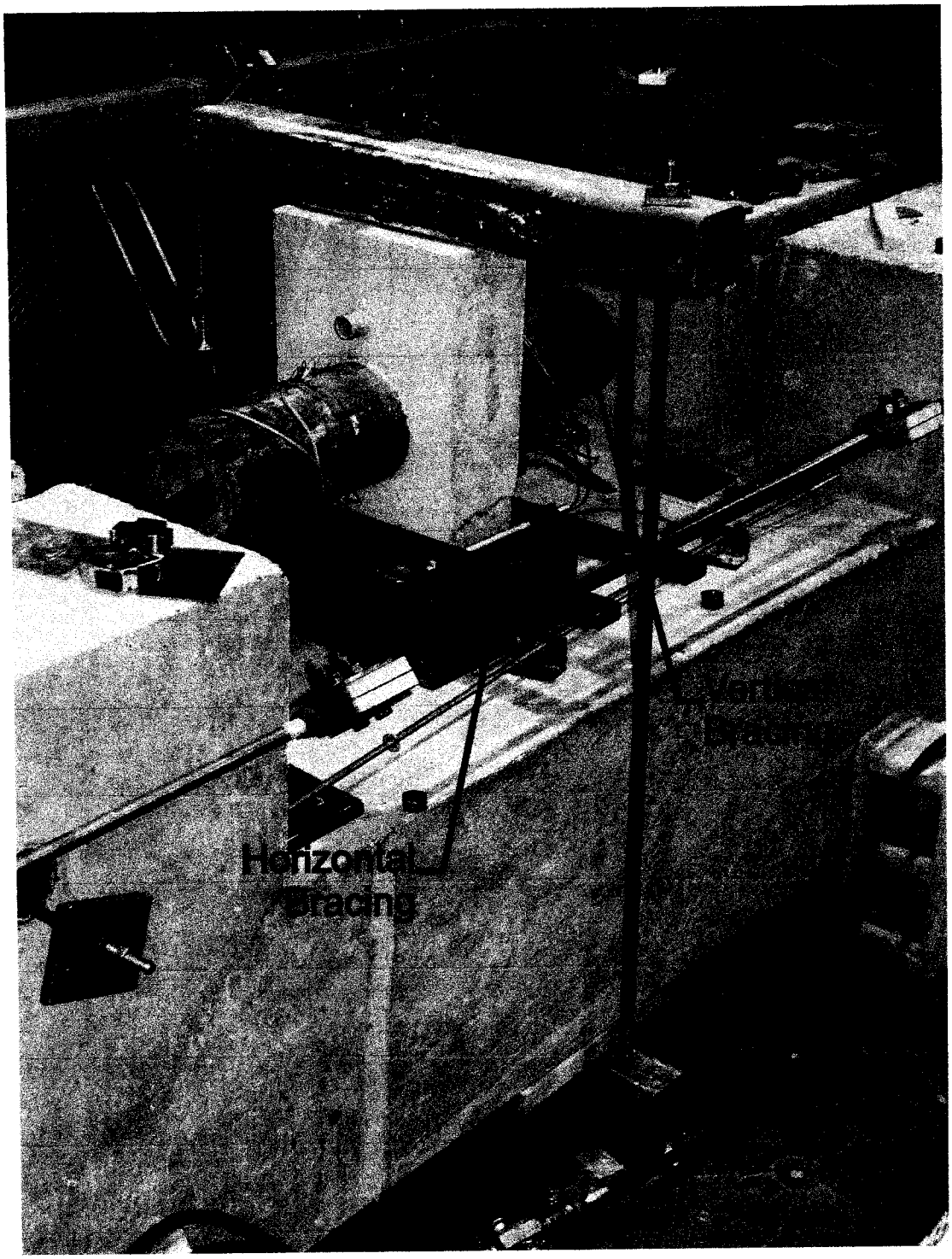


**Figure 3.9: Deviator support bracing**

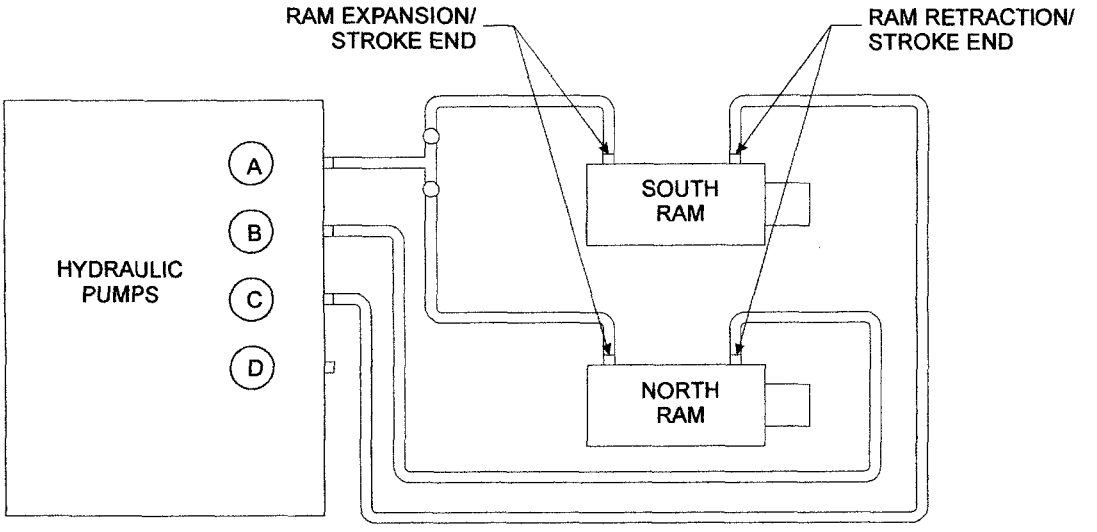


**Figure 3.10: Ram-hose-pump configuration**


**Figure 3.11: Deviator deflection LVDTs**

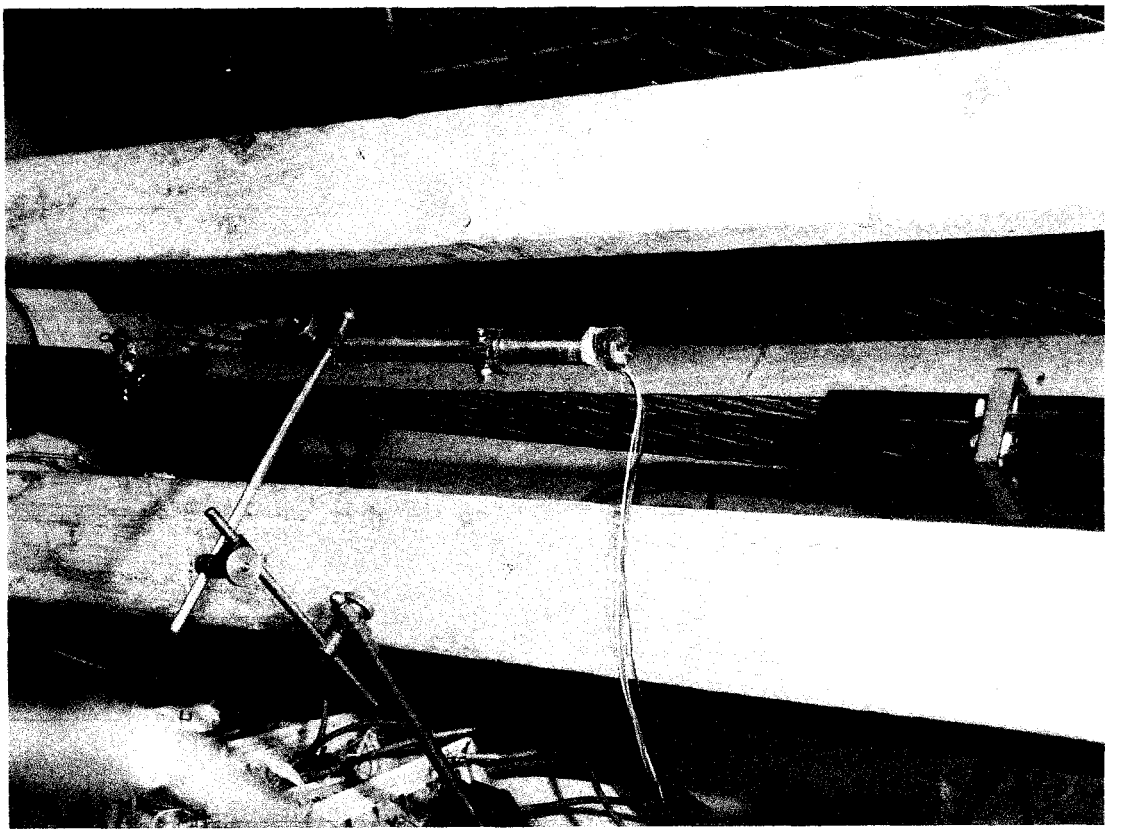

**Figure 3.12: Set-up for LVDT measuring strand movement through deviator**

# 4 EVALUATION AND DISCUSSION OF TEST RESULTS

## 4.1 OVERVIEW

This chapter presents a detailed analysis of the test results. Friction coefficient values at the deviator are assessed with special attention to differences in coefficient due to deviator size and load level. The stress-strain relationship in the failure tests is assessed and compared to that from the control tests as well as that of a single straight prestressing strand. In addition, the deflection, strains, and diameter changes in the deviators will be examined and compared to model predictions. From these results, a design methodology for composite diablo deviators is developed.

## 4.2 FRICTION TESTS

The objective of the friction tests was to determine the coefficient of friction between the tendon and the sheathing at the deviator.

The friction test was designed assuming the friction partners were the prestressing tendon and the HDPE sheathing. From markings made on the outside of the HDPE at the deviator face, it was noted that the sheathing did not move relative to the deviator and this assumption, therefore, was confirmed. Another assumption made was that the strands in the tendon would move as a unit through the deviator. As mentioned in Chapter 3, in order to test this assumption, the outsides of the strands were marked at a specific point prior to shifting the strands back and forth through the deviator.

These markings remained together, thus proving that the strands did move as a unit through the deviator.

The strands entered the deviator positioned as shown in Figure 4.1. The angled grooves seen along the interior of the sheathing (Figure 4.2) indicate that the strands twisted as they moved through the deviator. Further evidence of this can be seen in Figure 4.3 as the strands coiled around each other during a friction test. This was the case in all similar friction tests.

Figure 4.4 (a) provides an illustration of the forces acting between the strands and the sheathing. Because the vertical inclination of the forces from the tendon is so small, the forces can be simplified as shown in Figure 4.4(b). Figure 2.6 shows the resultant forces acting at the deviator. The friction coefficient, $\mu$, can then be determined using the following relationships:

$$F_n = (P_1 + P_2)\sin(\alpha/2) \qquad \textbf{(Eq. 4.1)}$$

$$\mu = \frac{P_2 - P_1}{F_n} \qquad \textbf{(Eq. 4.2)}$$

The angle change of the tendon, $\alpha$, was manually measured. The loads $P_1$ and $P_2$ were initially determined from the strain gauges on the tendon wires and their calibration values against load. Typical load results thus determined from the strain gauges are shown in Figure 4.5. The results from the strain gauges showed $P_2$ continuing to decrease throughout the entire tendon shift, often becoming even less than $P_1$. These results could not be explained. Similar results from other tests are

shown in Appendix B and confirm that this unexplained behaviour was typical for all tests.

The loads in the tendon were also determined from the pressures in the rams. As outlined in Chapter 3, to shift the tendon, oil was pumped into the retraction end of one ram while released from the retraction end of the other ram. For instance, to move the tendon towards the south (south ram extending and north ram retracting), oil would be pumped into the north ram retraction end while released at the south ram retraction end. Pressure would build at the north ram retraction end until the force on the ram piston was sufficient to overcome the friction in the two rams and the friction between the tendon and the deviator.

The friction in the rams occurs between the ram piston and the interior surface of the ram. When the rams were calibrated against the MTS, the relationship between pressure and load was determined in each ram, both for when the ram piston was extending and the ram piston was retracting. These relationships are noted in the following equations:

$$P_{S_{EXT}} = 0.0921\sigma_S + 10.541 \quad \text{(south ram – piston extending)} \qquad \textbf{(Eq. 4.3)}$$

$$P_{S_{RET}} = 0.0922\sigma_S + 18.127 \quad \text{(south ram – piston retracting)} \qquad \textbf{(Eq. 4.4)}$$

$$P_{N_{EXT}} = -0.0914\sigma_N + 13.675 \quad \text{(north ram – piston extending)} \qquad \textbf{(Eq. 4.5)}$$

$$P_{N_{RET}} = -0.0918\sigma_N + 19.856 \quad \text{(north ram – piston retracting)} \qquad \textbf{(Eq. 4.6)}$$

where $P_{S_{EXT}}$ and $P_{S_{RET}}$ are the loads (in kN) at the south ram when the piston is extending and retracting respectively, $P_{N_{EXT}}$ and $P_{N_{RET}}$ are the loads (in kN) at the north ram when the piston is extending and retracting respectively, and $\sigma_S$ and $\sigma_N$ are the pressure readings from the south and north rams (in psi) respectively. From Equations 4.3 - 4.6, the friction in each ram can be determined from the following relationships:

$$F_{f_S} = \frac{\left|P_{S_{EXT}} - P_{S_{RET}}\right|}{2} \qquad \textbf{(Eq. 4.7)}$$

$$F_{f_N} = \frac{\left|P_{N_{EXT}} - P_{N_{RET}}\right|}{2} \qquad \textbf{(Eq. 4.8)}$$

where $F_{fs}$ and $F_{fn}$ are the friction forces within the south and north rams respectively.

The pressure reading at the retraction valve was taken with dial gauges during the friction tests. The accuracy of the reading is ±50 psi (0.346 MPa). From this pressure reading, the load at the retraction end can be determined as

$$P_{ret} = \sigma_{ret} A_{ret} \qquad \textbf{(Eq. 4.9)}$$

where $P_{ret}$ is the load at the retraction end of the ram, $\sigma_{ret}$ is the pressure reading at the retraction end of the ram, and $A_{ret}$ is the effective area of the ram piston at its retraction end. The friction force, $P_f$, and coefficient of friction between the deviator and tendon is thus reduced to the following equations:

$$P_f = \sigma_{ret} A_{ret} - F_{f_N} - F_{f_S} \qquad \textbf{(Eq. 4.10)}$$

$$F_n = (P_N + P_S)\sin\left(\alpha/2\right) \qquad \textbf{(Eq. 4.11)}$$

$$\mu = \frac{P_f}{F_n} \qquad \textbf{(Eq. 4.12)}$$

where $P_N$ is the load at the north ram, as determined from either Equations 4.5 or 4.6 and $P_S$ is the load at the south ram, as determined from either Equations 4.3 or 4.4.

From the method outlined above, the coefficient of friction was determined for the various tests. The results from each test can be seen separately in Figure 4.6. The values determined are for the static coefficient of friction as the pressure values at initial movement of the tendon are used in the analysis. The results from the individual tests appear very scattered. The scatter of the results is explained by the low accuracy of the pressure reading at the retraction valve (±50 psi), for which the resulting error in friction coefficient is shown in Figure 4.7.

Figure 4.7 also shows how the test results are grouped into high data points, middle data points, and low data points. The vertical distance between the groups corresponds to an approximately 50 psi increment in pressure reading. With additional error from the other pressure gauge readings, the coefficient of friction values from each test have an accuracy of ±0.07. The mean value, therefore, has a standard error of ±0.01.

The friction coefficients were divided into two groups based on the direction of travel, as seen in Figure 4.8. Direction 1 is the direction of initial travel in the friction test, while Direction 2 is the opposite direction of travel. From these results, it can be seen that

there was no significant difference in the friction coefficient based on tendon travel direction.

The results from the tests with the R1500 and R4500 deviators were separated and are shown in

Figure 4.9. The average friction coefficients were fairly consistent with the R1500 deviator were 0.11, 0.10, and 0.11 at the 50%, 60%, and 70% $f_{pu}$ load levels, respectively. The average friction coefficients with the R4500 deviator were 0.11, 0.13, and 0.15 at the 50%, 60%, and 70% $f_{pu}$ load levels, respectively. While these latter results show a steady increase in friction coefficient with increasing load level, it is difficult to determine if this is, or to what degree this is, a significant trend as there are approximately half the test results from the R4500 deviators as with the R1500 deviators, with which there was no such trend. Furthermore, the results from the R4500 and R1500 deviators are within the error determined for the friction coefficients.

The test results were also separated according to their testing procedures, Method A and Method B (

Figure 4.10). The results from Method A, in which the direction of travel was alternating with every tendon shift, were higher than the results from Method B, in which the tendon was moved in shorter shifts at least three times in the same direction before changing tendon movement direction. The difference between the friction coefficients averaged at 0.02 at each load level. These results show that, when

changing the direction of tendon movement, there is a higher initial friction coefficient than when the direction of tendon movement is maintained.

When all results at each load level were averaged (also seen in Figure 4.7), the coefficients were 0.11, 0.12, and 0.13 for the 50%, 60%, and 70% $f_{pu}$ load levels respectively. These mean values of the coefficient of friction are important to note as, in real world applications, the friction losses in a tendon are the net effect at a number of points/deviators due to a number of tendon shifts. For this reason, the mean value for estimating friction losses is more appropriate that taking the extreme, or near extreme values, from the data set. The friction coefficient values determined are in agreement with the literature overviewed in Chapter 2 (see Table 2.1), with the exception of AASHTO LRFD (2000). This is as expected as the friction partners were the polyethylene sheathing and prestress tendon and the use of a bell-shaped deviator should not have affected the interaction between the materials.

From this investigation, it is recommended that, in the absence of vendor (post-tensioning systems supplier) specific data, one use the friction coefficient values outlined by CAN/CSA S6-00 (2000), ACI 318-02, or CEB-FIP 1990 (1993). The coefficient of friction used by AASHTO LRFD (2000) may warrant further investigation as it is significantly different from the results of the study as well as those from the other codes discussed in Chapter 2. Nonetheless, whenever possible, measured properties should be used in lieu of generic "textbook" values. In addition,

if the direction of tendon movement is changed, a slightly higher coefficient of friction is expected.

## 4.3 FAILURE TESTS

### 4.3.1 TENDON EFFICIENCY

The tests to tendon failure can be used to determine if the proposed deviators have adequate efficiency.

Tendon stress-strain curves for each failure test are shown in Figure 4.11. The stress-strain curves from the Control Tests are also shown in Figure 4.11 and showed a good correlation with the failure test results. The maximum tendon stress and strain in each test is shown in Table 4.1.

The tendon stress was computed from the tendon force and the area of the unbroken wires. The tendon strain was determined by dividing the total stroke length of the rams by the initial tendon length from north to south ram head. These strain values are reported in Table 4.1. As the tendon had been loaded to 70%$f_{pu}$ prior to the failure tests, additional wedge draw-in would have been insignificant and was, therefore, not considered in the determination of strain.

As a check, the strain for each strand was also determined by dividing the strand elongation by the initial length of the strand. The results from both strain assessment

methods showed a good correlation. The individual strand strains were also used to note any variations in strand strains for wedge chuck shimming.

Prior to the failure test, the tendon had travelled under load in the friction tests. The total amount of travel under load for each test is shown in Table 4.2 (see Appendix A for amount of travel in north and south directions). This movement under load resulted in wear of the sheathing.

From

Figure 4.11, it can be seen that the tendons in the failure tests and the control tests behaved similarly. Table 4.1 shows the maximum tendon stress and strain at each wire break in a test. In Test 1500A, testing ended after the first wire break in a strand. In all other tests, stressing continued until at least two wires had broken.

In deviators, bending stresses and radial forces ($w_p$) are induced in the tendon (see Figure 4.4). The axial strains in the tendon due to tendon curvature are 0.047% and 0.14% for the R4500 and R1500 deviators, respectively. These strains in the tendon can induce premature tendon failure. The smaller the radius of curvature in the deviator, the lower the expected tendon strength. CAN/CSA S6-00 (2000) requires anchorage hardware to not reduce tendon efficiency below 95%. A desirable deviator should not reduce strand efficiency below 95% efficiency. All the tests performed, except Tests 4500A and 4500B, achieved at least 95% of tendon ultimate strength before any wire failed. Since these tests were performed with the larger sized

deviator, and failure occurred at the wedges, it can be concluded that deviator size did not contribute to the low failure stress level.

The failure test results were controlled by the efficiency of the end anchorage hardware. All tendon failures occurred at the wedges where the wedge teeth press into the strands, creating a shear force. A typical wire failure from the failure tests can be seen in Figure 4.12(a), while a typical seven-wire failure from the preliminary tests can be seen in Figure 4.12(b). The seven-wire failure shown in Figure 4.12(b) occurred as each wire yielded, indicated by the necking of each wire. The wire from the failure tests, however, showed an angled shearing of the wire at the first wedge teeth. From preliminary testing, it was discovered that proper placement of the wedges was critical in achieving high stresses and strains in strands. If the wedges were placed incorrectly, the maximum stress and strain of the strands markedly dropped. Thus, wedge placement can account for much of the variation in maximum stress and strain in the tendons.

In Test 4500A, the first wire break occurred at 94.8% $f_{pu}$. While the failure was under the required 95% efficiency value, the 0.2% difference could easily be accounted for by poor wedge chuck placement. This hypothesis is further supported by the fact that the second wire failure occurred at 98.6% $f_{pu}$, well after the 95% efficiency was achieved.

In Test 4500B, the first wire break occurred at 87.5% $f_{pu}$. The wedge chuck at which this failure occurred was inspected after the test and showed visible signs of damage. The condition of the wedge may have caused the premature wire breaks. The wedge chuck was subsequently discarded.

From the experimental results, it can be concluded that deviator size did not affect the ultimate strength and ductility of the tendon. Wedge hardware was the determining factor for tendon efficiency in every test. The Rogowsky and Marti recommendation for minimum interior deviator curvature (with plastic sheathing) of

$$R_{\min} = 1.5\sqrt{P_u / 1000} \qquad \textbf{(Eq. 4.13)}$$

is supported and should be considered in the design requirements implemented by future codes.

### 4.3.2 Deviator Behaviour

The deviator deflections and strains can be used to determine if the grout and steel pipe act as a composite member or as a non-composite member.

The deviator strains and deflections are shown in Table 4.3 and Table 4.4. Strain results shown as N/A are from improperly functioning strain gauges while deflection results shown as N/A indicate poor LVDT connections and/or placement. Prediction and test result curves for load vs. deflection and load vs. deviator strain can be seen in Appendix B. Plots of typical results are given in Figure 4.13 to Figure 4.18. The deflection values are for the vertical deflections at the free ends of the deviator pipes.

The deviator strains are longitudinal strains measured on the extreme top and bottom fibres of the steel deviator pipe.

Prediction analyses were performed for the deviator strains and deflections, considering the deviator as: (a) fully composite and (b) fully non-composite. When the test results are compared to these analyses predictions, the degree of composite action in the deviators will be determined and a model for the deviator can be established. As with the friction analysis, the forces acting on the deviator can be simplified to those shown in Figure 4.4(b). The model can be further simplified by modelling one end of the deviator as a cantilever beam with the deviator support acting as a fixed end (Figure 4.4 (c)).

The 1500 series deviators had short tendon contact lengths and, as a result, the cantilever lengths ($l_c$), sometimes shorter than 20 mm (location of strain gauges), were too short to provide useful data because the deviator strains were negligibly small. Thus, only the results from the 4500 series tests are considered for the deviator strain model.

#### 4.3.2.1 Fully Composite Analysis

For the fully composite analysis, the shear forces ($V_p$), moments ($M_p$), strains ($\varepsilon_{comp}$), and deflections ($\delta_{comp}$) of the deviators are determined from the following relationships:

$$V_p(z) = 0 \quad when\, z < l_e \qquad \textbf{(Eq. 4.14)}$$

$$V_p(z) = w_p(z - l_e) \quad when\ l > z \geq l_e \qquad \textbf{(Eq. 4.15)}$$

$$M_p(z) = 0 \quad when\ z < l_e \qquad \textbf{(Eq. 4.16)}$$

$$M_p(z) = \frac{w_p(z - l_e)^2}{2} \quad when\ l > z \geq l_e \qquad \textbf{(Eq. 4.17)}$$

$$\varepsilon_{comp}(z) = \frac{M_p y}{E_g I_{comp}} \qquad \textbf{(Eq. 4.18)}$$

$$\theta_{comp}(z) = \int_l^{l-z} \frac{M_p}{E_g I_{comp}} d(l - z) \qquad \textbf{(Eq. 4.19)}$$

$$\delta_{comp}(z) = \int_l^{l-z} \theta_{comp} d(l - z) \qquad \textbf{(Eq. 4.20)}$$

$$\delta_{comp}(0) = \delta_{comp}(l_e) + l_e \sin(\theta_{comp}(l_e)) \qquad \textbf{(Eq. 4.21)}$$

where $z$, $l$, and $l_e$ are as defined in Figure 4.4, $y$ is the distance from the cross-section centroid to point of interest for strain, $E_g$ is the modulus of elasticity of deviator grout, $I_{comp}$ is the moment of inertia of composite section of deviator, transformed to grout ($I_{comp} = I_g + nI_s$), $I_g$ is the moment of inertia of the grout cross-section in the deviator, $I_s$ is the moment of inertia of the deviator steel pipe cross-section, $n$ is the ratio of steel modulus of elasticity to grout modulus of elasticity, and $\theta_{comp}$ is the slope of the deviator due to elastic bending.

Because the cross-sectional properties change along the length of the deviator, the integrals in the above equations are difficult to evaluate in closed form. To simplify the analysis, numerical integration was used with small $\Delta z$ intervals ($\Delta z$ = 10 mm for 4500 test series and $\Delta z$ = 1 mm for 1500 test series). The error resulting from numerical integration was checked and determined to be insignificant, provided small

$\Delta z$ values are used (less than 0.05% difference in deflections when $\Delta z$ = 10 mm and $\Delta z$ = 5 mm used for 4500 test series and less than 0.5% difference in deflections when $\Delta z$ = 1 mm and $\Delta z$ = 0.5 mm used for 1500 test series).

#### 4.3.2.2 Fully Non-Composite Analysis

In the non-composite analysis, the forces from tendon deviation acting on the deviator are the same as in the composite analysis. The problem is, however, statically indeterminate. Computer aided analyses were performed using the program S-Frame. The deviators were modeled as separate grout and steel cantilever members connected with rigid members. The members were connected at the same $\Delta z$ intervals as in the composite analyses ($\Delta z$ = 10 mm for 4500 test series and $\Delta z$ = 1 mm for 1500 test series). The section properties for the grout were defined separately for each section in consideration of its changing dimensions over the length of the deviator. The load applied was a constant vertical distributed load applied on the steel member over the length the tendon was in contact with the deviator. The deflection at each joint (located at $\Delta z$ intervals) and strain in the deviator over the length of each member were thus determined using S-Frame.

#### 4.3.2.3 Model Assessment

The degree composite behaviour was determined through the following relationship:

$$\%\,\text{Composite} = \left( \frac{\text{NonComposite Value} - \text{Test Result}}{\text{NonComposite Value} - \text{Composite Value}} \right) \cdot 100\% \qquad \textbf{(Eq. 4.22)}$$

The test results, prediction results, and percent composite action in each test is shown in Table 4.3 and Table 4.4.

The majority of the deviator strain measurements showed the deviator behaving as either a fully composite or partially composite member. The low accuracy of the composite behaviour predictions can account for why some tests showed more than 100% composite behaviour. From the strain information in Table 4.3, one may conclude that the deviator is 50%-100% composite.

The deviator deflection varied much more as it showed composite, non-composite and partially composite behaviour with about equal frequency. Figure 4.16 shows fully composite behaviour while Figure 4.17 shows fully non-composite behaviour. Figure 4.18, however, indicates partially composite behaviour as the test results are between the composite and non-composite predictions.

The loading history and construction details of deviators should be noted in the determination of composite behaviour. The deviators used in these tests had circumferential weld beads along the interior of the steel pipe to increase the connection between the grout and steel. The number and geometry of these weld beads was not controlled in the specimen design. Unfortunately, the interior surface condition of the pipes and the weld beads were not inspected prior to grouting of the deviator. More importantly, the handling and previous loading of the deviator may affect the amount of composite behaviour a deviator exhibits.

The degree of composite behaviour was shown to be variable and is therefore difficult to predict. In addition, the handling and loading history of the deviator may affect the degree of composite behaviour they exhibit. For these reasons, the conservative assumption of non-composite behaviour should be made.

### 4.3.3 DEVIATOR OVALLING

The diameters of the deviators were monitored to examine whether the diameters changed (ovalled) excessively and, thus, if transverse bending of the pipe wall was a design issue.

The results from the deviator diameter measurements can be seen in Table 4.5. Since contact between the tendon and the deviator interior was primarily along the length of the support, the 1500 test series deviators were not evaluated for ovalling. In addition, ovalling measurements were not taken for Test 4500B. For Tests 4500A and 4500A2, horizontal diameters were measured as described in Chapter 3. Diameter changes were predicted using Roark and Young's formula for diameter changes of circular rings, $\Delta D_H$, based on the load configuration shown in Figure 4.19 (Roark and Young, 1975),

$$\Delta D_H = \frac{W R_s^{\,3}}{E_s I_s}\left(\frac{2}{\pi} - \frac{k_3}{2}\right) \qquad \textbf{(Eq. 4.23)}$$

Equation 4.23 is in imperial units, where $\Delta D_H$ is in inches, $W$ is the resultant vertical load acting on the deviator (in pounds), $R_s$ is the outer radius of the deviator steel pipe (in inches), $E_s$ is the modulus of elasticity of the deviator steel pipe (in psi), $I_s$ is

moment of inertia of the deviator steel pipe cross-section (in $in^4$), and $k_3$ is a constant, as defined in Equations 4.24 to 4.26,

$$k_3 = 1 - a - b \quad \textbf{(Eq. 4.24)}$$

$$a = \frac{I_s}{A_{sec} R_c^{\,2}} \quad \textbf{(Eq. 4.25)}$$

$$b = \frac{F E_s I_s}{G A_{sec} R_c^{\,2}} \quad \textbf{(Eq. 4.26)}$$

where $a$ and $b$ are shape constants, $A_{sec}$ is the cross-sectional area of the steel pipe, $R_c$ is the radius to the centroid of the cross-section, $F$ is the shape factor for the steel pipe cross-section (0.878 for 1500 mm radius deviators and 0.870 for 4500 mm radius deviators), and $G$ is the shear modulus of elasticity of the steel pipe.

It is recognized that this model provides only a crude approximation of the real loading situation. For the 4500 deviators, assuming tendons were loaded to 100% with a total 0.14 rad angle deviation, the maximum diameter change predicted from Equation 4.23 was $0.21 \times 10^{-3}$ mm. The callipers used could not measure diameter changes that small. In addition, the exterior of the deviator was rough, which further reduced the accuracy of the diameter measurements. Nonetheless, as the diameter changes were all very small and in the range of what could be considered human error, the test results supported the belief that diameter changes would be insignificant.

The diameter changes could, in fact, have been even less than those predicted in Table 4.5. These predictions were made considering the steel pipe alone and its

deforming as a thin-walled circular ring. The interior grout was not considered in the prediction analysis. The grout would act as a thick-walled member and would restrain distortion of the thin walled steel pipe. Thus, the diameter changes predicted in Table 4.5 from Equation 4.23 are very conservative approximations.

Because of the strength of the steel pipe, in combination with the restraint the grout provides against its distortion, deviator ovalling is negligible and need not be considered in design. If examination is desired, however, the Roark and Young formulation in Equation 4.23 provides a conservative approximation for the horizontal diameter changes.

### 4.3.4 Sheathing Integrity

The sheathing was inspected to determine the nature and significance of the sheathing damage incurred from testing and thus, if HDPE sheathing is an acceptable form of sheathing.

The interior of the sheathing after all testing is shown in Figure 4.2. The tendons had made indentations in the sheathing, but the HDPE remained smooth elsewhere and there was no visible cracking anywhere. The indentations in the sheathing were made as the HDPE compressed under the load and movement of the tendon. Because the HDPE is compressed as opposed to gouged out, the density of the material increases with its deformation and it ultimately becomes more resistant to loading effects.

The indentations in the sheathing were, at most, less than 2 mm in depth, leaving an overall material thickness of over 2 mm. As noted in Chapter 2, CAN/CSA S6-00 (2000) states the sheathing wall must not be less than 1 mm after a tendon movement of 750 mm at a tendon stress of $0.80f_{pu}$. The amount of tendon movement through the deviator was not measured in the failure tests, though it would have been minimal as the tendon was pulled from both ends. Thus, the tendon likely did not travel through the sheathing at $0.80f_{pu}$ for 750 mm in the tests. Nonetheless, the tendon travelled through the deviator at various other load levels (see Table 4.2 for load levels and tendon travel lengths) and the sheathing retained over double the required wall thickness.

While no direct comparison can be made with the CAN/CSA S6-00 (2000) sheathing thickness requirements, the sheathing did have over double the required wall thickness after experiencing tendon travel at load levels as high as $0.70f_{pu}$. To the extent that the sheathing was tested, it can therefore be concluded that the HDPE sheathing alternative was acceptable. Furthermore, because the sheathing was compressed instead of gouged out, it is likely that the sheathing would be adequate at higher load levels as well.

**Table 4.1: Failure test tendon results**

| Test | Wires Broken | Tendon Load (kN) | Tendon Stress (MPa) | Tendon Stress $\%f_{pu}$ | Tendon Strain (%) |
|---|---|---|---|---|---|
| Control 1 | Break 1 | 742.3 | 1880 | 98.1 | 2.63 |
| | Break 2 | 722.1 | 1900 | 98.9 | 3.10 |
| Control 2 | Break 1 | 733.0 | 1880 | 97.8 | 2.77 |
| | Break 2 | 718.2 | 1910 | 99.7 | 3.24 |
| 1500A | Break 1 | 732.2 | 1860 | 96.7 | 2.15 |
| 1500B | Break 1 | 745.3 | 1890 | 98.5 | 2.89 |
| | Break 2 | 720.5 | 1890 | 98.9 | 3.02 |
| 1500A2 | Break 1 | 732.5 | 1860 | 96.8 | 2.06 |
| | Break 2 | 712.0 | 1870 | 97.5 | 2.17 |
| 4500A | Break 1 | 717.8 | 1820 | 94.8 | 1.52 |
| | Break 2 | 720.2 | 1890 | 98.6 | 2.65 |
| 4500B | Break 1 | 662.6 | 1680 | 87.5 | 0.96 |
| | Break 2 | 669.2 | 1760 | 91.6 | 1.09 |
| | Break 3 | 675.5 | 1840 | 96.0 | 1.46 |
| 4500A2 | Break 1 | 735.4 | 1860 | 97.2 | 2.23 |
| | Break 2 | 707.9 | 1860 | 96.9 | 2.37 |

**Table 4.2: Tendon travel under load prior to failure test**

| Test | Travel at Load Level (mm) | | | Total Travel (mm) |
|---|---|---|---|---|
| | 50% | 60% | 70% | |
| 1500A | 330 | 1282 | 350 | 1962 |
| 1500B | 550 | 575 | 589 | 1714 |
| 1500A2 | 560 | 560 | 560 | 1680 |
| 4500A | 840 | 785 | 440 | 2065 |
| 4500B | 695 | 695 | 695 | 2085 |
| 4500A2 | 640 | 570 | 577 | 1787 |

**Table 4.3: Deviator strains from failure tests**

(a) Test deviator strain results and percent composite behaviour

| Test | Tendon Load (kN) | Test Results Deviator Strain (με) | | | | | | | | | | | | | | | | Ave % Comp |
|---|---|---|---|---|---|---|---|---|---|---|---|---|---|---|---|---|---|---|
| | | Top N20 | % Comp | Top N40 | % Comp | Top S20 | % Comp | Top S40 | % Comp | Bot N20 | % Comp | Bot N40 | % Comp | Bot S20 | % Comp | Bot S40 | % Comp | |
| 4500A | 710.1 | 132 | 78.9 | 106 | 82.0 | 102 | 55.0 | 82.9 | 49.2 | 143 | 66.2 | N/A | N/A | 78.8 | 95.5 | 42.4 | 139 | 80.8 |
| | 712.6 | 132 | 79.2 | 106 | 82.5 | 102 | 55.5 | 82.5 | 50.6 | 147 | 62.1 | N/A | N/A | 84.3 | 86.4 | 41.7 | 141 | 79.6 |
| 4500B | 651.6 | 122 | 93.3 | N/A | N/A | 0.56 | 231 | 1.13 | 229 | 111 | 106 | 91.2 | 108 | 2.47 | 228 | 2.32 | 227 | 175 |
| | 658.2 | 127 | 88.3 | N/A | N/A | 0.57 | 232 | 0.94 | 231 | 122 | 94.1 | 94.3 | 105 | 3.09 | 228 | 3.13 | 226 | 172 |
| | 664.5 | 129 | 88.0 | N/A | N/A | 0.75 | 232 | 1.13 | 231 | 119 | 98.4 | 95.2 | 105 | 3.50 | 228 | 3.63 | 227 | 173 |
| 4500A2 | 724.5 | 143 | 68.8 | N/A | N/A | 136 | -1.72 | N/A | N/A | N/A | N/A | N/A | N/A | N/A | N/A | N/A | N/A | 33.6 |
| | 696.9 | 137 | 70.2 | 98.0 | 91.3 | 129 | 3.56 | N/A | N/A | 122 | 87.8 | 60 | 146 | 93.3 | 67.3 | N/A | N/A | 77.6 |

Note: 1) N/A indicates strain gauges that were not functioning properly
2) N20 and N40 refer to the strain gauges north of the deviator support by 20 mm and 40 mm respectively. S20 and S40 refer to the strain gauges south of the deviator support by 20 mm and 40 mm respectively. (See Figure 3.3 for schematic)

(b) Predicted deviator strain results (composite and non-composite)

| Test | Tendon Load (kN) | Predicted Deviator Strain (με) (Composite) | | | | | | | | Predicted Deviator Strain (με) (Non-Composite) | | | | | | | |
|---|---|---|---|---|---|---|---|---|---|---|---|---|---|---|---|---|---|
| | | N20 | ± | N40 | ± | S20 | ± | S40 | ± | N20 | ± | N40 | ± | S20 | ± | S40 | ± |
| 4500A | 710.1 | 114 | 42 | 93.7 | 37 | 76.2 | 28 | 59.9 | 14 | 200 | 46 | 165 | 40 | 134 | 30 | 105 | 25 |
| | 712.6 | 114 | 43 | 94.0 | 37 | 76.5 | 28 | 60.1 | 14 | 200 | 46 | 165 | 40 | 134 | 30 | 105 | 25 |
| 4500B | 651.6 | 116 | 98 | 97.2 | 84 | 84.3 | 70 | 68.7 | 59 | 204 | 83 | 171 | 72 | 148 | 59 | 121 | 50 |
| | 658.2 | 117 | 99 | 98.3 | 85 | 85.2 | 71 | 69.4 | 59 | 205 | 83 | 173 | 72 | 149 | 59 | 122 | 50 |
| | 664.5 | 118 | 100 | 99.2 | 86 | 86.0 | 72 | 70.1 | 60 | 206 | 84 | 174 | 73 | 150 | 60 | 123 | 50 |
| 4500A2 | 724.5 | 117 | 44 | 95.6 | 37 | 77.8 | 28 | 61.1 | 24 | 201 | 46 | 166 | 40 | 135 | 30 | 106 | 25 |
| | 696.9 | 112 | 42 | 91.9 | 36 | 74.8 | 27 | 58.8 | 23 | 196 | 45 | 162 | 39 | 131 | 29 | 103 | 25 |

Note: Errors (±) listed are one standard deviation

**Table 4.4: Deviator deflections from failure tests**

(a) Test deviator deflection results and percent composite behaviour

| Test | Tendon Load (kN) | Test Results Deflection (μm) | | | |
|---|---|---|---|---|---|
| | | North | % Composite | South | % Composite |
| 4500A | 484.5 | 46.43 | 3.20 | 5.900 | 115.4 |
| 4500B | 568.5 | 47.72 | 5.94 | N/A | N/A |
| 4500A2 | 721.5 | N/A | N/A | 15.75 | 95.49 |
| | 554.4 | 15.57 | 105.7 | 13.59 | 91.53 |
| 1500B | 734.1 | 0.19 | 69.5 | 0.070 | 60.2 |
| 1500A2 | 721.6 | N/A | N/A | 0.040 | 33.6 |
| | 701.1 | N/A | N/A | 0.040 | 32.3 |

(b) Predicted deviator deflection results (composite and non-composite)

| Test | Tendon Load (kN) | Predicted Deviator Deflection (Fully Composite) (μm) | | | | Predicted Deviator Deflection (Fully Non-Composite) (μm) | | | |
|---|---|---|---|---|---|---|---|---|---|
| | | North | ± | South | ± | North | ± | South | ± |
| 4500A | 484.5 | 17.07 | 2.23 | 11.40 | 1.49 | 47.40 | 5.84 | 47.09 | 5.84 |
| 4500B | 568.5 | 17.78 | 2.17 | 10.67 | 1.35 | 49.61 | 5.54 | 49.14 | 5.46 |
| 4500A2 | 721.5 | 22.57 | 2.76 | 13.55 | 1.71 | 62.95 | 7.03 | 62.36 | 6.92 |
| | 554.4 | 17.35 | 2.12 | 10.41 | 1.32 | 48.40 | 5.41 | 47.95 | 5.33 |
| 1500B | 734.1 | 0.118 | 0.047 | 0.006 | 0.005 | 0.338 | 0.117 | 0.164 | 0.090 |
| 1500A2 | 721.6 | 0.023 | 0.013 | 0.003 | 0.003 | 0.066 | 0.033 | 0.060 | 0.038 |
| | 701.1 | 0.022 | 0.013 | 0.003 | 0.003 | 0.064 | 0.032 | 0.058 | 0.037 |

Note: Errors (±) listed are one standard deviation

**Table 4.5: Ovalling results**

| | Test | Load (kN) | Dia. N1 (mm) | Dia. N2 (mm) | Dia. N3 (mm) | Dia. S1 (mm) | Dia. S2 (mm) | Dia. S3 (mm) |
|---|---|---|---|---|---|---|---|---|
| Original | 4500A | 0 | 158.62 | 158.66 | 158.33 | 159.47 | 159.08 | 158.65 |
| | 4500A2 | 0 | 158.48 | 158.53 | 158.67 | 158.28 | 158.41 | 158.84 |
| Under Load | 4500A | 546.4 | 158.80 | 158.77 | 158.42 | 159.47 | 159.11 | 158.18 |
| | 4500A2 | 557.9 | 158.85 | 158.74 | 158.91 | 158.35 | 158.45 | 158.75 |
| Test Difference | 4500A | 546.4 | 0.18 | 0.11 | 0.09 | 0.00 | 0.03 | -0.47 |
| | 4500A2 | 557.9 | 0.37 | 0.21 | 0.24 | 0.07 | 0.04 | -0.09 |
| Predicted Difference | 4500A | 546.4 | $0.15 \times 10^{-3}$ | $0.13 \times 10^{-3}$ | $0.09 \times 10^{-3}$ | $0.13 \times 10^{-3}$ | $0.10 \times 10^{-3}$ | $0.07 \times 10^{-3}$ |
| | 4500A2 | 557.9 | $0.16 \times 10^{-3}$ | $0.13 \times 10^{-3}$ | $0.09 \times 10^{-3}$ | $0.13 \times 10^{-3}$ | $0.10 \times 10^{-3}$ | $0.07 \times 10^{-3}$ |

Note: 1) N1, N2, and N3 measured 10 mm, 50 mm, and 100 mm north of the deviator support face respectively. S1, S2, and S3 measured 10 mm, 50 mm, and 100 mm south of the deviator support face respectively.

2) Test values listed are the average of 3 measurements with a standard deviation varying from 0.00 mm to 0.27 mm

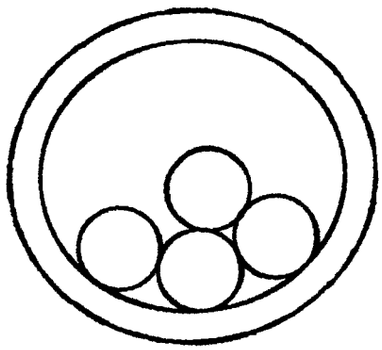

**Figure 4.1: Strand positioning upon entering deviator**

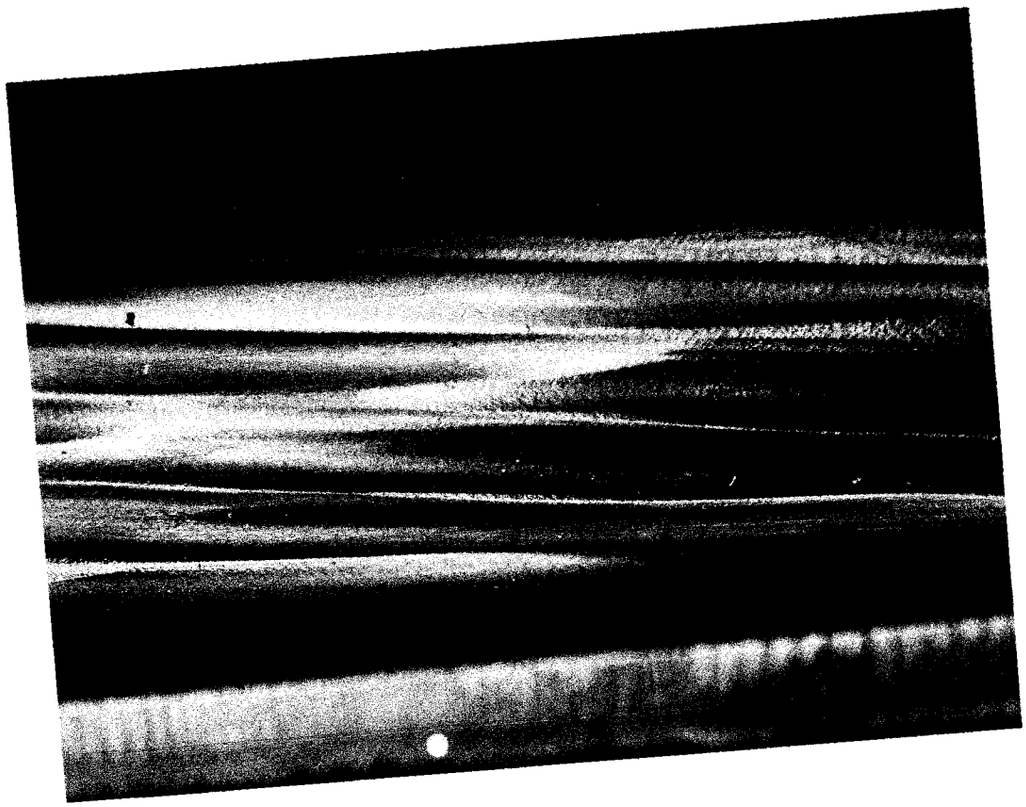

**Figure 4.2: Sheathing interior after testing**

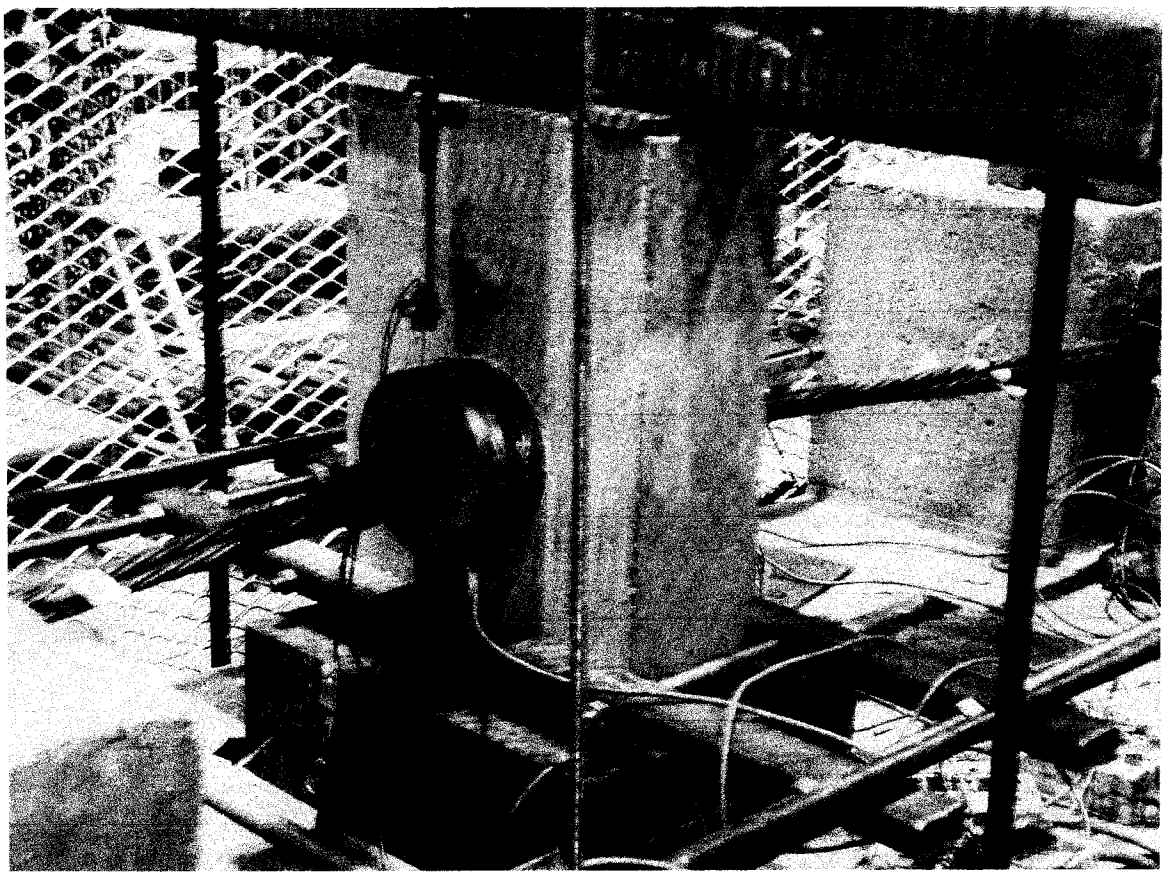

**Figure 4.3: Strand alignment after rotating ("coiling") in a friction test**

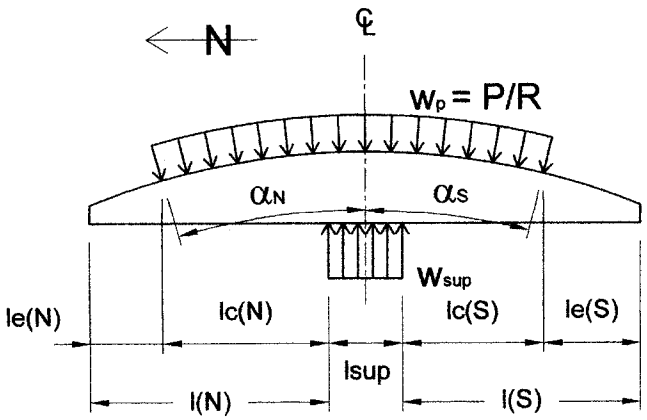


(a) Actual forces on deviator

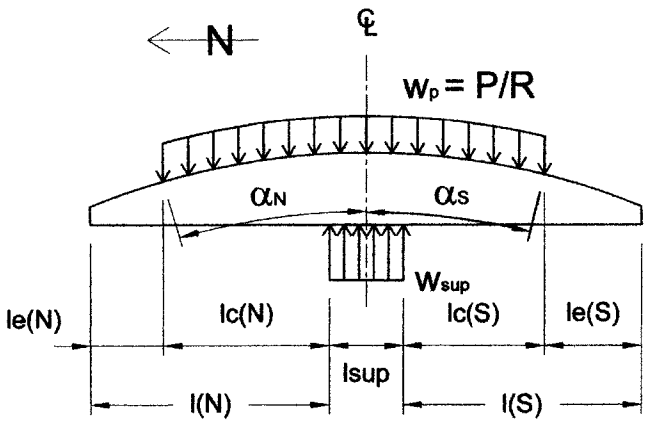


(b) Simplified forces acting on deviator

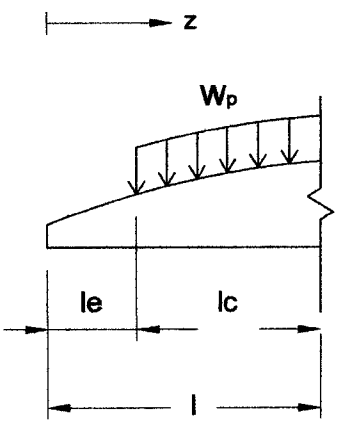


(c) Cantilever model of deviation forces

Note: For simplicity, friction forces are not shown

**Figure 4.4: Forces acting on deviator**

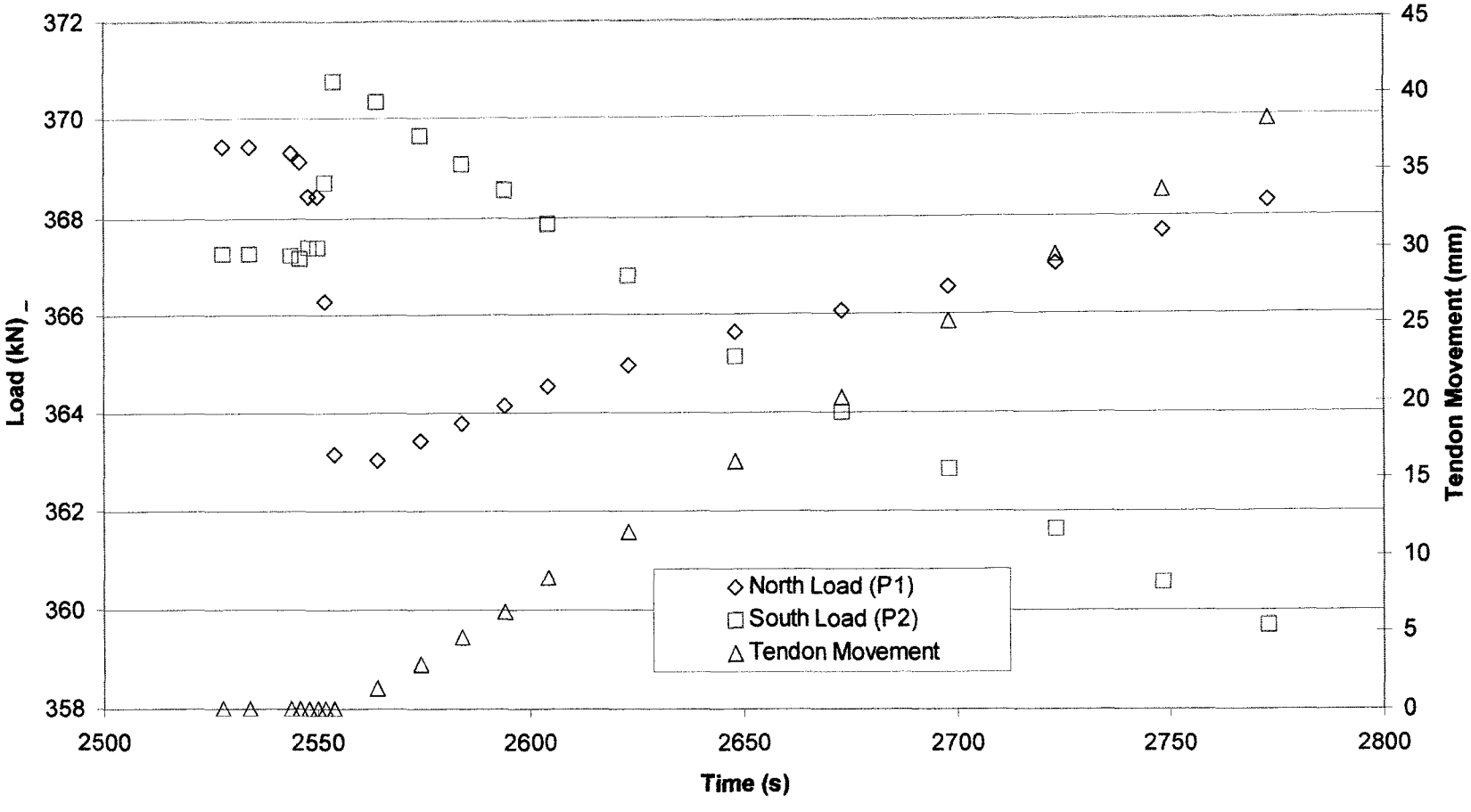


**Figure 4.5: Time vs. load (from strand strain gauges) for third tendon shift (movement of tendon towards the south in Test 4500B – 50%B)**

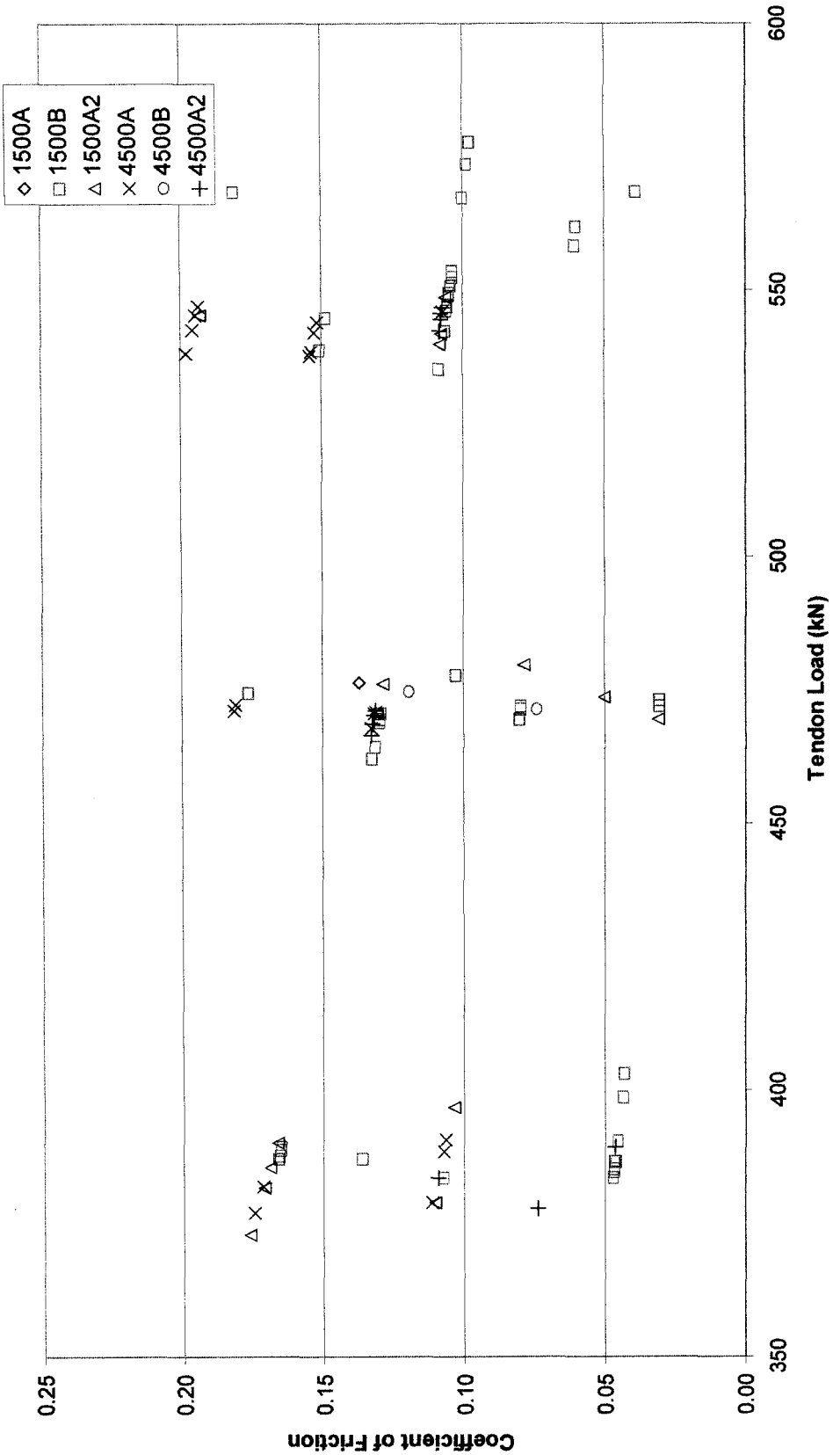


**Figure 4.6: Load vs. friction coefficient (individual test results)**

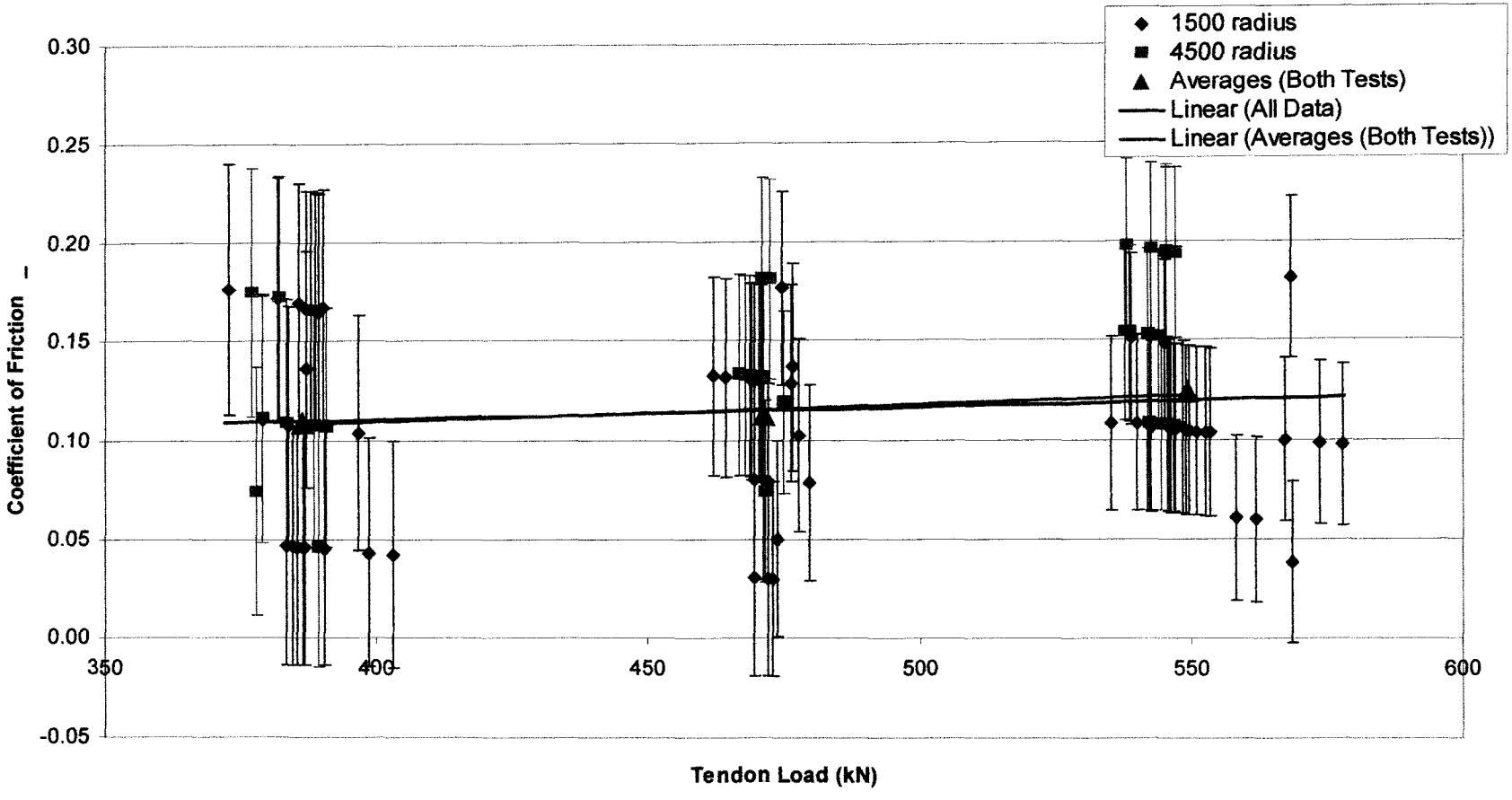


Note: 1) Error bars indicate error associated with ±50 psi reading in pressure
2) 33 readings with 4500R deviators; 61 readings with 1500R deviators

**Figure 4.7: Tendon load vs. coefficient of friction (errors and average readings)**

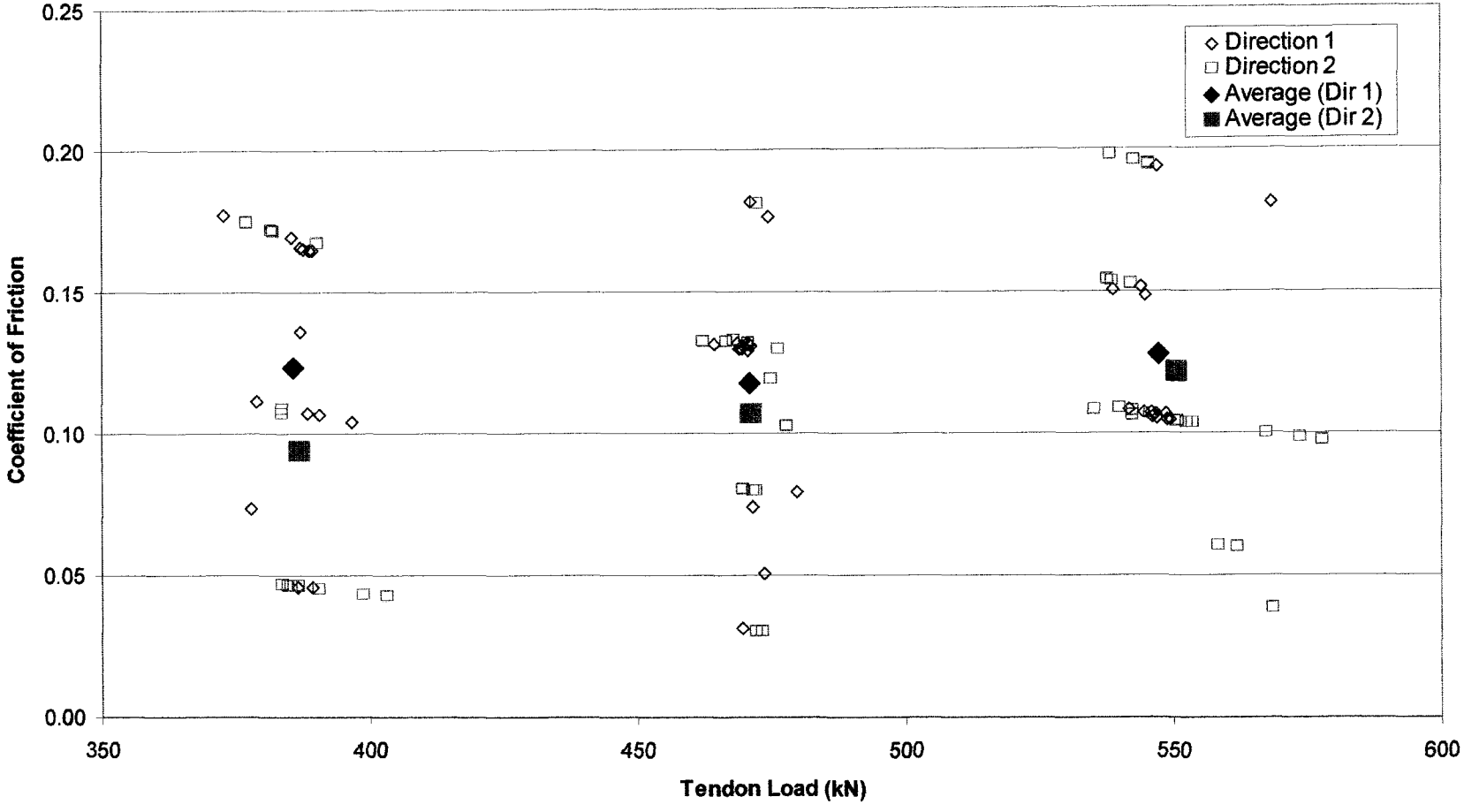


**Figure 4.8: Tendon load vs. coefficient of friction (effect of direction of travel)**

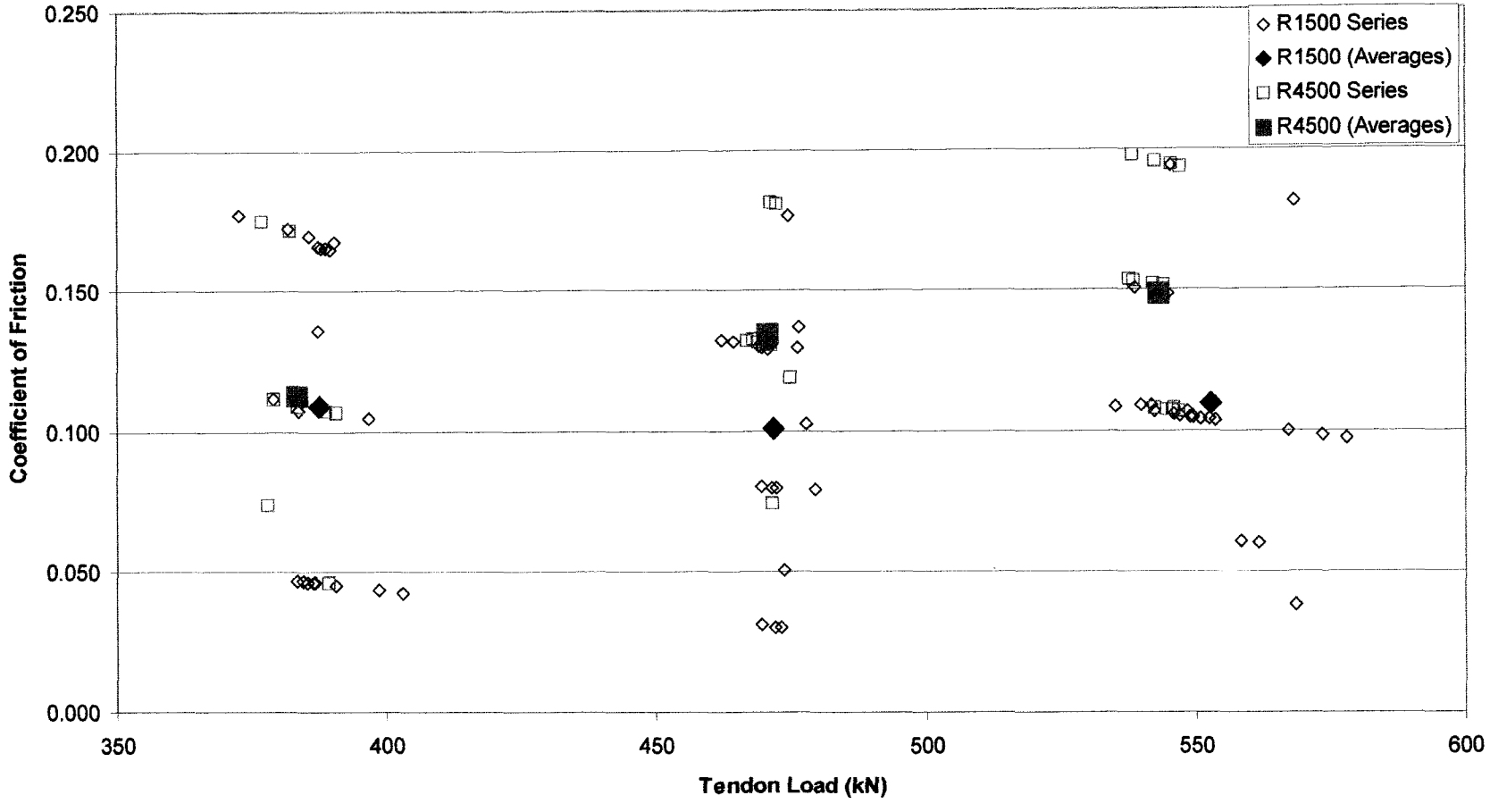


* 33 readings with 4500R deviators; 61 readings with 1500R deviators

**Figure 4.9: Tendon load vs. coefficient of friction (R1500 deviators vs. R4500 deviators)**

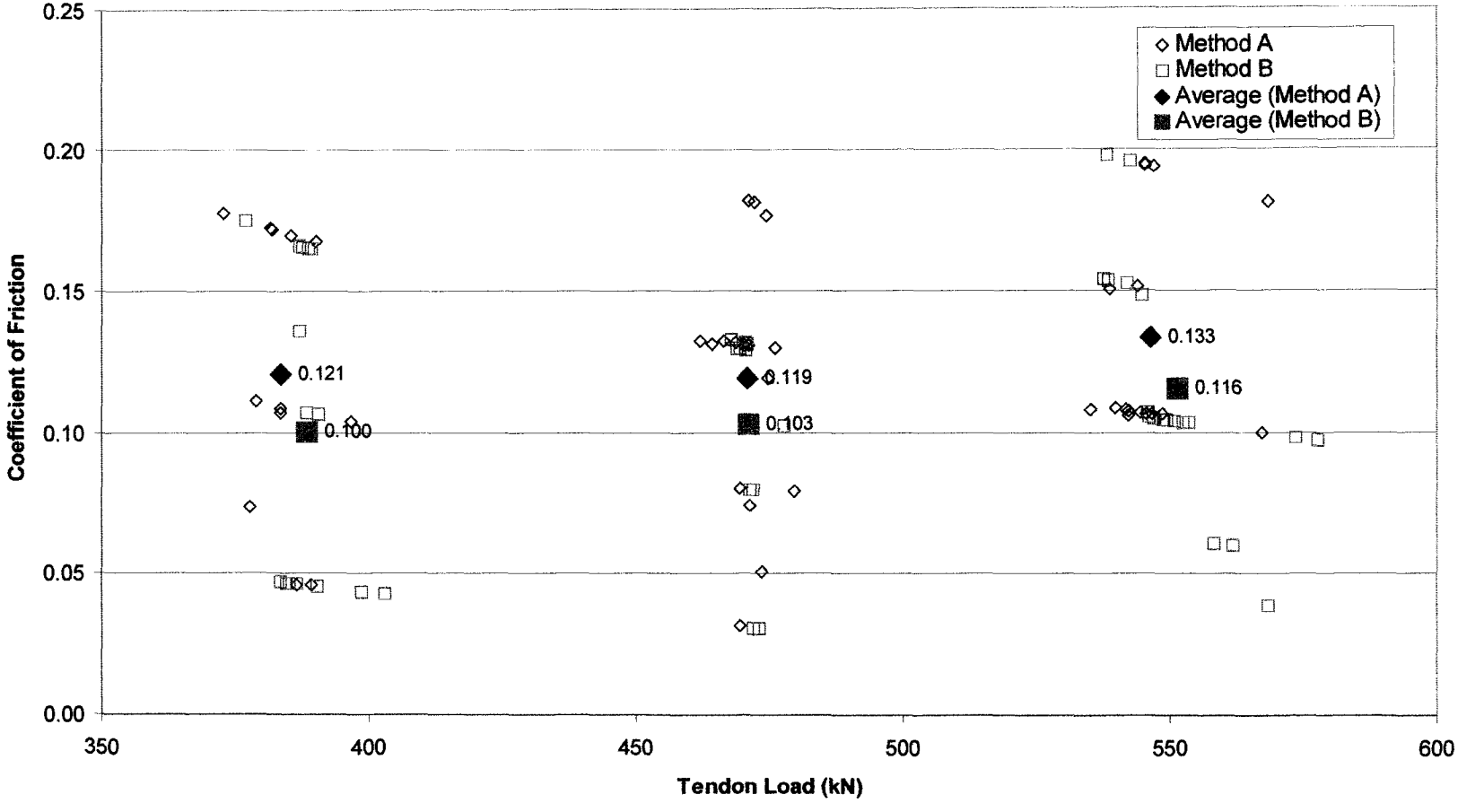


**Figure 4.10: Tendon load vs. coefficient of friction (Method A vs. Method B)**

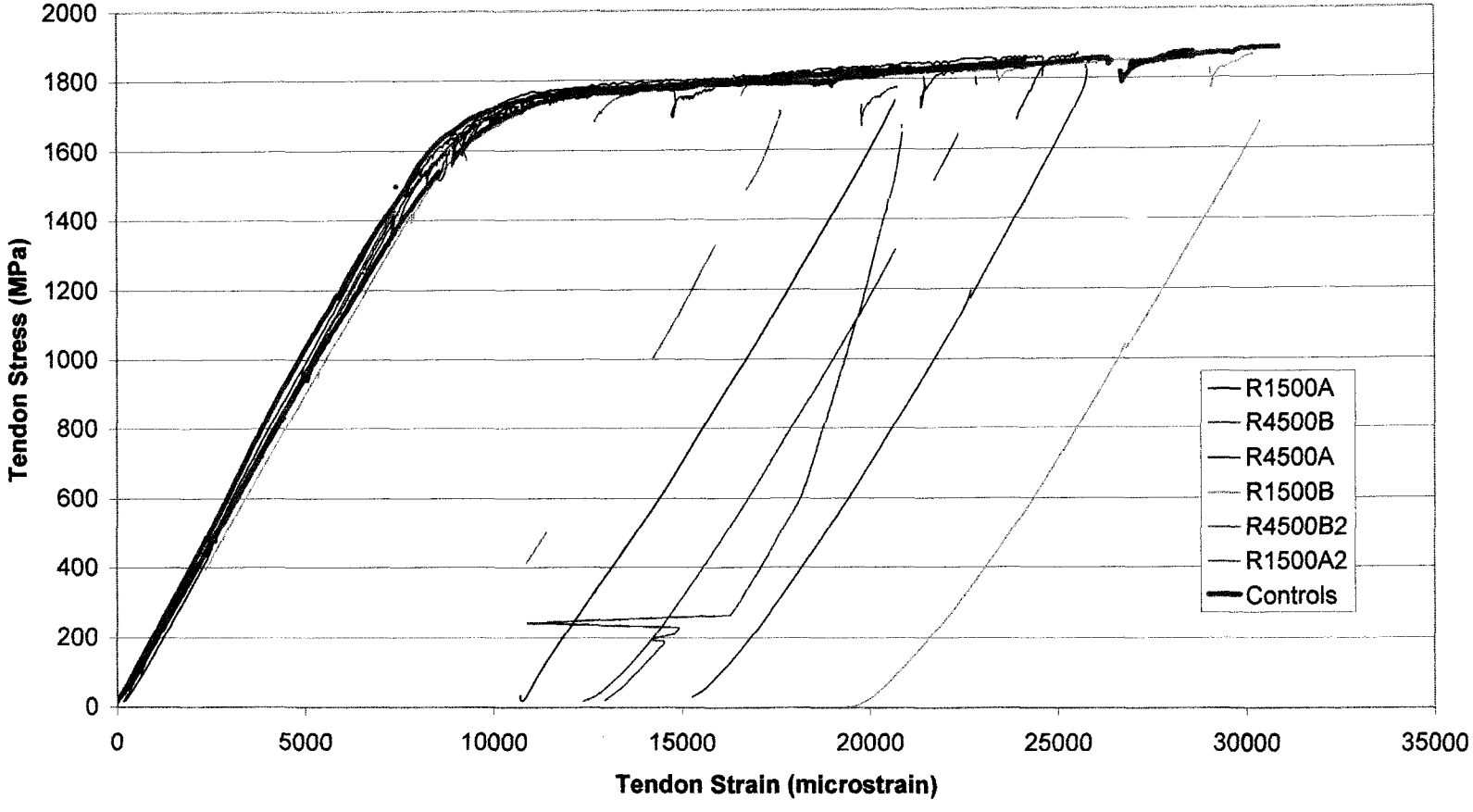


**Figure 4.11: Stress-tendon strain relationship for tests to ultimate tendon failure**

(a) Typical wire break at end anchorage wedge in failure tests

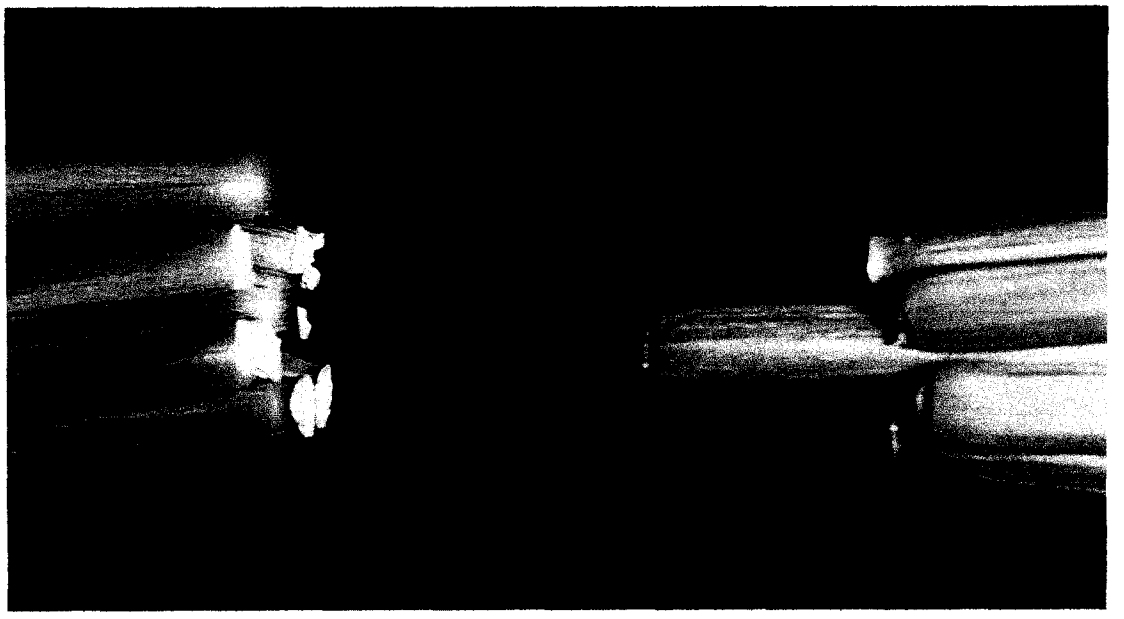

(b) Seven-wire strand break in free length away from wedge grips (gives 100% $f_{pu}$)

**Figure 4.12: Strand wire breaks**

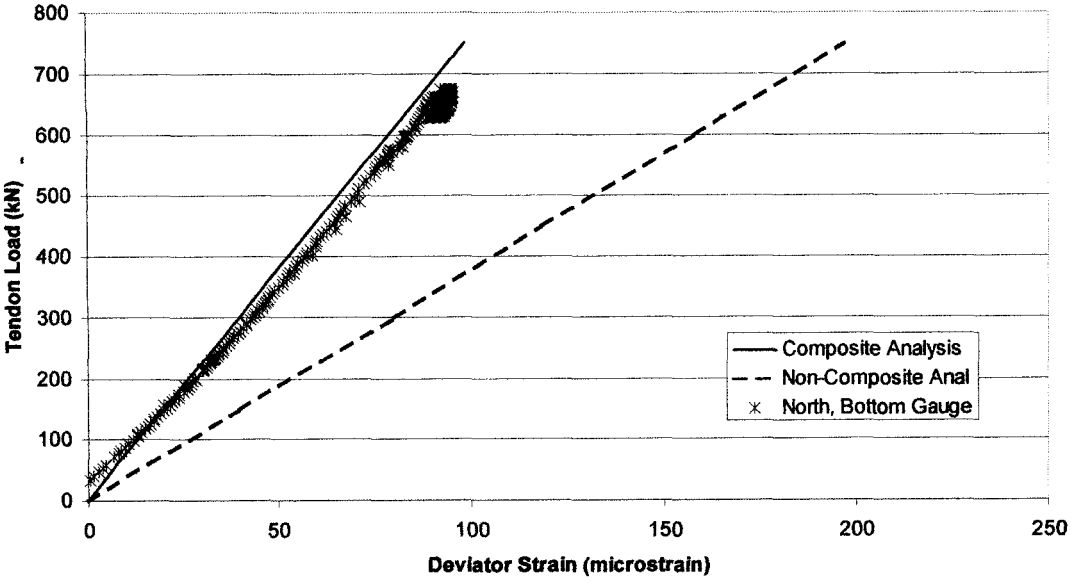


**Figure 4.13: Typical fully composite strain results (Test 4500B, 40 mm cantilever)**

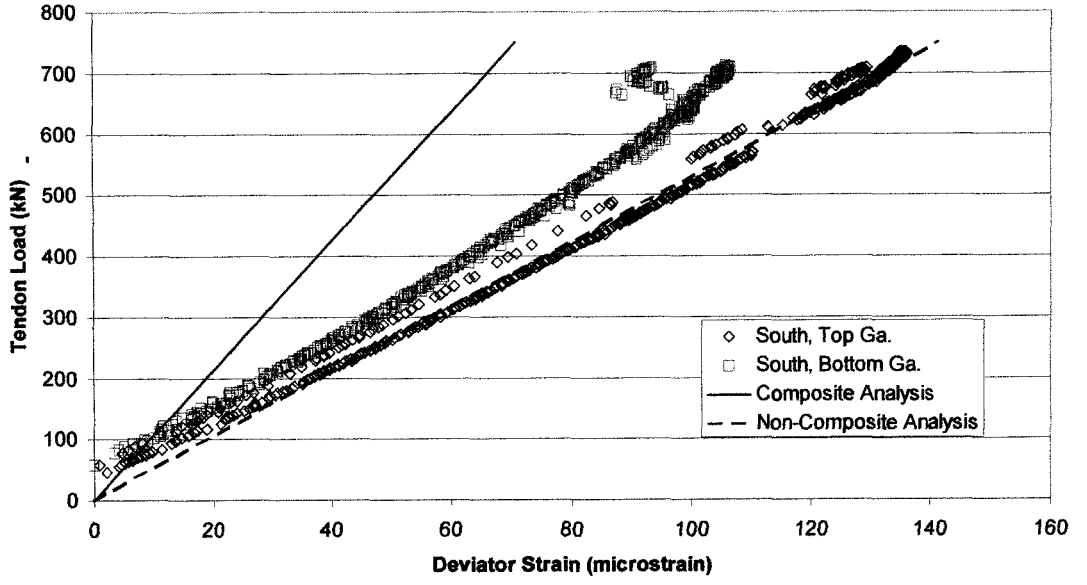


**Figure 4.14: Typical fully non-composite deviator strain results (Test 4500A2)**

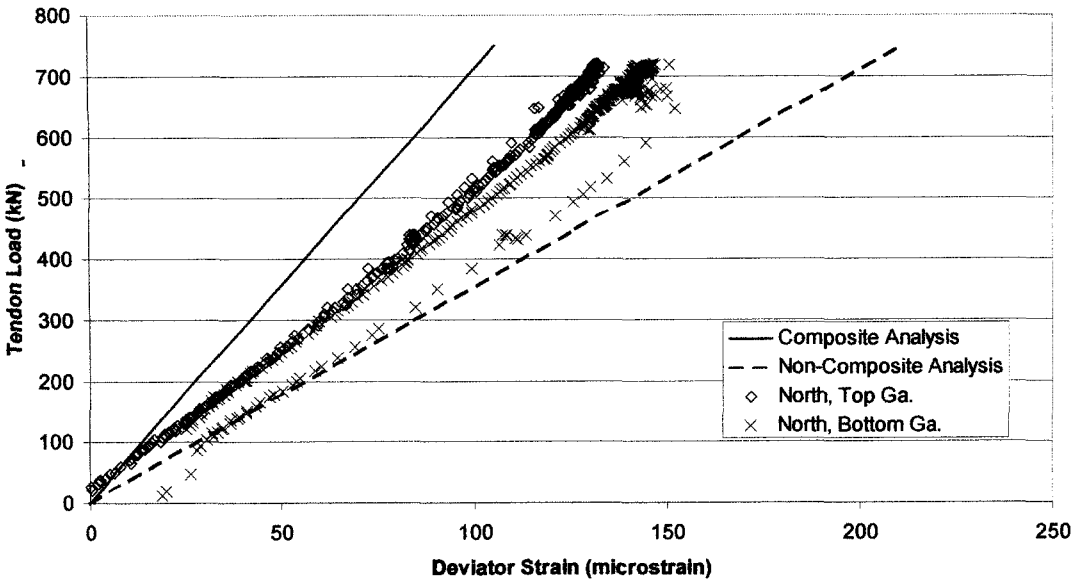


**Figure 4.15: Typical partially composite deviator strain results (Test 4500A, 20 mm cantilever)**

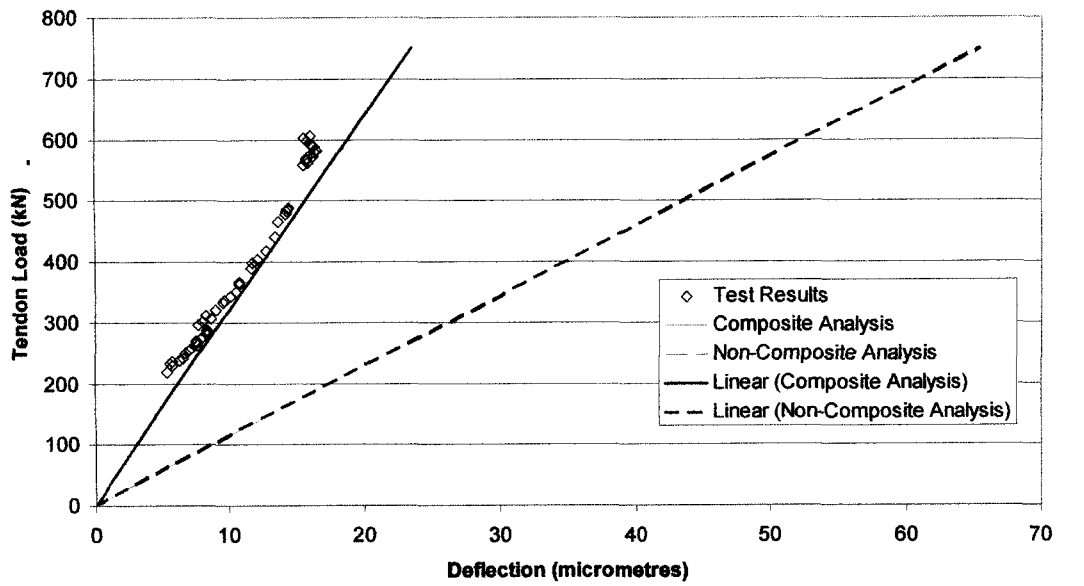


**Figure 4.16: Typical fully composite deviator deflection results (Test 4500A2, north end of deviator)**

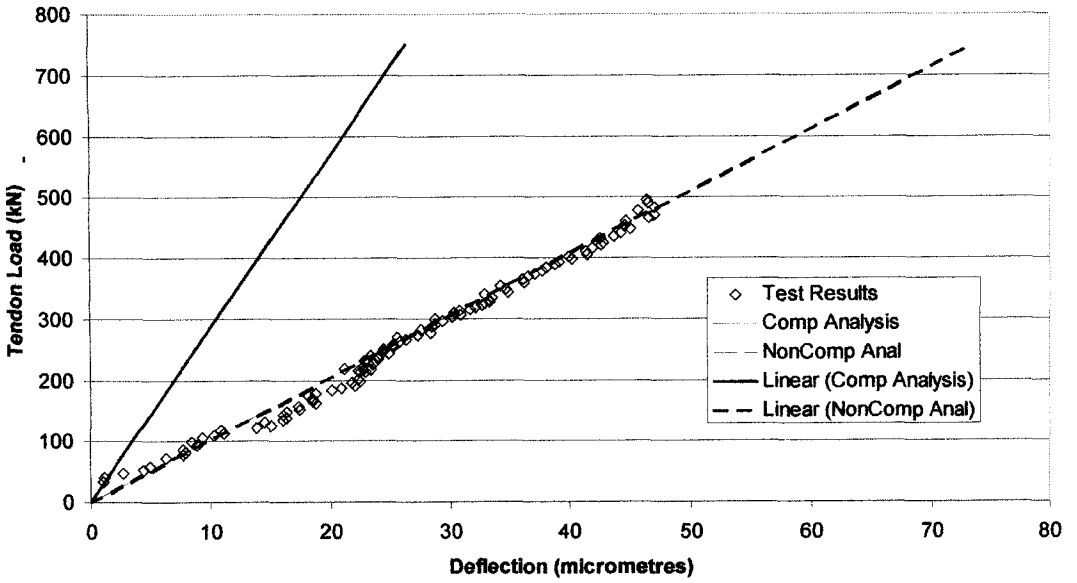


**Figure 4.17: Typical fully non-composite deviator deflection results (Test 4500B, north end of deviator)**

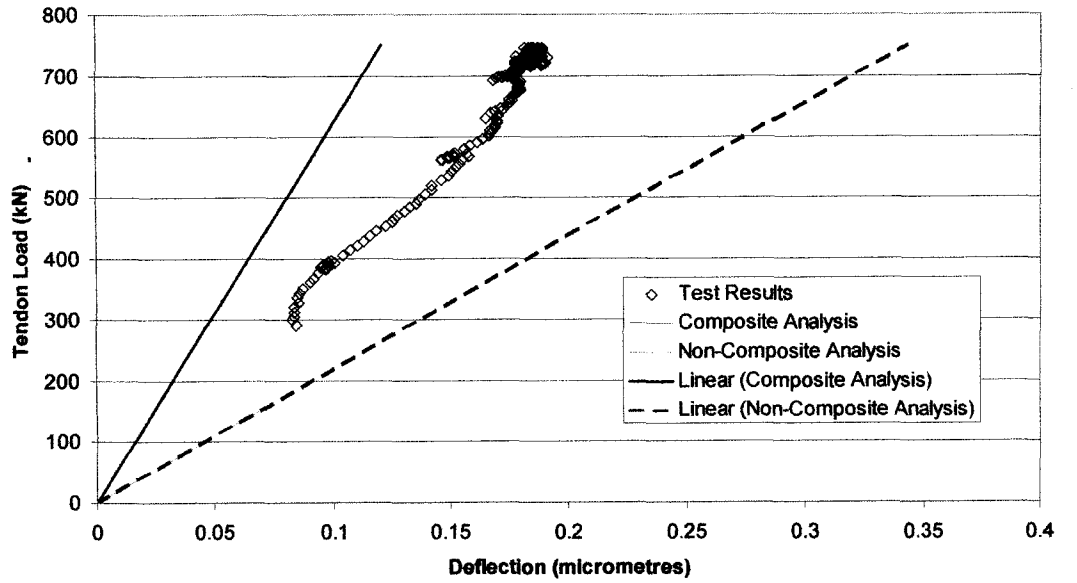


**Figure 4.18: Typical partially composite deviator deflection results (Test 1500B, north end of deviator)**

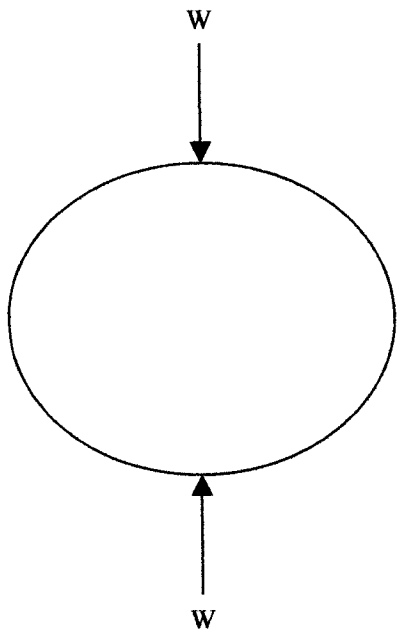


**Figure 4.19: Loading condition for Equation 4.23 (Roark and Young, 1975)**

# 5 SUMMARY AND CONCLUSIONS

## 5.1 SUMMARY

This study examined the characteristics of the composite diablo deviator, with emphasis on the friction characteristics, tendon efficiency, and general behaviour of the deviator due to tendon deviation forces. Composite deviators with internal radius of curvatures of 1500 mm and 4500 mm were designed and tested with multistrand tendons.

Friction tests were performed during which the tendon movement and the tendon load on each side of the deviator was monitored. The friction coefficient was determined from these results and compared to the friction coefficients from the literature surveyed. Failure tests were performed to determine the effects of the deviators on tendon efficiency and the behaviour of the deviator under the loads due to tendon deviation. The stress-strain relationship of the tendon in the failure tests were compared to that from control tests in which undeviated tendons were tested. The deflection at the deviator ends and axial strains of the deviator were monitored and compared to analyses performed assuming fully composite and fully non-composite deviator behaviour. The horizontal diameters of the deviator were also monitored and compared to Roark and Young's formulation for diameter changes in thin walled pipes.

## 5.2 CONCLUSIONS

From the investigation performed, the following conclusions were made:

1. The use of "diablo" type deviators, when compared to bent-steel pipe deviators, would reduce misalignment errors and possible kinking of the tendon at deviator entry and exit points.
2. The friction partners were confirmed to be the sheathing and tendon when high-density polyethylene sheathing and low-relaxation mulistrand tendons were passed through a composite diablo deviator with an interior grout surface.
3. The friction coefficients from the experimental results (0.11 – 0.13) were in good agreement with those from the codes and literature surveyed, with the exception of AASHTO LRFD (2000). It is recommended that a friction coefficient between 0.10 and 0.15 be used with high-density polyethylene sheathing in the absence of other information. However, when possible, results from experiments using design materials and/or models should be used.
4. AASHTO LRFD (2000) may want to re-examine its use of 0.23 as the coefficient of friction when high-density polyethylene sheathing is employed. This coefficient is significantly higher than those found in the experimental investigation and in all the literature surveyed.
5. The tendon moved as a unit through the deviator. The strands coiled around each other as the tendon twisted as it moved through the deviator.

6. The tendon efficiency was controlled by the anchorage hardware as all tendon failures occurred at the wedges.
7. Deviator size did not affect the ultimate strength and ductility of the tendon, thus supporting the recommendation of Rogowsky and Marti, for tendons with plastic duct, that

$$R_{\min} = 1.5\sqrt{P_u / 1000} \qquad \textbf{(Eq. 5.1)}$$

8. The conservative design assumption of non-composite behaviour is recommended for the assessment of deviator strain and deflection. While deviators did show composite behaviour in some tests, the behaviour was not consistent. The degree of composite action is further affected by factors that are difficult to predict, including the quality of construction and handling of the deviator.
9. Deviator diameters do not change significantly due to tendon deviation forces and therefore need not be considered in design. This is in large part due to the relatively large size of pipe used (as in accordance with the bent-steel pipe deviator requirements). Nonetheless, while the steel pipe by itself would be considered a thin walled member, the interior grout is considered a thick walled member and is therefore even less likely to experience any ovalling. Thus, any diameter changes the steel pipe might experience under the deviation forces would further be restrained by the grout.
10. To the extent that it was tested, the HDPE pipe is an acceptable alternative for sheathing. Furthermore, because of the way that it deforms under tendon

load, it would likely be in accordance with the requirements outlined by CAN/CSA S6-00 (2000).

## 5.3 Recommendations for Further Research

Further research is necessary before code stipulations can be made on "diablo" deviators. Areas for future investigation include:

1. A full-size test should be performed on deviators. Based on the design principles outlined in this thesis, a deviator should be designed as it would be used in a bridge. A common size for a tendon in a bridge would be 19-13 mm $\phi$ strands. Such a test could possibly be performed as part of a bridge with supplemental external tendons with bell-shaped deviators.
2. The sheathing integrity with tendon travel of 750 mm at a tendon stress of $0.80f_{pu}$ should be tested to ensure it meets the requirements of CAN/CSA S6-00 (2000).
3. The long-term behaviour of the plastic sheathing at high pressure with a tight radius should be examined.
4. The effects of weld beads (size and quantity) and internal surface condition of the pipe on the composite action of the deviator could be investigated.
5. Alternatives to reinforced concrete deviator supports should be studied to allow for alternatives such as steel deviator supports.
6. The friction data collected in these tests had a low accuracy. More reliable data should be collected to determine the friction coefficient for HDPE sheathing and multistrand tendons.

# REFERENCES

"AASHTO LRFD Bridge Design Specifications – SI Units", Second Edition, American Association of State Highway and Transportation Officials, Washington DC, 2000

"ACI 318-02, Building Code Requirements for Structural Concrete", ACI Committee 318, ACI, Michigan, USA, 2002

Aeberhard, H.V., Buergi P., Ganz, H., Marti, P., Matt, P., and Sieber, T., "External Post-Tensioning", VSL International Ltd, Berne Switzerland, 1992, 31pp.

Ariyawardena, N.D., and Ghali, A., "Design of Precast Prestressed Concrete Members Using External Prestressing," PCI Journal, Vol.47 No.2, Precast Concrete Institute, March-April 2002, pp. 84-94

Bowden, F.P. and Tabor, D., "Friction and Lubrication", Methuen & Co. Ltd., Great Britain, 1956 150pp.

Bruggeling, A.S.G., "External Prestressing – a State of the Art" External Prestressing in Bridges, ACI SP-120, ed. Naaman, A. and Breen, John, American Concrete Institute, Detroit Michigan, 1990, pp.61-81

Burns, N.H., Helwig, T., and Tsujimoto, T., "Effective Prestress Force in Continuous Post-Tensioned Beams with Unbonded Tendons" ACI Structural Journal, Vol.88, Jan-Feb 1991, pp.84-90

"CAN/CSA S6-00 Canadian Highway Bridge Design Code", Canadian Standards Association, Toronto ON, 2000

"CAN/CSA S6.1-00, Commentary on CAN/CSA-S6-00", Canadian Highway Bridge Design Code, Canadian Standards Association, Toronto ON, 2001

"CEB-FIP Model Code 1990 Design Code", Comité Euro-International du Béton, 1993, Thomas Telford, London, UK

"Chevron; Driscopipe® 8100 Series Polyethylene Piping Produced from PE 3408/PE100 Material"; www.cpchem.com/enu/docs_pipe/pp3028100.pdf ; Chevron Chemical Company; May 2004

Collins, M.P. and Mitchell, D., "Prestressed Concrete Basics", Canadian Prestressed Concrete Institute, Ottawa ON, 1987, 614pp.

"CPCI Design Manual, Precast and Prestressed Concrete", Third Edition, Canadian Prestressed Concrete Institute, Ottawa ON, 1996

"CSA A23.3-94 Design on Concrete Structures", Canadian Standards Association, Ontario, CAN, 1995

Diep, Bui Khac and Tanabe, Tada-aki, "Modified Formulation of Cable Strain in Finite Element Analysis of Externally Prestressed Concrete Beams" Transactions of the Japan Concrete Institute, Vol.22, 2000, pp.325-330

Diep, B.K. and Umehara, H., "Non-linear Analysis of Externally Prestressed Concrete Beams" Electronic Journal of Structural Engineering, Vol.2, 2002, pp.85-97 http://www.civag.unimelb.edu.au/ejse/Archives/Fulltext/200201/07/20020107.pdf

Dow Chemical Company, http://www.dow.com/sal/design/guide/physchar.htm, 2006

Hewson, N.R.; "The Use of External Tendons for the Bangkok Second Stage Expressway" The Structural Engineer, http://www.istructe.org.uk/thestructuralengineer/HC/Terms.asp?id=5714, Vol. 71 No. 23, Dec 1993

Hewson, Nigel R., "Prestressed Concrete Bridges: Design and Construction"; Thomas Telford Ltd., 2003, London GB, 371pp.

Jartoux, P. and Lacroix, R., "Development of External Prestressing in Bridges – Evolution of the Technique" External Prestressing in Bridges, ACI SP-120, ed. Naaman, A. and Breen, John, American Concrete Institute, Detroit Michigan, 1990, pp.83-106

Kinsella, M.E., Lilly, B., Gardner, B.E., and Jacobs, N.J., "Experimental determination of friction coefficients between thermosplastics and rapid tooled injected mold materials" Rapid Prototyping Journal, Vol. 11 No.3, Emerald Group Publishing Ltd., July 2005, pp.167-173

Leonhardt, Fritz, "Prestressed Concrete Design and Construction" Second Edition, Wilhelm Ernst & Sohn, Berlin-Wilmersdorf, 1964, 677pp.

Macovei-Benczur, S. and Rogowsky, D.M., "Developments in External Post-Tensioning" Annual Conference of the Canadian Society for Civil Engineering, June 5-8 2002, Montreal Canada; 13pp.

Manisekar, R. and Rao, M.V.B., "Behaviour of Deviators in External Prestressing: A Review" The Indian Concrete Journal, Vol. 77, Sept 2003, pp. 1332-1338

Nave, R., http://hyperphysics.phy-astr.gsu.edu/hbase/frict2.html

Pisani M.A. and Nicoli, E., "Beams Prestressed with Unbonded Tendons at Ultimate" Canadian Journal of Civil Engineering, Vol.23, Dec. 1996, pp.1220-1230

Rao, P. Srinivasa and Mathew, George, "Behaviour of Externally Prestressed Concrete Beams with Multiple Deviators" ACI Structural Journal, Vol. 93 No. 4, July-August 1996, pp.387-396

Roark, Raymond J. and Young, Warren C., "Roark's Formulas for Stress and Strain" 5th Ed.; McGraw-Hill, New York, 1975, 763pp.

Roberts, C.L.; "Measurement-Based Revisions for Segmental Bridge Design and Construction Criteria"; University of Texas at Austin, 1993, UMI Dissertation Services, Ann Arbor, MI, 529pp.

Rogowsky, D.M. and Marti, P., "Detailing for Post-Tensioning", VSL Report Series, VSL International Ltd., 1991, Berne Switzerland, 49pp.

Tan, K-H and Ng, C-K, "Effects of deviators and tendon configuration on behavior of externally prestressed beams" ACI Structural Journal, Vol.94 No.1, Jan-Feb 1997 pp.14-22

# APPENDIX A

**Table A.1: Test 1500A friction test tendon travel**

| 1500A-60% A | | 1500A -70% A | | 1500A -50% B | | 1500A -60% B | |
|---|---|---|---|---|---|---|---|
| Travel Direction | Approx. Travel Distance (mm) | Travel Direction | Approx. Travel Distance (mm) | Travel Direction | Approx. Travel Distance (mm) | Travel Direction | Approx. Travel Distance (mm) |
| North | 25 | South | 25 | South | 20 | South | 20 |
| South | 25 | North | 25 | South | 20 | North | 75 |
| North | 25 | South | 40 | South | 20 | South | 10 |
| South | 25 | North | 40 | North | 70 | North | 10 |
| North | 25 | South | 10 | South | 25 | South | 20 |
| South | 25 | North | 10 | South | 25 | South | 20 |
| North | 25 | North | 40 | South | 20 | South | 20 |
| North | 10 | South | 40 | North | 70 | North | 60 |
| South | 10 | North | 40 | South | 20 | South | 15 |
| North | 10 | South | 40 | South | 20 | South | 15 |
| South | 10 | North | 40 | South | 20 | South | 15 |
| North | 10 | | | | | North | 40 |
| South | 10 | | | | | South | 7 |
| North | 10 | | | | | South | 15 |
| South | 40 | | | | | South | 10 |
| North | 40 | | | | | South | 20 |
| South | 40 | | | | | North | 20 |
| North | 40 | | | | | South | 20 |
| South | 40 | | | | | South | 20 |
| North | 40 | | | | | North | 25 |
| North | 20 | | | | | North | 20 |
| North | 20 | | | | | North | 10 |
| South | 20 | | | | | South | 10 |
| North | 20 | | | | | South | 20 |
| South | 20 | | | | | North | 20 |
| North | 20 | | | | | North | 20 |
| South | 20 | | | | | North | 20 |
| North | 20 | | | | | South | 20 |
| | | | | | | South | 20 |
| | | | | | | South | 20 |
| | | | | | | | |
| TOTALS | | | | | | | |
| South | 285 | South | 155 | South | 190 | South | 317 |
| North | 360 | North | 195 | North | 140 | North | 320 |
| | 645 | | 350 | | 330 | | 637 |
| | | | | | | | |

**Table A.2: Test 1500B friction test tendon travel**

| 1500B-50% A | | 1500B -60% A | | 1500B -70% A | | 1500B -50% B | | 1500B -60% B | | 1500B -70% B | |
|---|---|---|---|---|---|---|---|---|---|---|---|
| Travel Direction | Approx. Travel Distance (mm) | Travel Direction | Approx. Travel Distance (mm) | Travel Direction | Approx. Travel Distance (mm) | Travel Direction | Approx. Travel Distance (mm) | Travel Direction | Approx. Travel Distance (mm) | Travel Direction | Approx. Travel Distance (mm) |
| North | 40 | North | 40 | South | 40 | South | 10 | North | 10 | South | 10 |
| South | 40 | South | 40 | North | 75 | South | 10 | North | 10 | South | 14 |
| North | 40 | North | 40 | South | 40 | South | 10 | North | 10 | South | 10 |
| South | 40 | South | 40 | North | 40 | South | 10 | North | 10 | South | 10 |
| North | 40 | North | 40 | South | 40 | South | 10 | North | 10 | South | 10 |
| South | 40 | South | 40 | North | 40 | North | 10 | South | 10 | South | 10 |
| North | 40 | North | 30 | South | 40 | North | 10 | North | 10 | North | 10 |
| South | 40 | North | 15 | North | 40 | North | 10 | South | 10 | North | 10 |
| North | 40 | South | 40 | South | 40 | North | 10 | South | 10 | North | 10 |
| South | 40 | North | 40 | North | 40 | North | 10 | South | 10 | North | 10 |
| | | South | 40 | | | South | 10 | South | 10 | North | 10 |
| | | | | | | South | 10 | South | 10 | North | 10 |
| | | | | | | South | 10 | North | 10 | South | 10 |
| | | | | | | South | 10 | North | 10 | South | 10 |
| | | | | | | South | 10 | North | 10 | South | 10 |
| | | | | | | | | North | 10 | | |
| | | | | | | | | North | 10 | | |
| **TOTALS** | | | | | | | | | | | |
| South | 200 | South | 205 | South | 200 | South | 100 | South | 110 | South | 94 |
| North | 200 | North | 200 | North | 235 | North | 50 | North | 60 | North | 60 |
| | 400 | | 405 | | 435 | | 150 | | 170 | | 154 |
| | | | | | | | | | | | |

**Table A.3: Test 1500A2 friction test tendon travel**

| 1500A2-50%A | | 1500A2-60%A | | 1500A2-70%A | |
|---|---|---|---|---|---|
| Travel Direction | Approx. Travel Distance (mm) | Travel Direction | Approx. Travel Distance (mm) | Travel Direction | Approx. Travel Distance (mm) |
| South | 40 | South | 40 | South | 40 |
| North | 40 | North | 40 | North | 40 |
| South | 40 | South | 40 | South | 40 |
| North | 40 | North | 40 | North | 40 |
| South | 40 | South | 40 | South | 40 |
| North | 40 | North | 40 | North | 40 |
| South | 40 | South | 40 | South | 40 |
| North | 40 | North | 40 | North | 40 |
| South | 40 | South | 40 | South | 40 |
| North | 40 | North | 40 | North | 40 |
| South | 40 | South | 40 | South | 40 |
| North | 40 | North | 40 | North | 40 |
| South | 40 | South | 40 | South | 40 |
| North | 40 | North | 40 | North | 40 |
| | | | | | |
| TOTALS | | | | | |
| South | 280 | South | 280 | South | 280 |
| North | 280 | North | 280 | North | 280 |
| | 560 | | 560 | | 560 |
| | | | | | |

**Table A.4: Test 4500A friction test tendon travel**

| 4500A-50% A | | 4500A -60% A | | 4500A -70% A | | 4500A -50% B | | 4500A -60% B | |
|---|---|---|---|---|---|---|---|---|---|
| Travel Direction | Approx. Travel Distance (mm) | Travel Direction | Approx. Travel Distance (mm) | Travel Direction | Approx. Travel Distance (mm) | Travel Direction | Approx. Travel Distance (mm) | Travel Direction | Approx. Travel Distance (mm) |
| South | 40 | South | 40 | North | 40 | South | 30 | North | 20 |
| North | 40 | North | 40 | South | 40 | South | 25 | North | 20 |
| South | 40 | South | 40 | North | 40 | South | 13 | North | 10 |
| North | 40 | North | 40 | South | 40 | North | 25 | South | 30 |
| South | 40 | South | 40 | North | 40 | North | 37 | South | 30 |
| North | 40 | North | 40 | South | 40 | North | 25 | South | 20 |
| South | 40 | South | 40 | North | 40 | South | 25 | South | 20 |
| North | 40 | North | 40 | South | 40 | South | 25 | North | 30 |
| | | | | North | 40 | South | 25 | North | 30 |
| | | | | South | 40 | South | 15 | North | 30 |
| | | | | North | 40 | North | 25 | South | 25 |
| | | | | | | North | 25 | South | 25 |
| | | | | | | North | 25 | South | 25 |
| | | | | | | South | 25 | North | 25 |
| | | | | | | South | 25 | North | 25 |
| | | | | | | South | 25 | North | 25 |
| | | | | | | North | 25 | South | 25 |
| | | | | | | North | 25 | South | 25 |
| | | | | | | North | 25 | South | 25 |
| | | | | | | South | 25 | | |
| | | | | | | South | 25 | | |
| | | | | | | | | | |
| TOTALS | | | | | | | | | |
| South | 160 | South | 160 | South | 200 | South | 283 | South | 250 |
| North | 160 | North | 160 | North | 240 | North | 237 | North | 215 |
| | 320 | | 320 | | 440 | | 520 | | 465 |
| | | | | | | | | | |

**Table A.5: Test 4500B friction test tendon travel**

| 4500B-50%A | | 4500B -60%A | | 4500B -70%A | | 4500B -50%B | | 4500B -60%B | | 4500B -70%B | |
|---|---|---|---|---|---|---|---|---|---|---|---|
| Travel Direction | Approx. Travel Distance (mm) | Travel Direction | Approx. Travel Distance (mm) | Travel Direction | Approx. Travel Distance (mm) | Travel Direction | Approx. Travel Distance (mm) | Travel Direction | Approx. Travel Distance (mm) | Travel Direction | Approx. Travel Distance (mm) |
| South | 20 | South | 40 | South | 55 | South | 20 | South | 10 | South | 10 |
| North | 20 | North | 40 | North | 40 | South | 20 | South | 10 | South | 10 |
| South | 30 | South | 40 | South | 40 | North | 20 | South | 10 | South | 10 |
| North | 40 | North | 40 | North | 40 | North | 20 | South | 10 | South | 10 |
| South | 30 | South | 40 | South | 40 | North | 15 | South | 10 | South | 10 |
| North | 45 | North | 40 | North | 40 | South | 20 | North | 10 | North | 10 |
| South | 40 | South | 40 | South | 40 | South | 20 | North | 10 | North | 10 |
| North | 40 | North | 40 | North | 40 | South | 15 | North | 10 | North | 10 |
| South | 40 | South | 40 | South | 40 | South | 20 | North | 15 | North | 10 |
| North | 40 | North | 40 | North | 40 | North | 20 | South | 10 | South | 10 |
| | | | | South | 40 | North | 20 | South | 10 | South | 10 |
| | | | | North | 40 | North | 20 | South | 10 | South | 10 |
| | | | | | | South | 10 | South | 10 | South | 10 |
| | | | | | | South | 10 | North | 10 | South | 10 |
| | | | | | | South | 10 | North | 10 | South | 10 |
| | | | | | | South | 10 | North | 10 | North | 10 |
| | | | | | | South | 10 | North | 10 | North | 10 |
| | | | | | | South | 10 | North | 10 | North | 10 |
| | | | | | | North | 10 | South | 10 | North | 10 |
| | | | | | | North | 10 | South | 10 | North | 10 |
| | | | | | | North | 10 | South | 10 | | |
| | | | | | | North | 10 | South | 10 | | |
| | | | | | | North | 10 | South | 10 | | |
| | | | | | | North | 10 | South | 10 | | |
| | | | | | | | | North | 10 | | |
| | | | | | | | | North | 10 | | |
| | | | | | | | | North | 10 | | |
| | | | | | | | | North | 10 | | |
| | | | | | | | | North | 10 | | |
| | Total | | | | | | | | | | |
| South | 160 | South | 200 | South | 255 | South | 175 | South | 150 | South | 110 |
| North | 185 | North | 200 | North | 240 | North | 175 | North | 145 | North | 90 |
| | 345 | | 400 | | 495 | | 350 | | 295 | | 200 |
| | | | | | | | | | | | |

**Table A.6: Test 4500A2 friction test tendon travel**

| 4500A2-50% A | | 4500A2-60% A | | 4500A2-70% A | |
|---|---|---|---|---|---|
| Travel Direction | Approx. Travel Distance (mm) | Travel Direction | Approx. Travel Distance (mm) | Travel Direction | Approx. Travel Distance (mm) |
| South | S ~40 | South | S ~40 | South | S ~40 |
| North | N ~40 | North | N ~40 | North | N ~40 |
| South | S ~40 | South | S ~40 | South | S ~40 |
| North | N ~40 | North | N ~40 | South | S ~17 |
| South | S ~40 | South | S ~40 | North | N ~40 |
| North | N ~40 | North | N ~40 | South | S ~40 |
| South | S ~40 | South | S ~40 | North | N ~40 |
| North | N ~40 | South | S ~10 | South | S ~40 |
| South | S ~40 | North | N ~40 | North | N ~40 |
| North | N ~40 | South | S ~40 | South | S ~40 |
| South | S ~40 | North | N ~40 | North | N ~40 |
| North | N ~40 | South | S ~40 | South | S ~40 |
| South | S ~40 | North | N ~40 | North | N ~40 |
| North | N ~40 | South | S ~40 | South | S ~40 |
| South | S ~40 | North | N ~40 | North | N ~40 |
| North | N ~40 | | | | |
| | | | | | |
| **TOTALS** | | | | | |
| South | 320 | South | 290 | South | 297 |
| North | 320 | North | 280 | North | 280 |
| | 640 | | 570 | | 577 |
| | | | | | |

# APPENDIX B

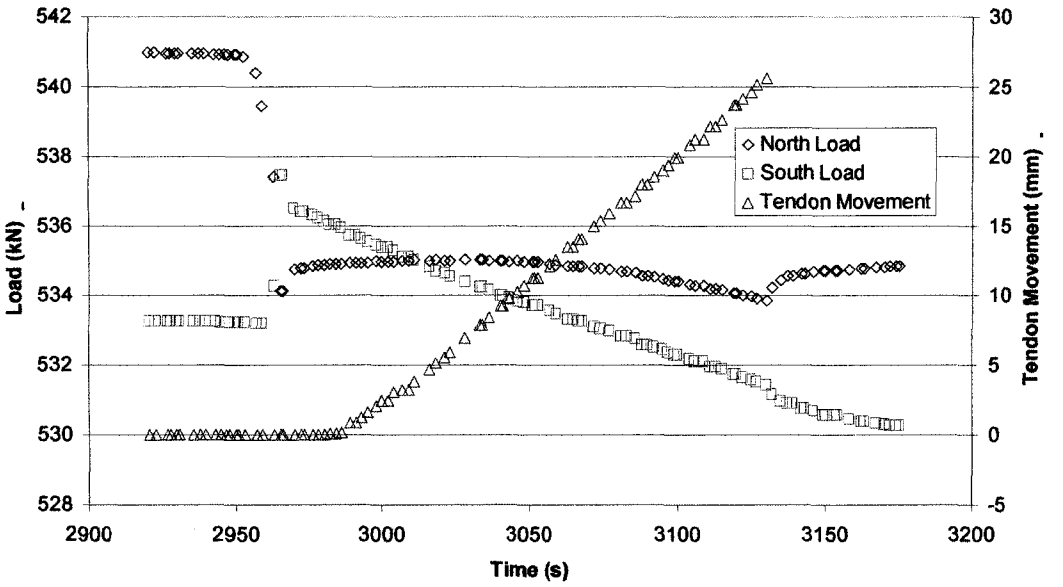


**Figure B.1: Time vs. load and tendon movement (Test 1500A - 70%A, first tendon shift south)**

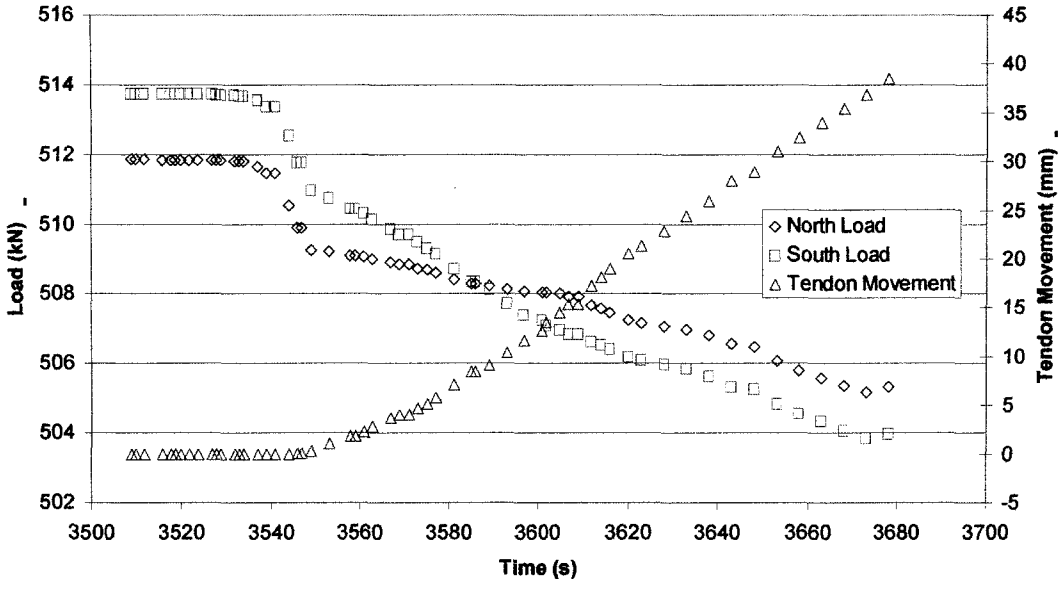


**Figure B.2: Time vs. load (determined from strain gauges on strands) and tendon movement (Test 1500B - 70%A, second tendon shift south)**

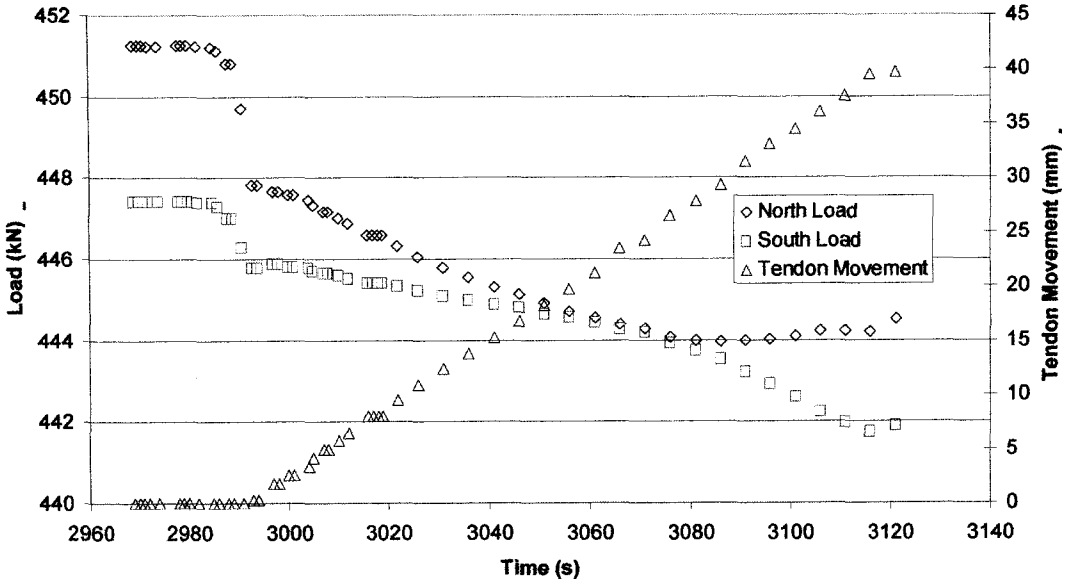


**Figure B.3: Time vs. load (determined from strain gauges on strands) and tendon movement (Test 4500A - 60%A, first tendon shift south)**

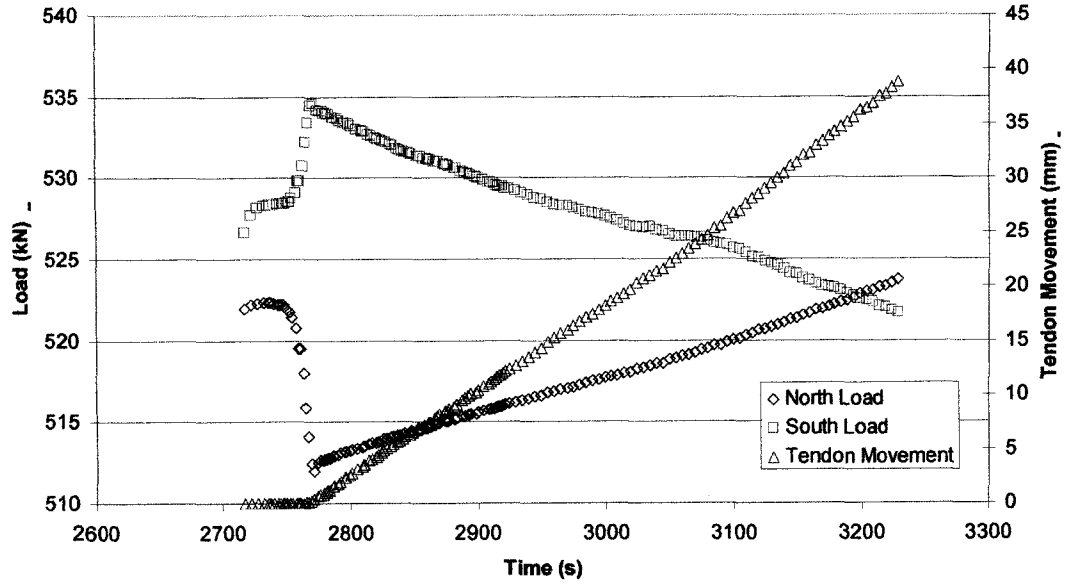


**Figure B.4: Time vs. load (determined from strain gauges on strands) and tendon movement (Test 4500B - 70%A, first tendon shift south)**

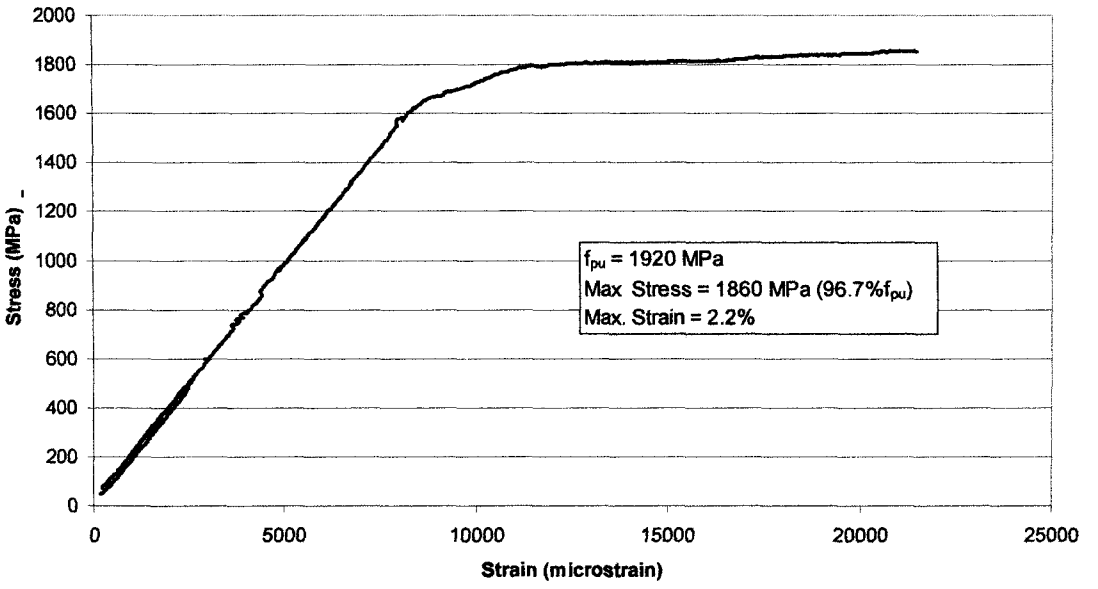


**Figure B.5: Tendon stress vs. strain (1500A)**

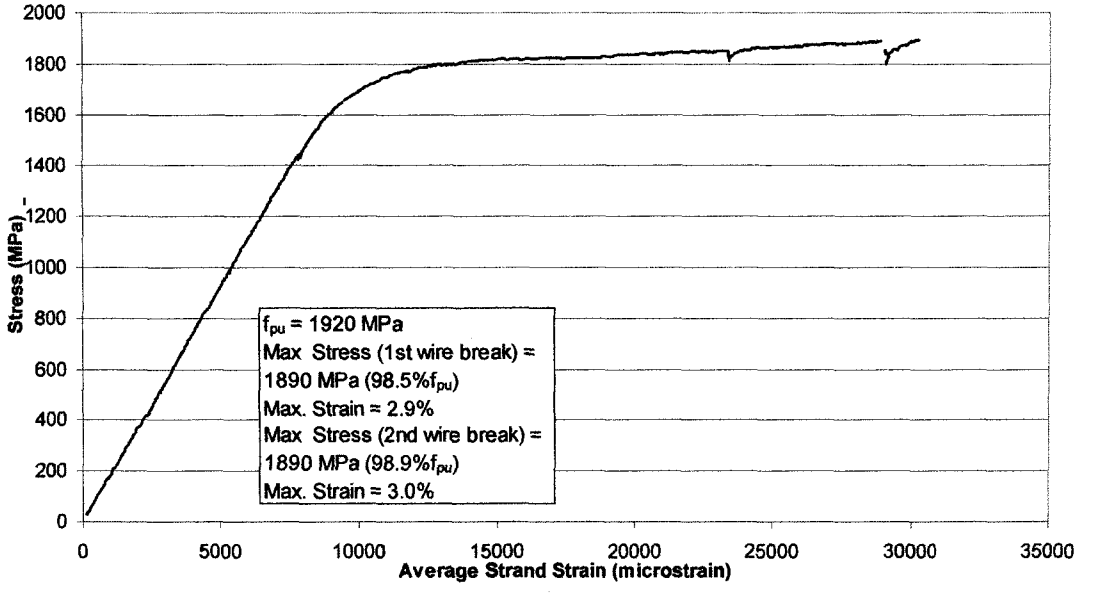


**Figure B.6: Tendon stress vs. strain (1500B)**

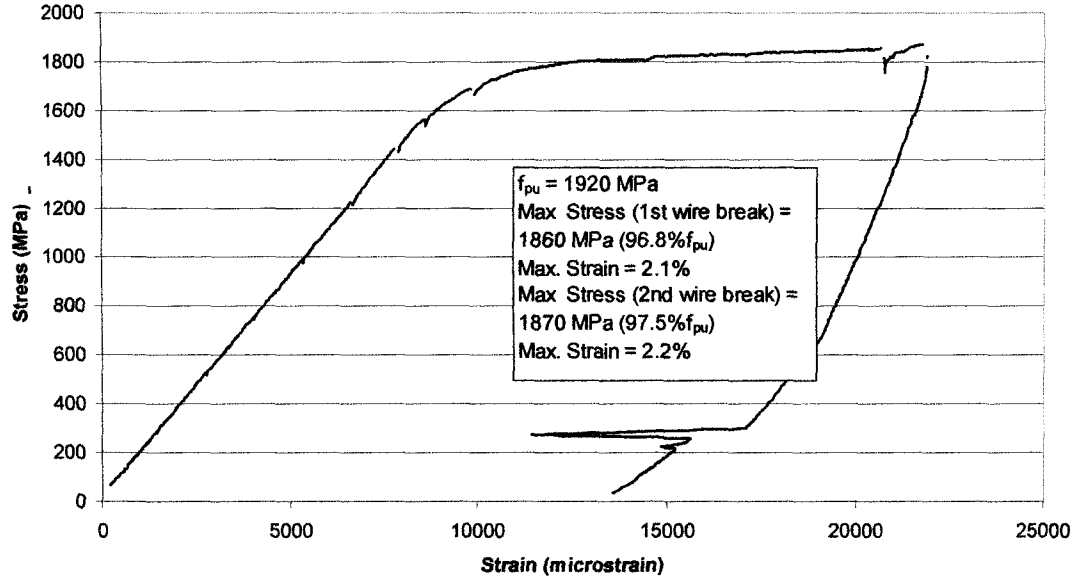


**Figure B.7: Stress vs. strand strain (1500A2)**

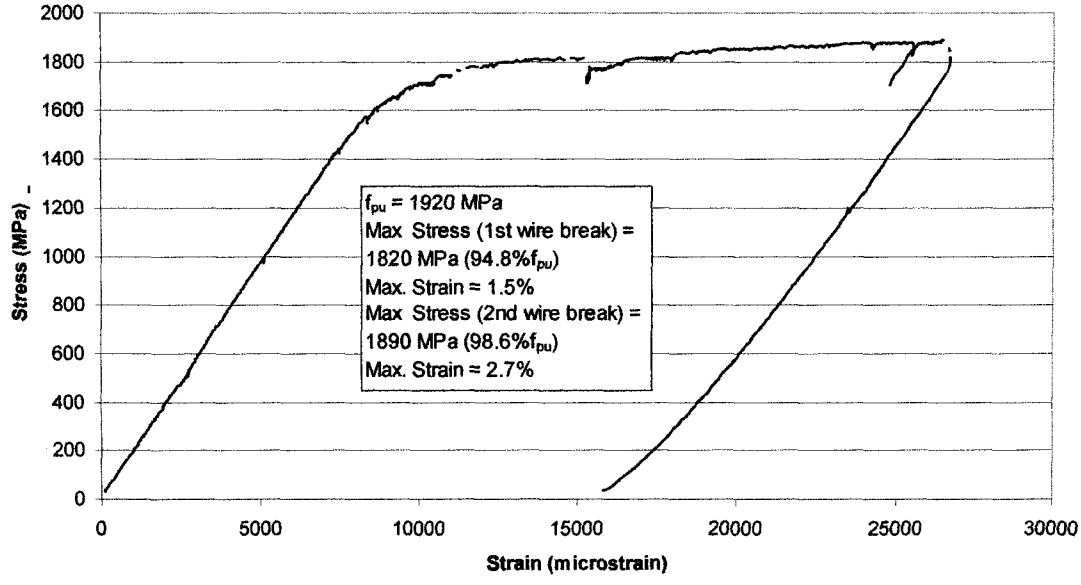


**Figure B.8: Tendon stress vs. strain (4500A)**

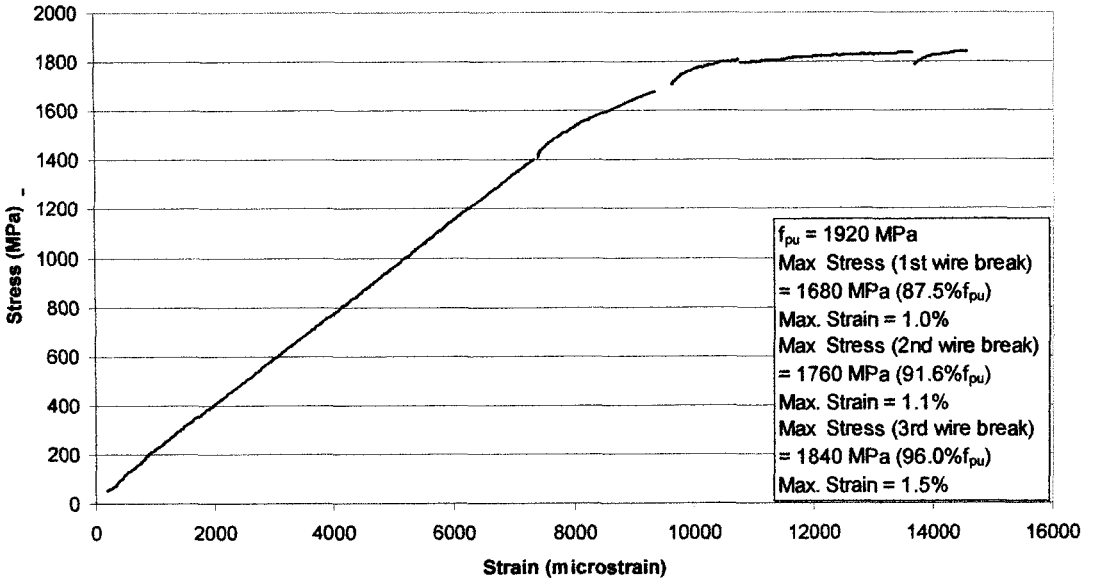


**Figure B.9: Tendon stress vs. strain (4500B)**

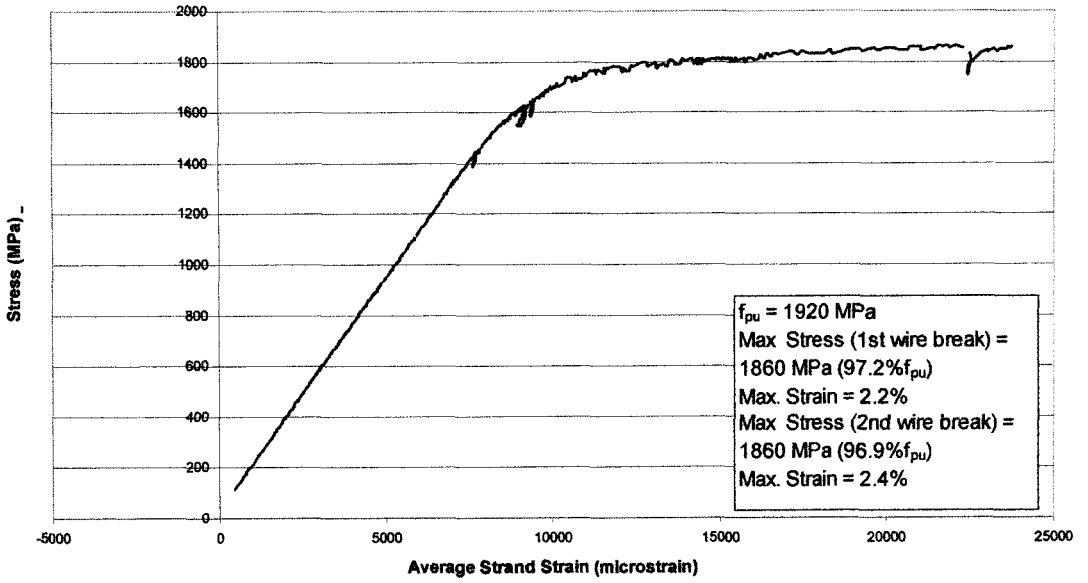


**Figure B.10: Tendon stress vs. strain (4500A2)**

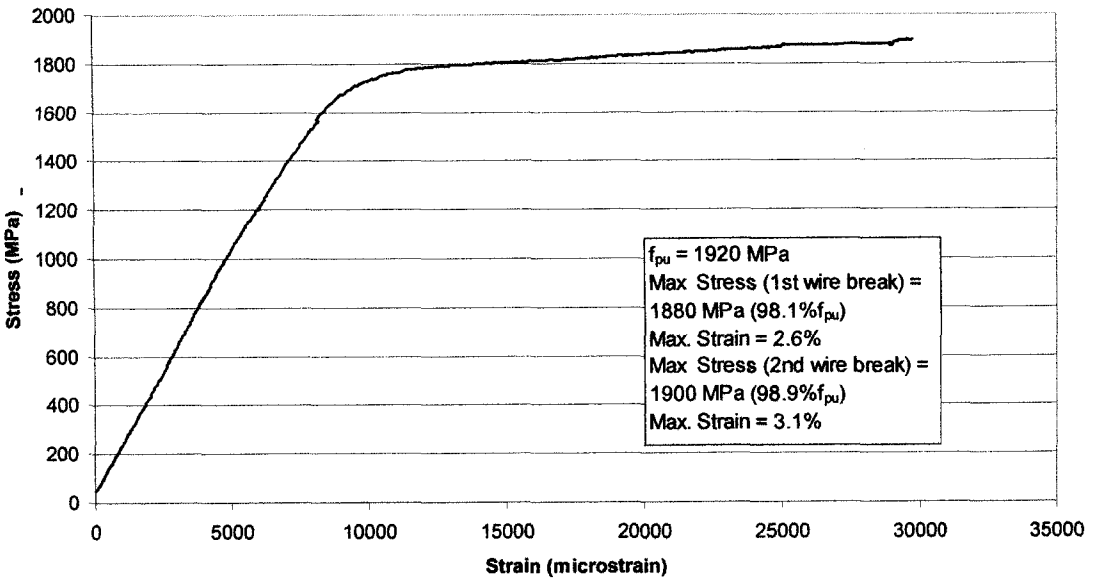


**Figure B.11: Control Test 1 results**

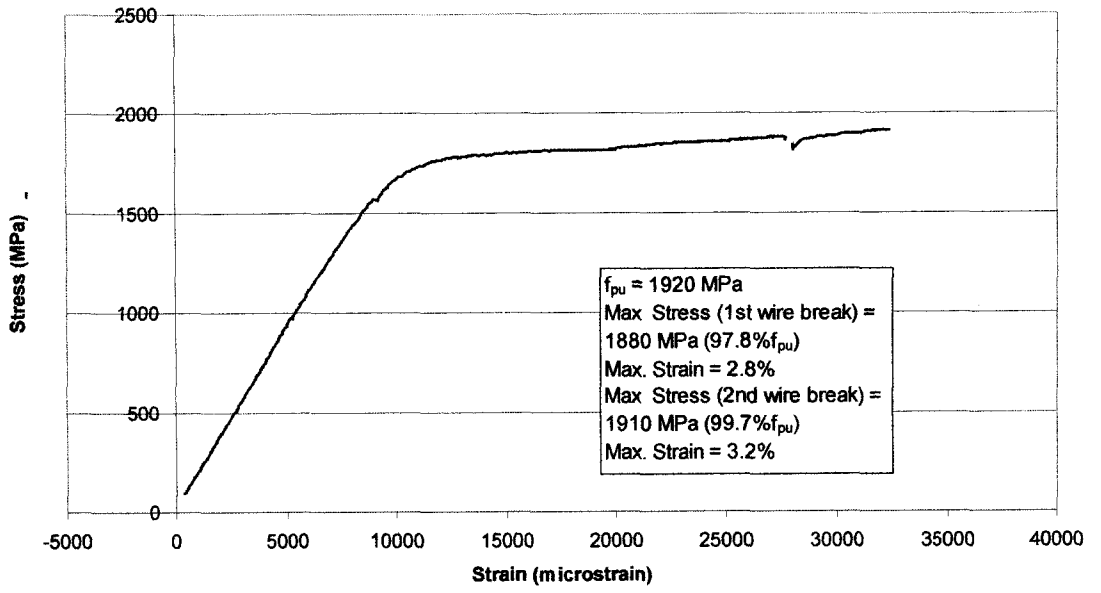


**Figure B.12: Control Test 2 results**

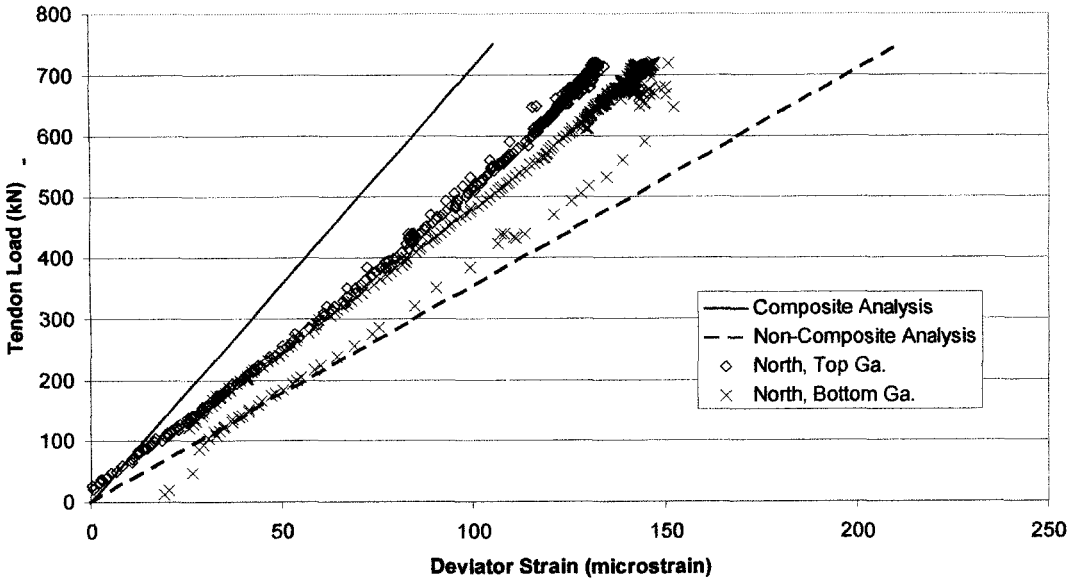


**Figure B.13: Tendon load vs. deviator strains (4500A) – 20 mm cantilever, north end**

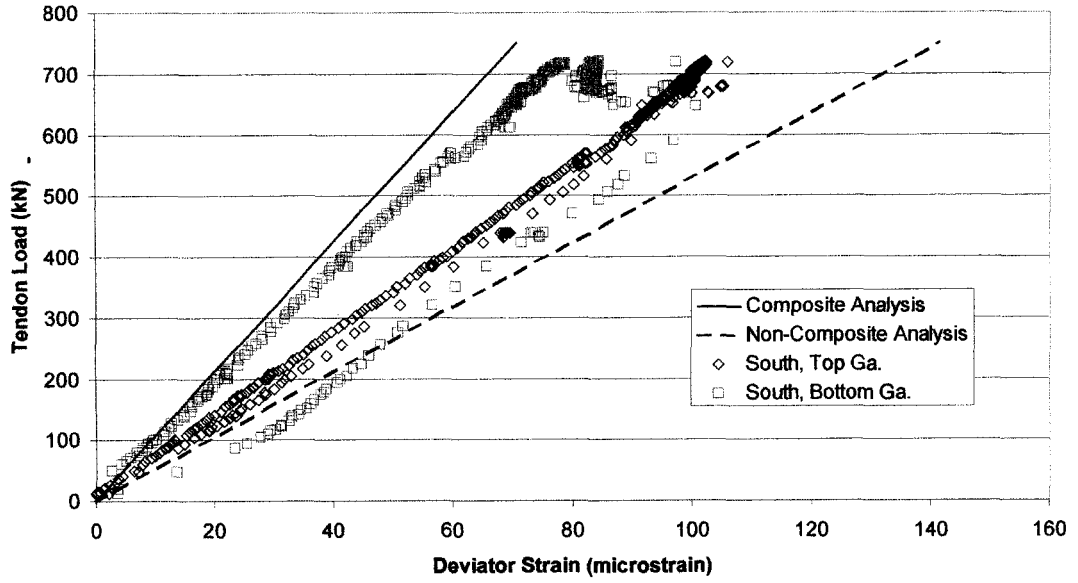


**Figure B.14: Tendon load vs. deviator strains (4500A) – 20 mm cantilever, south end**

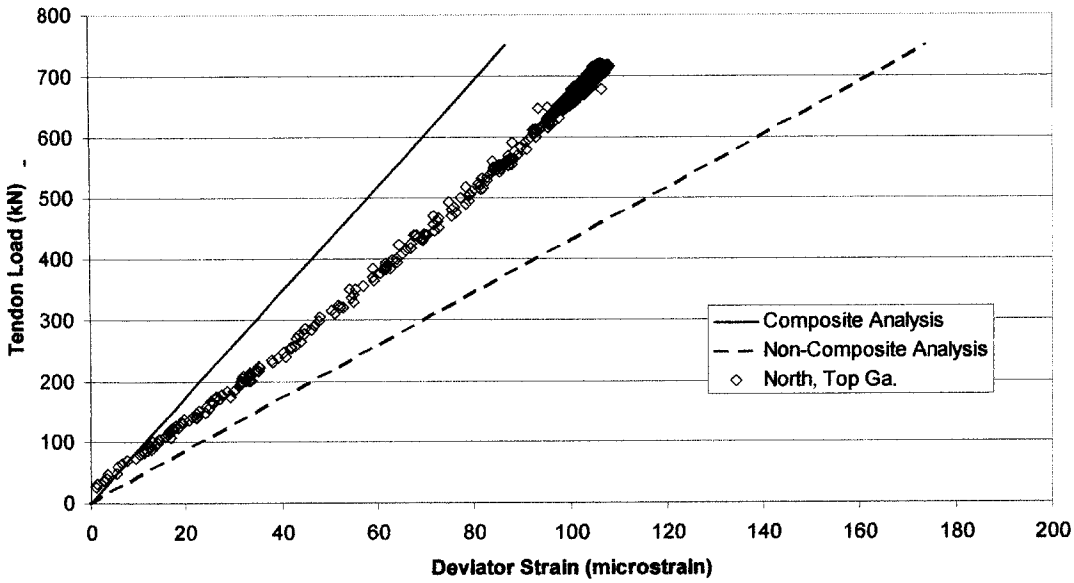


**Figure B.15: Tendon load vs. deviator strains (4500A) – 40 mm cantilever, north end**

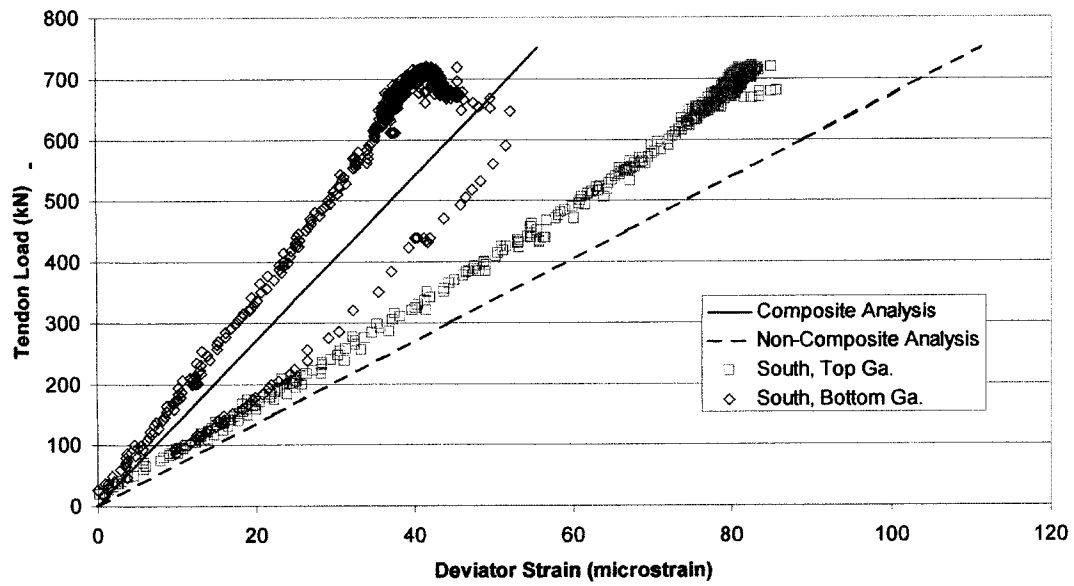


**Figure B.16: Tendon load vs. deviator strains (4500A) – 40 mm cantilever, south end**

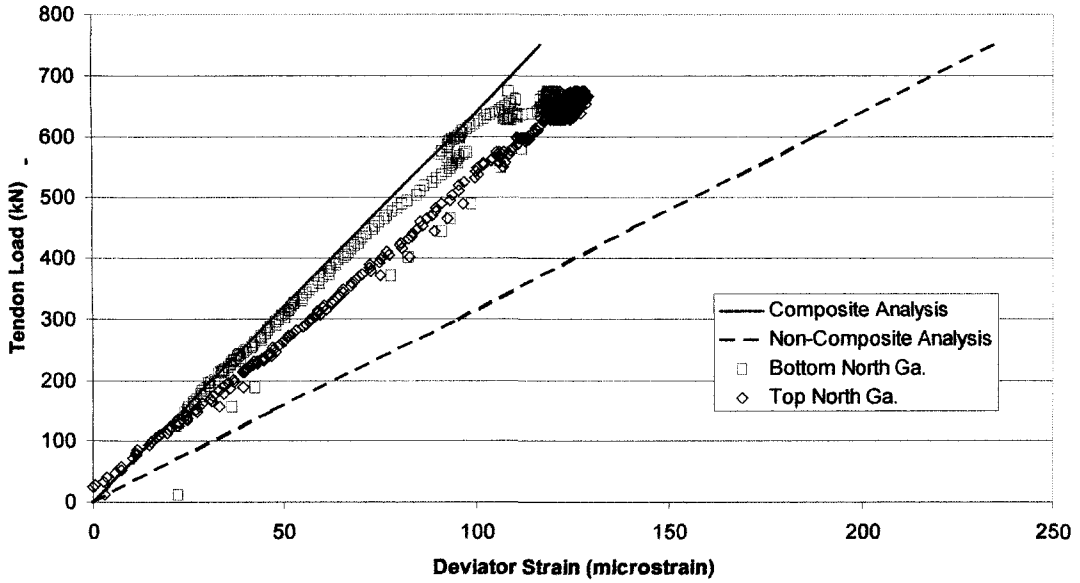


**Figure B.17: Tendon load vs. deviator strains (4500B) – 20 mm cantilever, north end**

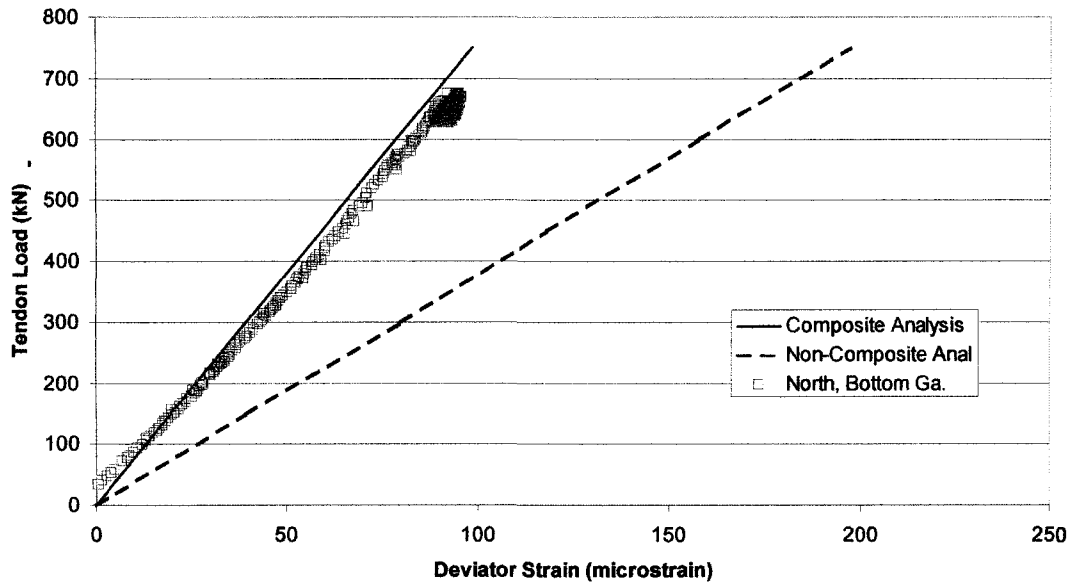


**Figure B.18: Tendon load vs. deviator strains (4500B) – 40 mm cantilever, north end**

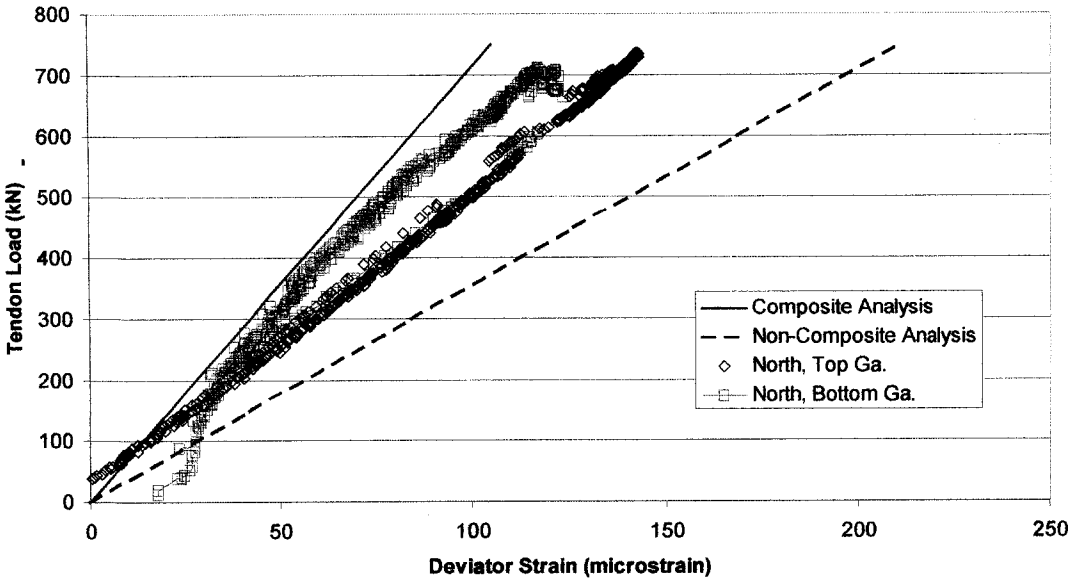


**Figure B.19: Tendon load vs. deviator strains (4500A2) – 20 mm cantilever, north end**

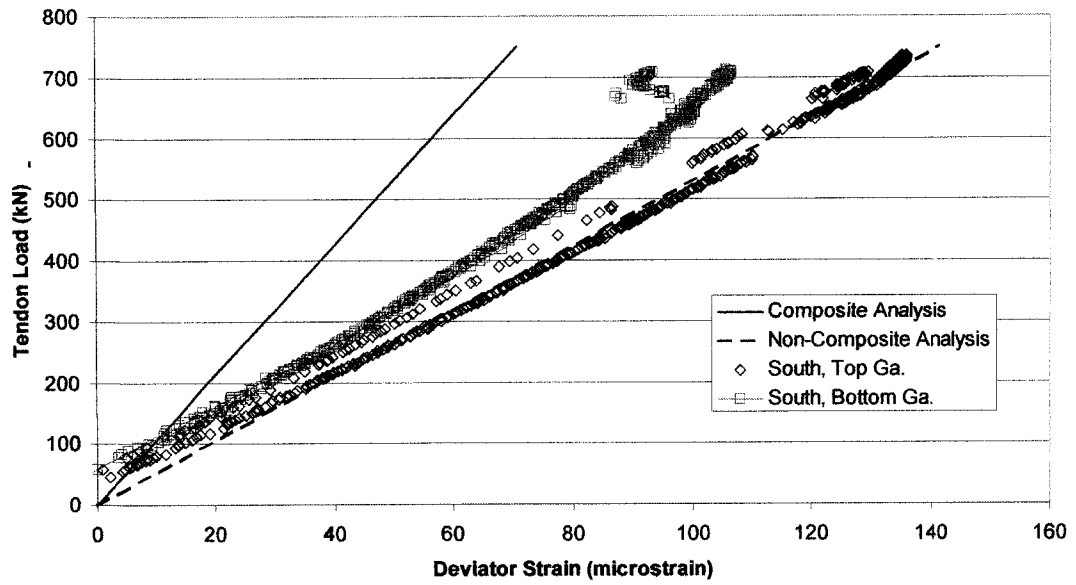


**Figure B.20: Tendon load vs. deviator strains (4500A2) – 20 mm cantilever, south end**

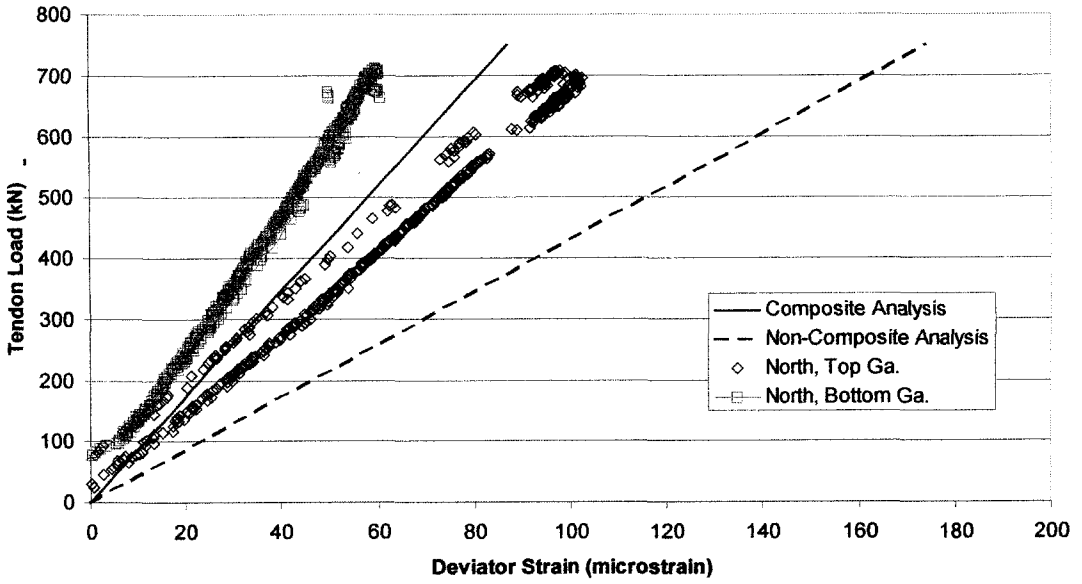


**Figure B.21: Tendon load vs. deviator strains (4500A2) – 40 mm cantilever, north end**

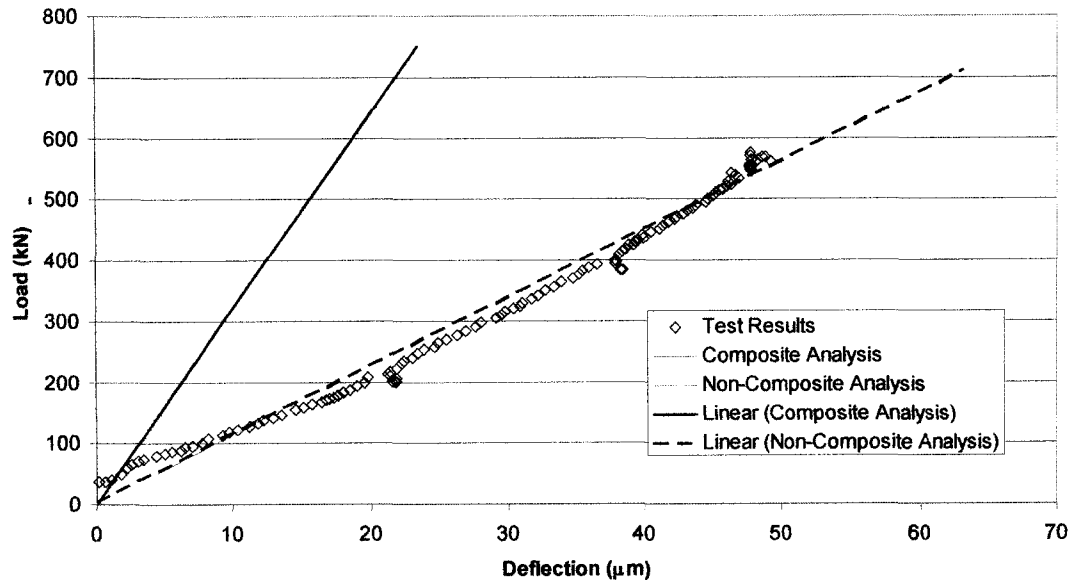


**Figure B.22: Tendon load vs. deviator deflection (4500A), north end**

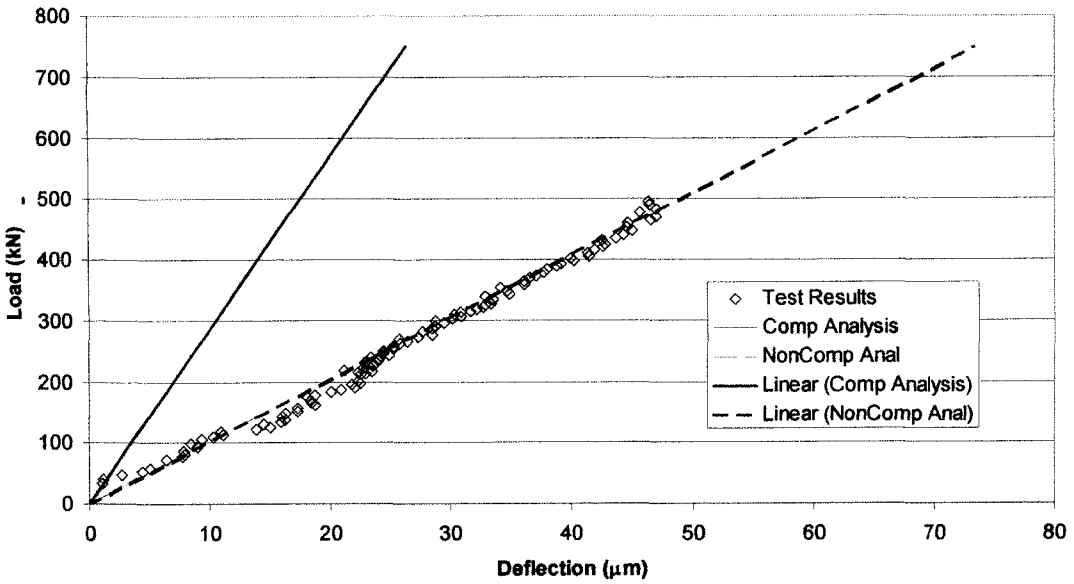


**Figure B.23: Tendon load vs. deviator deflection (4500B), north end**

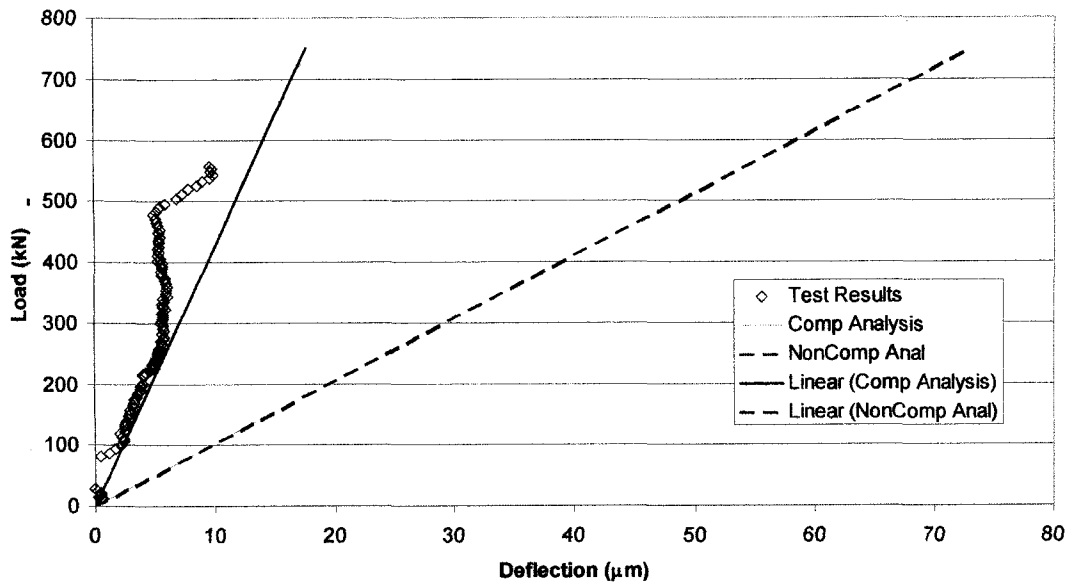


**Figure B.24: Tendon load vs. deviator deflection (4500B), south end**

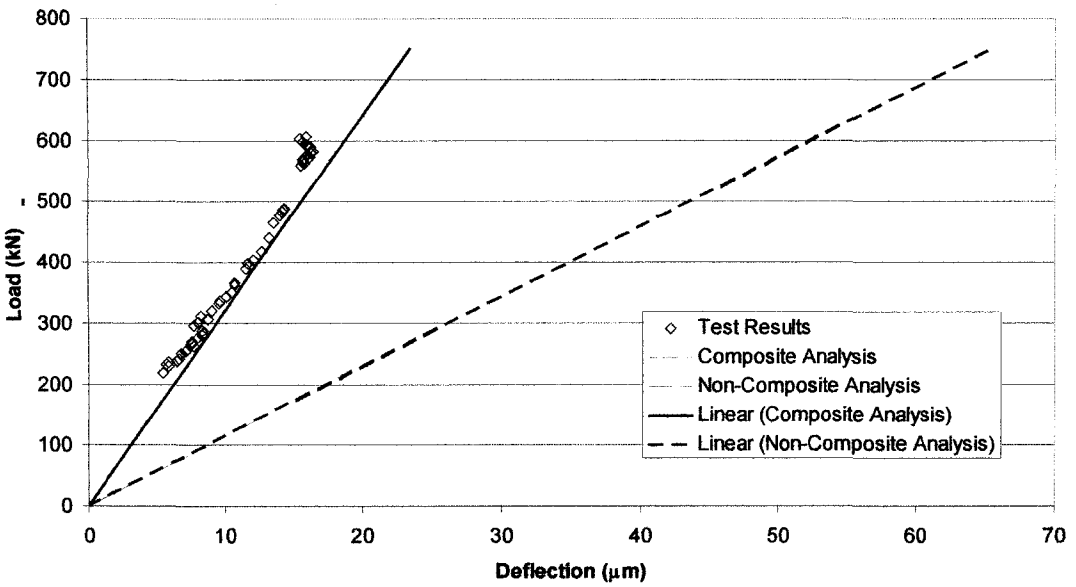


**Figure B.25: Tendon load vs. deviator deflection (4500A2), north end**

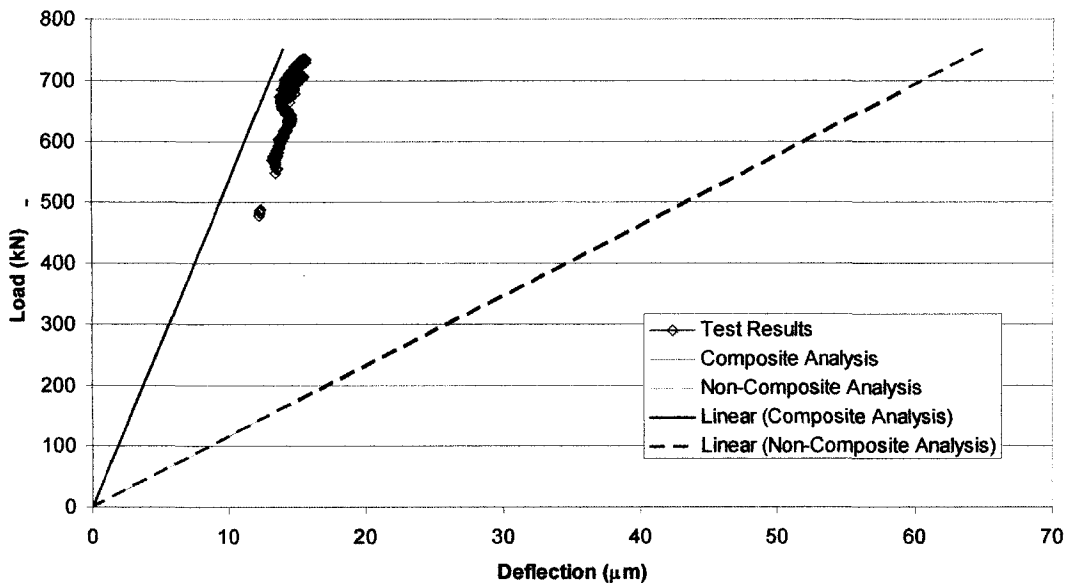


**Figure B.26: Tendon load vs. deviator deflection (4500A2), south end**

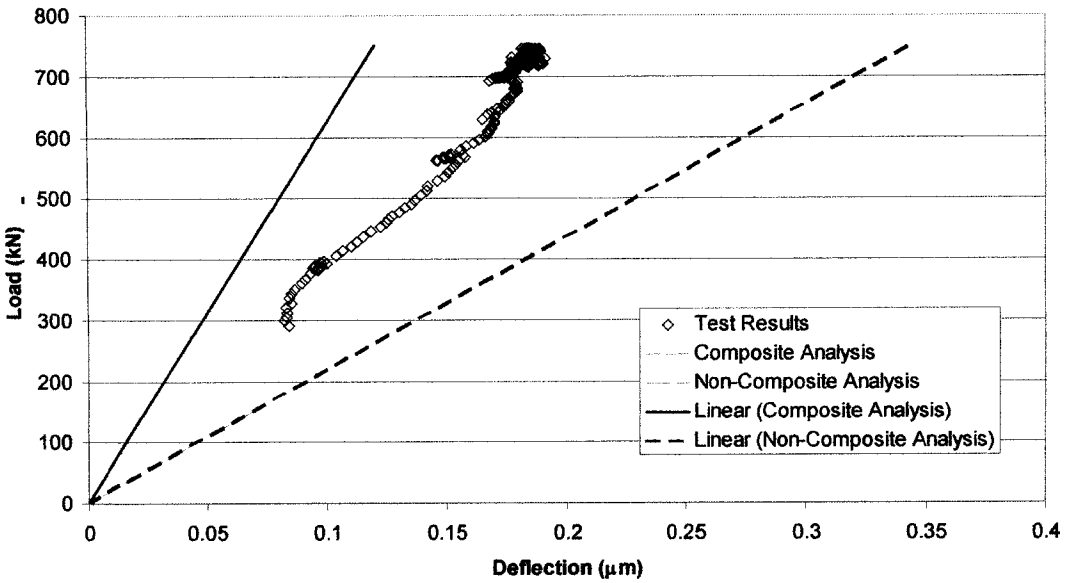


**Figure B.27: Tendon load vs. deviator deflection (1500B), north end**

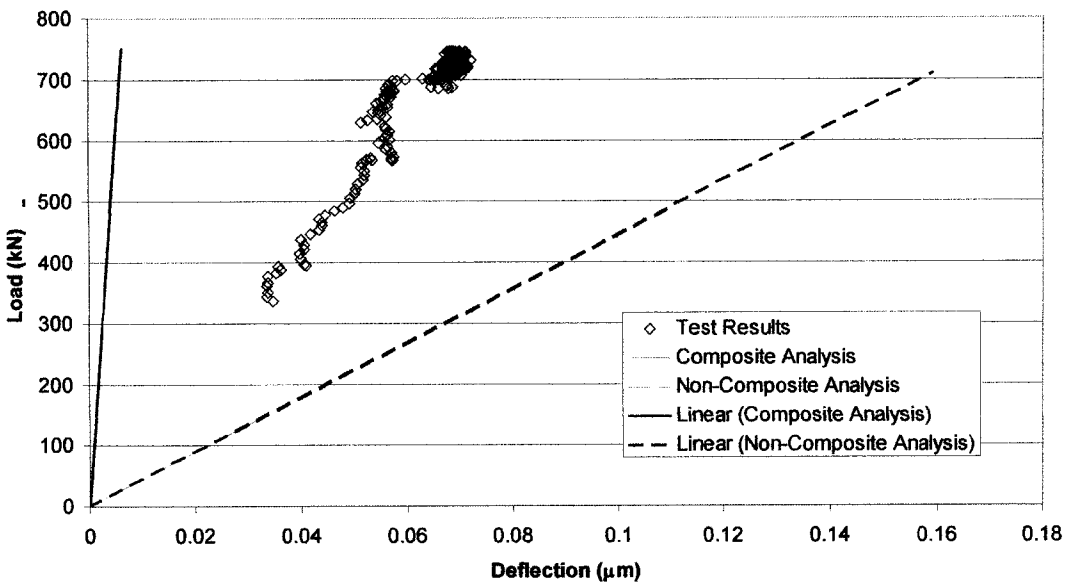


**Figure B.28: Tendon load vs. deviator deflection (1500B), south end**

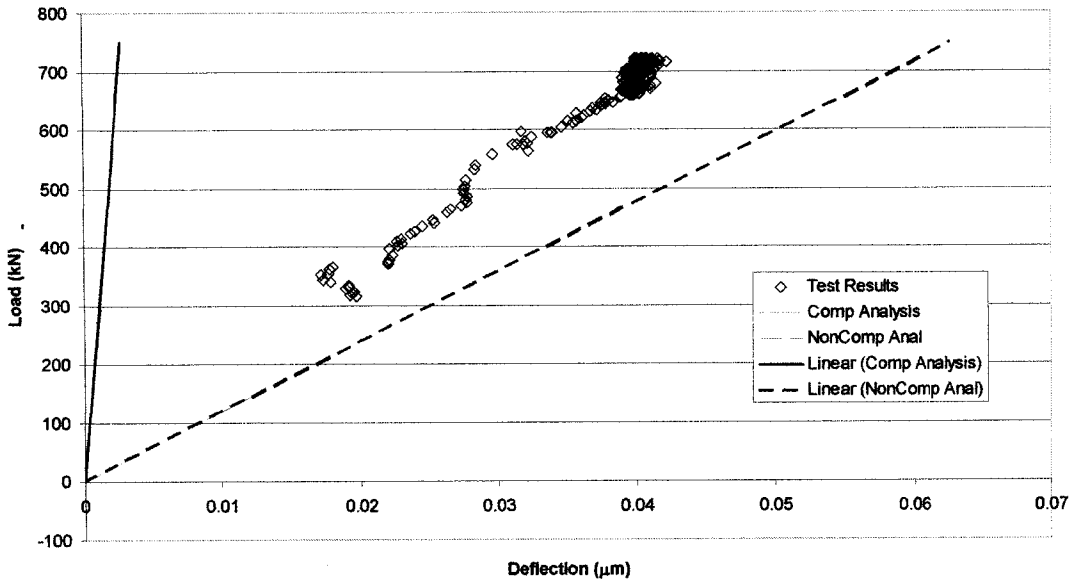


**Figure B.29: Tendon load vs. deviator deflection (1500A2), south end**